

*Mineral Processing and Coal Preparation*



## Concentration Procedure and Mineralogical and Chemical Composition of Raw Quartz Sand

Z Sekulic, N Came, & Z Bartulovic

*Institute for Technology of Nuclear and Other Mineral Raw Materials, 11 000 Belgrade,  
86 Franchet d'Esperey Street, Serbia and Montenegro*

M Ignjatovic

*Chamber of Commerce and Industry of Serbia Belgrade*

**ABSTRACT:** The investigation, presented in this paper, was carried out on raw quartz sand from three different deposits "Slatma", Cucuge" and "Avala", within the locality of Ub (Serbia) Main scope of the investigation was determination of the optimal concentration procedure for production of the quartz sand concentrate adequate for application in the glass industry

Performed investigation undoubtedly showed that concentration procedure depends on mineralogical and chemical composition of raw quartz sand

The optimal concentration procedure for quartz sand "Slatma", consisting of quartz, chalcedony, feldspar, mica, amphibolites, carbonates and clay minerals, involved washing, classifying and attrition scrubbing For quartz sand "Cucuge", which mineralogical composition includes quartz, chalcedony, feldspar, hornstone and limonite-goethite, it was necessary to involve the high intensity magnetic concentration together with washing, classifying and attrition scrubbing At the end, quartz sand "Avala" that consists of quartz chalcedony mass, potassium feldspar, limonite goethite, mica and rutile, required washing, classifying, attrition scrubbing, high intensity magnetic concentration and flotation concentration in order to obtain the concentrate of required quality

**Key words** *quartz sand, glass industry, sizing, attrition scrubbing, magnetic concentration, flotation concentration*

### 1. INTRODUCTION

The Company "Kopovi", Ub (Serbia) produce quartz sand Within the Company there are three quartz sand deposits In these deposits, the grain size of the raw quartz sands is different, as well as their mineralogical and chemical composition [1] The investigations, presented in this paper, were carried out on raw quartz sand from these three deposits The samples were denoted as "Slatma", Cucuge" and "Avala",

The main application of high quality quartz sand concentrate is in the glass industry [1] Glass industry [2] has high criteria concerning the quality of the quartz sand, as follows

#### Granulometric composition

> 0,500 max 0 05 %  
< 0,100 max 1 %

#### Chemical composition

Al<sub>2</sub>O<sub>3</sub> max 0 5 %  
Fe<sub>2</sub>O<sub>3</sub> 0 035 % (+/- 0 005)  
TiO<sub>2</sub> max 0 08 %  
K<sub>2</sub>O max 0 25 %  
Na<sub>2</sub>O max 0 006 %  
CaO max 0 05 %  
MgO max 0 05 %  
IL max 0 30 %

In our previous papers, the investigation results related with various possibilities for obtaining high quality quartz sand concentrate, were presented [3,4] as well as the results concerning the application of various reagents in the process of flotation concentration [5,6]

In this paper, the investigation results of selection of concentration procedure in dependence on mineralogical and chemical composition of raw quartz sand are presented

2. EXPERIMENTAL

2.1. Material properties

2.1.1 Granulometric composition of raw quartz sand samples

Granulometric composition of investigated samples was determined by wet sieving, with standard labora-

tory sieves. The obtained results are presented in Table 1

From the results presented in Table 1 it can be seen that quartz sand "Cucuge" has 2.42% of class +0.5 mm and 5.71% of class -0.1+0.0 mm. Quartz sand "Slatina" has 0.84% of class +0.5 mm and 2.40% of class -0.1+0.0 mm, while quartz sand "Avala" has 1.42% of class +0.5 mm and 13.96% of class -0.1+0.0

Table 1 Granulometric composition of raw quartz sand samples

Class, mm	Sample								
	"Cucuge"			"Slatina"			"Avala"		
	W,%	I	2W% I	W,%	zw% I	T	MW%	sw% T	zw% T
+0.5	2.42	2.42	100.00	0.84	0.84	100.00	1.42	1.42	100.00
-0.5+0.3	34.01	36.43	97.58	76.41	77.25	99.16	18.5	3.27	98.58
-0.3+0.2	52.76	89.19	63.57	18.28	95.53	22.75	12.70	15.97	96.73
-0.2+0.1	5.10	94.29	10.81	2.07	97.60	4.47	70.07	86.04	84.03
-0.1+0.0	5.71	100.00	5.71	2.40	100.00	2.40	13.96	100.00	13.96
Feed	100.00			100.00			100.00		

2.1.2 Chemical analysis of raw quartz sand samples

Results of chemical analysis of raw quartz sand samples from three deposits are presented in Table 2

According to results, given in Table 2, it can be seen that content of SiO<sub>2</sub> in investigated samples

was 92.53% - sample "Avala", 96.50% - sample "Cucuge" and 98.23% - sample "Slatina". The content of Fe<sub>2</sub>O<sub>3</sub> in samples varied from 0.214% to 0.390%. This chemical composition of investigated samples indicated that for obtaining required quality of quartz sand concentrate for the glass industry the application of concentration procedures was necessary.

Table 2 Chemical composition of raw quartz sand samples

Sample	Content, %								
	SiO <sub>2</sub>	Al <sub>2</sub> O <sub>3</sub>	Fe <sub>2</sub> O <sub>3</sub>	K <sub>2</sub> O	Na <sub>2</sub> O	CaO	MgO	TiO <sub>2</sub>	EL
"Cucuge"	96.50	1.66	0.39	0.34	0.024	0.042	0.054	0.133	0.68
"Slatina"	98.23	0.832	0.214	0.16	0.02	0.028	0.019	0.050	0.49
"Avala"	92.53	3.97	0.33	1.16	0.07	0.22	0.032	0.40	1.25

2.1.3 Mineralogical analysis of raw quartz sand samples

Microscopic analysis of the sample "Slatina"

Mineral composition: quartz, chalcedony, feldspar, mica, amphiboles, carbonate and clay minerals. Micro description: Mica minerals (biotite, uncommonly muscovite) were found in minor quantities. The rest of minerals occurred in insignificant percentage. Feldspar and quartz minerals were partly or completely alternated (sencited). The grains of all present miner-

als were uniform in size and had oval to isometric shape.

Microscopic analysis of the sample "Cucuge"

Mineral composition: quartz, chalcedony, feldspar, mica, amphiboles, carbonates and clay minerals. Micro description: Form, size and the level of alternation are very similar to one of "Slatina" quartz sand.

#### Microscopic analysis of the sample "Avala"

Mineral composition: quartz-chalcedony mass, quartz-muscovite mass, potassium feldspar, limonite-goethite, micas and rutile.

Based on the mineralogical composition of investigated samples, the following may be concluded:

- >In quartz sand "Slatina", the main impurities are feldspar, carbonates and clay minerals
- >Feldspar, mica, amphibolites, carbonates and clay minerals are the main impurities in quartz sand "Cucuge"
- >In quartz sand "Avala", the main impurities are potassium feldspar, limonite-goethite, rutile and mica minerals

Due to different mineralogical origin of the impurities, different concentration procedures are needed for their separation and removal from quartz sand.

#### 2.2. Classifying, attrition scrubbing and washing procedure

Classifying (wet sieving) was the first procedure applied, on raw quartz sand samples previously soaked in water. Vibration sieves were used. The results of chemical analysis of obtained products is presented in Table 3

Table 3 Chemical composition of classifying products

Content, %						
Cucuge deposit						
	SiO <sub>2</sub>	Al <sub>2</sub> O <sub>3</sub>	Fe <sub>2</sub> O <sub>3</sub>	K <sub>2</sub> O	Na <sub>2</sub> O	Loi
Feed	96.50	1.660	0.390	0.340	0.024	0.68
Classifying product	99.33	0.265	0.049	0.041	0.008	0.25
Slatina deposit						
Feed	98.23	0.832	0.214	0.16	0.02	0.49
Classifying product	99.20	0.34	0.054	0.113	0.011	0.22
Avala deposit						
Feed	93.015	3.78	0.326	1.039	0.072	1.109
Classifying product	97.03	1.43	0.08	0.83	0.06	0.23

As it can be seen in Table 3, for all samples, classifying is unable to provide satisfying quality of quartz sand concentrate. The content of Fe<sub>2</sub>O<sub>3</sub> is ranged from 0.049% to 0.08%.

Attrition scrubbing tests were performed in laboratory attrition machine, under the following conditions: pulp density during the attrition was 75% of solid, time of procedure was 15 minutes. After attrition, samples were washed on vibration sieve. Mass balances are presented in Table 4.

Results presented in Table 4, indicate that attrition scrubbing, gave the satisfying quality of the final product only for the quartz sand "Slatina" (content of Fe<sub>2</sub>O<sub>3</sub> was 0.031%) and for this sample further treatment is not needed, while other two samples from "Avala" and "Cucuge" deposits required additional treatment.

#### 2.3. Magnetic concentration procedure

Magnetic concentration tests were carried out in high intensity magnetic separator "BOXMAG

RAPID IRB 2-250. Magnetic induction used in these tests was 2.0 Tesla The obtained results are shown in Table 5.

The magnetic concentration was efficient procedure for sample from "Cucuge" deposit with which the content of Fe<sub>2</sub>O<sub>3</sub> in non magnetic fraction decreased to 0.034%. The obtained concentrate satisfied the criteria which regulates glass industry. For quartz sand "Avala", magnetic concentration was insufficient to provide required quality and this sample needs the additional treatment.

#### 2.4. Flotation concentration procedure

The flotation concentration was done on sample of quartz sand "Avala", using the procedure of an inverse flotation. R-825, ARMAC-C, FLOTIGAM-ENA and AERO 3030C were used as collectors of impurities (heavy metal minerals, mica, feldspar). NaF was used as deprimator for quartz sand.

The three experiments (Tests, 1, 2 and 3) with different regimes of reagents were done with the aim to

investigate the efficiency of applied reagents in flotation concentration of quartz sand

Test procedure were carried out according to the flow sheets, illustrated in Figures 2A, 2B and 2C, while the mass balance is shown in Table 6

Table 4 Results of attrition tests

Product	M, % per frac- tion	M, % per raw sample	Sample Cucuge					
			Content, %					
			SiO <sub>2</sub>	Al <sub>2</sub> O <sub>3</sub>	Fe <sub>2</sub> O <sub>3</sub>	K <sub>2</sub> O	Na <sub>2</sub> O	Loi
FEED	100 00	91 87	99 33	0 265	0 049	0 041	0 008	0 25
Attrition product	96 13	88 31	99 35	0 265	0 046	0 039	0 008	0 19
Attrition slurry	3 87	3 56	98 83	0 265	0 124	0 091	0 008	1740
Sample Slatina								
FEED	100 00	96 76	99 2	0 34	0 054	0 113	0 011	0 22
Attrition product	98 38	95 19	99 5	0 189	0 031	0 034	0 005	0 18
Attrition slurry	162	157	80 98	9 510	1451	4911	0 375	2 649
Sample Avala								
FEED	100 00	84 62	97 03	143	0 08	0 83	0 06	0 23
Attrition product	98 69	83 51	97 26	135	0 08	0 75	0 05	0 20
Attrition slurry	131	1 11	79 70	7 74	0 08	7 05	0 526	231

Table 5 Results of magnetic concentration tests at magnetic induction of 2.0 T

Product	M, % per fraction	M % per raw sam- ple	Sample Cucuge					
			Content, %					
			SiO <sub>2</sub>	Al <sub>2</sub> O <sub>3</sub>	Fe <sub>2</sub> O <sub>3</sub>	K <sub>2</sub> O	Na <sub>2</sub> O	Loi
Feed (Attrition product)	100 00	88 31	99 35	0 265	0 046	0 039	0 008	0 19
Non magnetic fraction	99 60	87 96	99 49	0 227	0 034	0 038	0 005	0 10
Magnetic fraction	0 40	0 35	64 49	9 727	3 034	0 288	0 755	22 60
Sample Avala								
Feed (Attrition product)	100 00	83 51	97 26	135	0 08	0 75	0 05	0 20
Non-magnetic fraction	98 82	82 52	98 54	1 02	0 049	0 73	0 05	0 16
Magnetic fraction	1 18	0 99	67 60	3 10	10 91	140	0 11	17 80

Comparing results of flotation concentration obtained in these three tests, it can be concluded that the best quality of quartz sand concentrate was achieved with collector AERO 3030C, used in

amount of 400 g/t (Test 3) Thus, the obtained quartz sand concentrate contain 99 28% of SiO<sub>2</sub>, 0 26% of Al<sub>2</sub>O<sub>3</sub>, 0 031% of Fe<sub>2</sub>O<sub>3</sub>, 0 005% of Na<sub>2</sub>O and 0 05% of K<sub>2</sub>O

Table 6 Results of flotation concentration of quartz sand AVALA

Tests	Product	M, % per fracuon	M, % per raw sam pie	Chemical composition %					
				SiO <sub>2</sub>	Al <sub>2</sub> O <sub>3</sub>	Fe <sub>2</sub> O <sub>3</sub>	K <sub>2</sub> O	Na <sub>2</sub> O	Loi
1	Feed	100 00	82 52	98 54	102	0 049	0 73	0 05	0 16
	C/SiO <sub>2</sub>	91 19	77 99	99 03	0 34	0 05	0 06	0 01	0 17
	C/C(impurities)	8 81	4 53	78 94	1180	0 35	7 89	0 45	0 51
2	Feed	100 00	82 52	98 54	102	0 049	0 73	0 05	0 16
	C/SiO <sub>2</sub>	93 50	77 16	98 81	0 45	0 06	0 11	0 016	0 17
	C/C(impurities)	6 50	5 36	74 96	14 30	0 37	9 94	0 539	0 63
3	Feed	100 00	82 52	98 54	102	0 049	0 73	0 05	0 16
	C/SiO <sub>2</sub>	90 10	74 35	99 28	0 26	0 03	0 05	0 005	0 16
	C/C(impurities)	9 90	8 17	78 87	1127	0 53	7 12	0 460	0 56

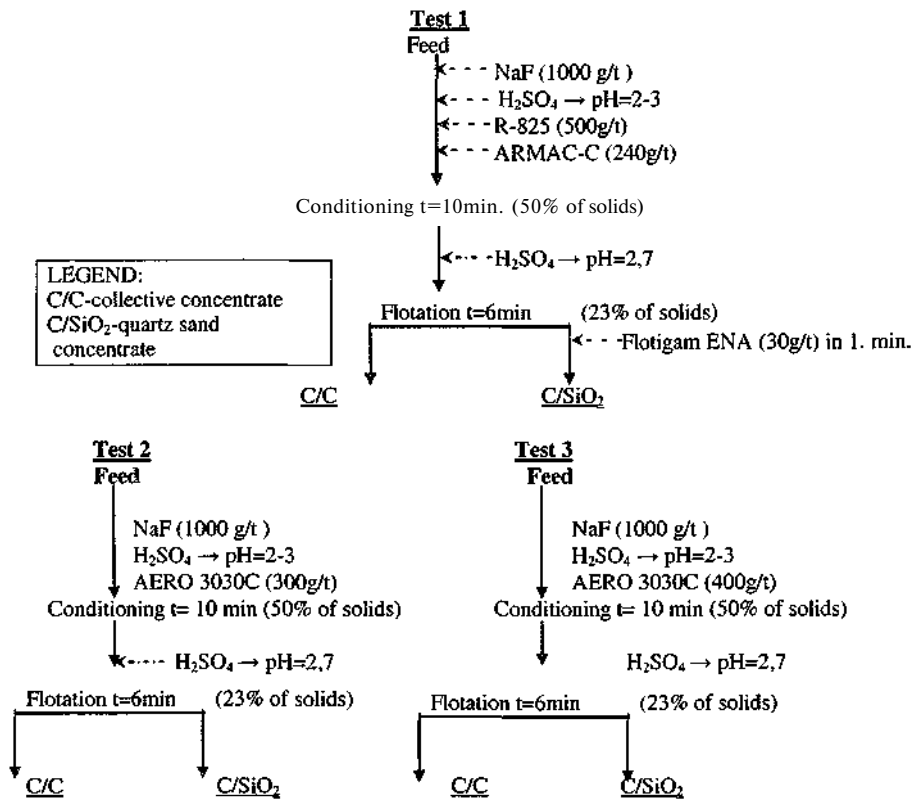


Figure 1. Flotation concentration procedure and conditions

Based on the results of chemical analysis (Table 6) it can be seen that with flotation concentration, the quartz sand concentrate which had the satisfying quality for application in glass industry was obtained, especially in third test

### 3. DISCUSSION

Summarized results of chemical composition, through the different concentration phases, are presented in Table 7. On obtained quartz sand concentrates, chemical analysis was done. These results are summarized in Table 8, together with the data for quality of quartz sand concentrate required for the glass industry. According to results of performed investigation, the technological procedures for valorization of quartz sand from three different deposits are proposed and illustrated in Figure 3A, 3B and 3C.

The summarized results of performed investigations, presented in Table 7, clearly show that selec-

tion of concentration procedure, for valorization of quartz sands from "Avala", "Slatina" and "Cucuge" deposits, directly is dependent on mineralogical and chemical composition of raw quartz sands. Therefore, for "Slatina" quartz sand valorization, classifying and attritional scrubbing were sufficient to apply, for obtaining high quality final product with 99.5% of SiO<sub>2</sub>, and only 0.189% of Al<sub>2</sub>O<sub>3</sub> and 0.031% of Fe<sub>2</sub>O<sub>3</sub>. Quartz sand "Cucuge", besides classifying and attritional scrubbing, required additionally magnetic concentration, in order to increase the concentrate quality to the satisfactory level. In this concentrate the content of SiO<sub>2</sub> was 99.49%, Al<sub>2</sub>O<sub>3</sub> 0.227% and 0.034% of Fe<sub>2</sub>O<sub>3</sub>. However, in order to obtain high quality concentrate from quartz sand "Avala", it was necessary to apply flotation concentration subsequent to classifying, attrition scrubbing and high intensity magnetic concentration. With flotation concentration the feldspar was successfully removed, using collector Aero 3030C, and the final quartz sand concen-

träte had 99.28% of  $\text{SiO}_2$ , 0.26% of  $\text{Al}_2\text{O}_3$  and 0.03% of  $\text{Fe}_2\text{O}_3$

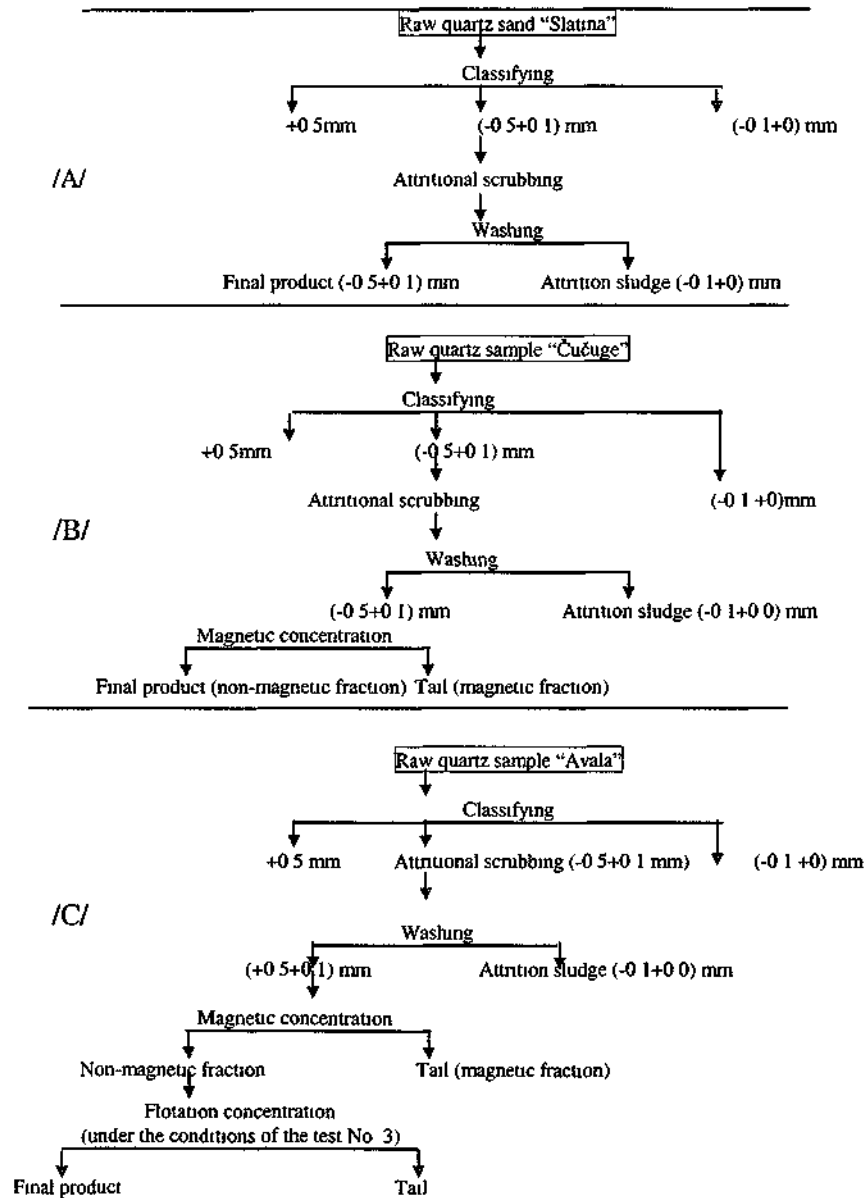


Figure 2 Proposed technological flow sheet for valorization of raw quartz sands from. A/ Slatina deposit, B/ Čučuge deposit and C/ Avala deposit

Chemical composition of quartz sand concentrates, obtained with different technological procedures

Applied technological procedure	Content, %					
	SiO <sub>2</sub>	Al <sub>2</sub> O <sub>3</sub>	Fe <sub>2</sub> O <sub>3</sub>	K <sub>2</sub> O	Na <sub>2</sub> O	Loi
Raw quartz sand from Slatina deposit						
Wet sieving	99.20	0.34	0.054	0.113	0.011	0.22
Attritional scrubbing	99.50	0.189	0.031	0.034	0.005	0.18
Raw quartz sand from Cucuge deposit						
Wet sieving	99.33	0.265	0.049	0.041	0.008	0.25
Attritional scrubbing	99.35	0.265	0.046	0.039	0.008	0.19
Magnetic concentration	99.49	0.227	0.034	0.038	0.005	0.10
Raw quartz sand from Cucuge deposit						
Wet sieving	97.03	1.43	0.08	0.83	0.06	0.23
Attritional scrubbing	97.26	1.35	0.08	0.75	0.05	0.20
Magnetic concentration	96.54	-	0.049	-	-	-
Flotation concentration, Test 1	99.03	0.34	0.05	0.06	0.011	0.17
Flotation concentration, Test 2	98.91	0.45	0.06	0.11	0.016	0.17
Flotation concentration, Test 3	99.28	0.26	0.03	0.05	0.005	0.16

Table 8 Comparative review of achieved quartz sand concentrates as well as the required quality of quartz sand for glass industry

Particle size, mm	Required quality	Achieved quality		
		Cucuge	Slatina	Avala
>0,500	max 0.05 %	0.02 %	0.2 %	0.1 %
<0,100	max 1 %	0.2 %	0.2 %	0.2 %
Chemical composition, %				
Al <sub>2</sub> O <sub>3</sub>	max 0.5 %	0.22 %	0.19 %	0.25 %
Fe <sub>2</sub> O <sub>3</sub>	0.035 % (+/- 0.005)	0.034 %	0.026 %	0.03 %
TiO <sub>2</sub>	max 0.08 %	0.033 %	0.03 %	0.03 %
K <sub>2</sub> O	max 0.25 %	0.032 %	0.034 %	0.03 %
Na <sub>2</sub> O	max 0.006 %	0.005 %	0.005 %	0.005 %
CaO	max 0.05 %	0.005 %	0.005 %	0.04 %
MgO	max 0.05 %	0.010 %	0.012 %	0.008 %
IL	max 0.30 %	0.10 %	0.11 %	0.16 %

Comparing the quality of quartz sand concentrates obtained in these investigations by treatment of raw quartz sand from three deposits, with the quality of concentrate required for application in glass industry, it can be concluded that produced concentrates fully satisfy the criteria regarding to granulometric composition as well as to chemical composition.

#### 4. CONCLUSION

Investigations were carried out on raw quartz sand samples from three different deposits ("Slatina", "Cucuge" and "Avala"), with the aim to determine the optimal valorization procedure for production of high quality quartz sand for application in glass industry. From obtained results following can be concluded:

- The main impurities in raw quartz sand "Slatina" are clay minerals while Fe<sub>2</sub>O<sub>3</sub> is pre-

sent in the form of limonite, which enables their separation and removal by classifying and attritional scrubbing. The quality of produced concentrate is satisfactory for application in glass industry.

According to mineralogical and chemical composition, quartz sand "Cucuge" is very similar to one from "Slatina" deposit but the main and most important difference is the form of the iron minerals. Free goethite grains, present in this quartz sand, may be removed only with magnetic concentration.

Quartz sand "Avala" differs from previous two quartz sands in mineralogical and chemical composition: the content of SiO<sub>2</sub> is much lower and the content of potassium feldspar is higher. Therefore, it is necessary to apply the flotation concentration subsequent to classifying, attrition

*Ā. Sekuĥc N Came Z. Bartulovic & M Iġnjatovic*

scrubbing and magnetic concentration in order to obtain the concentrate of satisfactory quality

- Based on the obtained results, a complete technological process is proposed, for quartz sand from each deposit, which will provide the final quartz sand concentrate with the required quality for the glass industry

Acknowledgments

This work is conducted under the Project "Development and application of novel technologies of preparation of raw non-metal materials and revitalization of active industries" financed by Ministry of Science, Technology and Development of Republic of Serbia (2002-2004)

REFERENCES

- IX J Group of authors, (1998) *Domestic non-metallic mineral raw materials for industrial application*, Belgrade, Serbia and Montenegro, (ITNMS), - ISBN 86-82867 09-5
- [2] *Technical quality conditions of the glass factory «OwShaze» form 2004*, Hungary
- [3] Sekuĥc Z, Bartulovic Z, Came N, (2002) Laboratory investigations of efficiency of magnetic concentration of quartz sand for application in glass industry, *Proceedings of 18<sup>th</sup> Yugoslav Symposium of Mineral Processing*, Banja Vruĥci, pp181-185
- [4] Sekuĥc Z, Came N, Bartulovic Z, Mihajlovic S, Dakovic A Valorization of quartz sand from »Avala« - Ub deposit with different mineral processing and concentration procedures. *Proceedings of X Balkan Mineral Processing Congress*, pp 627-633, Varna
- [5] Hanumantha Rao, K & Forsberg, KSE(1993) Solution chemistry of mixed Cationic/Anionic collectors and flotation separation of feldspar from quartz - *XVIII International Mineral Processing Congress*, pp 837-844, Sydney, Australia
- [6] Shehu N, & Spaziam, E (1999) Separation of feldspar from quartz using edta as modifier - *Minerals Engineering*, Vol 12, No 11, pp 1393-1397

## Obtaining Metallurgical Data from Drill Core Samples Using a Mini Pilot Plant

V L L Andrade, N A Santos, K L C Gonçalves,  
*Companhia Vale Do Rio Dote Mineral Development Center BR262 km 296 Santa Luzia MG, Brasil*

H Wyslouzū, G Dāvila,  
*Canadian Process Technologies Ine Unit 1 7168 Honeyman Street Delta British Columbia Canada V4G 1G1*

**ABSTRACT** :When confronted with the difficult decisions on advancing an exploration project to the feasibility and construction stages, it is important to know how various regions of the ore body will react in the milling and concentration processes. While bench scale test work is common and inexpensive, the results and information provided are somewhat limited due to the difficulty in accurately predicting the effects of recirculating middling streams or gradual changes in solution chemistry.

Conventional Pilot Plants, processing 100 to 1,000 kg/hour of sample ore, provide the detailed engineering data required to develop a final process flowsheet and to size the equipment. They are, however, expensive to set up and operate, and are really only viable for major projects that are well advanced.

In the latter part of 1999, the Mineral Development Center at CVRD (MDC) purchased a new piece of mineral processing equipment which can run continuous flotation tests using drill core samples. To evaluate its performance, and to compare it with conventional testing methods, various types of flotation tests were carried out using two different types of copper ore. The limitations and advantages of open circuit and locked cycle bench tests, as well as the Mini Pilot Plant and the Conventional Pilot Plant were evaluated.

Open circuit tests carried out at the bench scale only provide basic information. More complete and trustworthy information is obtained, in terms of the recirculation of flows and reaching a permanent and stable flotation regime as the dynamics and complexity of the tests increases. The data obtained showed that the MPP's metallurgical performance was equivalent to that of a conventional pilot plant.

### 1. INTRODUCTION

The future of the mining industry lies in its ability to find and develop new mineral deposits. According to figures published by the Mining Association of Canada, more than \$US2.34 Billion was budgeted for exploration in 2000 by some 656 mining companies operating worldwide. In Canada alone, over \$500 million was spent on exploration and deposit appraisal during this period.

The proper evaluation of a new mineral deposit is a complex and involved process requiring input from many disciplines including exploration geologists, mining engineers, mineral processors, economists and marketing specialists. The mineral processing engineer is a key member of the team, for it is he who has the task of finding a treatment process that is both economical and robust enough to handle the expected variations in ore types. Capital and operating costs are very sensitive to the process

selected. Over the years, many projects have failed due to high operating costs resulting from unexpected metallurgical responses to mill feed ore blends. A better understanding of the nature and variability of the deposit means a lower risk for the investor.

When confronted with the difficult decisions on advancing an exploration project to the feasibility and construction stages it has always been the dream of process engineers to know, with greater certainty, how various regions of the ore body will react in the milling and concentration processes. While bench scale test work is common and inexpensive, the results and information provided are somewhat limited due to the difficulty in accurately predicting the effects of recirculating middling streams or gradual changes in solution chemistry.

Conventional Pilot Plants, processing 100 to 1,000 kg/hour of sample ore, are used to provide the

detailed engineering data required to develop a final process flowsheet and to size equipment. They are, however, expensive to set-up and operate, and are really only viable for major projects that are well advanced. Typical sample and manpower requirements for different testing options are compared in Table 1.

**Table 1 Comparison of Testing Methods**

	<b>Bench</b>	<b>Mini Pilot Plant</b>	<b>Conventional Pilot</b>
Amount of ore	1-4 kg per test	5-15 kg/h	100 - 1000 kg/h
Origin of the ore	Drill core	Drill core	Underground gallery
Cost of the ore	Included in exploration costs	Included in exploration costs	- \$US 500,000 - 2 million
Cost of operation and analyses	- \$US 150 00 per test	- \$US 6,500 per 20 hr test	- \$US 10 - 20,000 per 20 hr test
Personnel	1 technician and 1 assistant	1 technicians and 1 to 2 assistants per shift	1 to 2 technicians and 4 assistants per shift
Attained Information	<ul style="list-style-type: none"> <li>• Ore characteristics</li> <li>• Stages and kinetics of flotation, reagents, reagent dosages</li> </ul>	<ul style="list-style-type: none"> <li>• Mass balances</li> <li>• Metallurgical &amp; water balances</li> <li>• Detailed engineering information</li> </ul>	<ul style="list-style-type: none"> <li>• Mass balances</li> <li>• Metallurgical &amp; water balances</li> <li>• Detailed engineering information</li> </ul>
Limitations	Does not allow evaluation of continuous	Produces small quantities of concentrates flows	Expensive, demands much ore generates great mass of tailings
Advantages	Simple and inexpensive	<ul style="list-style-type: none"> <li>° Allows evaluation of continuous streams with a small amount of ore</li> <li>° Is operationally inexpensive and allows ore evaluation from different regions of the deposit</li> <li>» Is much more environmentally friendly</li> </ul>	<ul style="list-style-type: none"> <li>° Provides reliable data for industrial scale-up</li> <li>° Can generate large concentrate samples for smelter tests</li> </ul>

The process development for new projects involving flotation normally consists of bench scale studies followed by pilot plant testing and subsequent scale up to the industrial plant. The bench scale studies permit determination of basic parameters for the process. These parameters include such items as mineralogical and liberation characteristics, a preliminary treatment flowsheets, flotation kinetics, reagent types and dosages, etc. The studies are also used to estimate the variability of the ore body by testing samples of different lithologies obtained from different zones within the deposit. The preliminary flotation tests are usually done using drill core samples obtained from the exploration program as these tests require small amounts of sample, usually from 1 to 4 kg of ore. Operationally, they are simple and inexpensive tests, and they are usually carried out in open circuit.

To obtain a preliminary estimation of recirculating loads, it is possible to conduct locked cycle tests which are of greater complexity but provide more detailed information. Locked cycle tests can produce good results for simple ores. Knowing when steady state has been reached,

however, and being able to interpret the results correctly, is not always an easy task (Ounpuu, 2000). In general, the principle limitation of bench scale testing is its inability to replicate the mixing regimes and process conditions of a continuous closed circuit operation.

To evaluate the process on a continuous basis, pilot scale tests are performed which allow mass, metallurgical and water balances to be obtained along with more detailed information for the project engineering studies. These tests are expensive and demand considerable operational effort. Continuous pilot plants also consume great quantities of ore, ranging between 100 and 1,000 kg/h per test. As these tests are conducted during the feasibility phase of the project, it is often necessary to develop an underground adit exclusively for obtaining the bulk ore samples, making the investment in terms of cash outlay and project schedule even greater.

In 1999, the Mineral Development Center at CVRD purchased new laboratory equipment referred to as the Mini Pilot Plant (MPP), designed and fabricated by Canadian Process Technologies (CPT). This equipment, originally developed at Comco's

research center at Trail, is designed to allow flotation testing with continuous flows, similar to a traditional pilot plant, but operating with a minimum amount of ore and personnel. A major part of Cominco's original justification was to reduce the need to conduct locked cycle tests. The Mini Pilot Plant developed by CPT was specifically designed to make use of the samples obtained from exploration drilling campaigns. The MPP is the first equipment of its type to be used in Brazil and has proven very useful in the evaluation of flotation processes.

This paper presents comparative tests results for three types of flotation studies: bench scale tests, locked cycle tests and continuous flow tests making use of the MPP as well as a larger conventional pilot plant. Two copper ores of varying complexity were used for this comparative test work.

## 2. DEVELOPMENT OF MINI PILOT PLANT (MPP)

As outlined earlier, the benefits of conducting continuous closed circuit tests using small sample quantities are numerous. There are certain challenges, however, when working with very low flow rates. The basic philosophy and design criteria for the equipment can be summarized as follows:

- The scale of the equipment should be convenient to handle feed rates ranging from 5 to 15 kg/h.
- Grinding should be done in batches of 30 to 50 kg as continuous grinding / classification at this scale would be too difficult to control.
- The circuit should be arranged to permit

maximum flexibility for circuit configuration.

- The flotation cells should be modeled after standard laboratory flotation cells and use the same impeller and tank design to eliminate cell design as a variable.
- The unit should use a high level of instrumentation to permit replication of conditions from test to test. Instrumentation should include digital air flow measurement, pH / eH measurement, precision reagent addition, variable speed froth paddles, impeller speed measurement and variable speed slurry transfer pumps.
- It should include ancillary equipment such as a continuous regrind mill and a miniature flotation column to permit testing of common industrial circuits.

The MPP comprises 12 flotation cells, each of 1.7 L capacity. The cells were modeled after the Denver D12 laboratory flotation machine and use the same impeller and stator design. The shape of the tank is also the same as the Denver cell but includes an adjustable level control system. Concentrates and tailings are transferred from cell to cell with small peristaltic pumps. A wide variety of flotation circuits can be reproduced in the MPP, including the most common combinations of rougher, scavenger and cleaning stages. The equipment acquired by CVRD includes a pin mill for the continuous regrinding of intermediate concentrates.

The following photographs show some of the individual components and the final assembly.

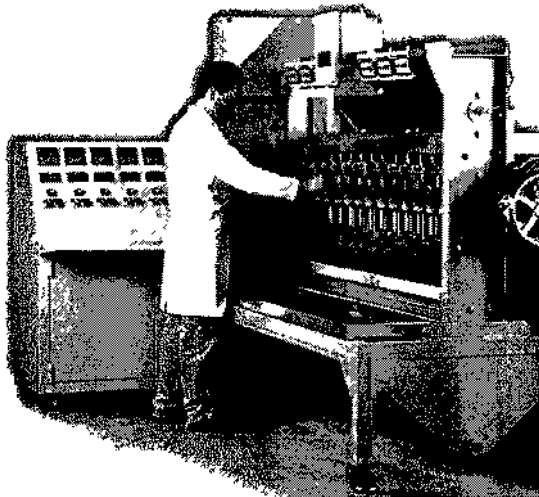


Figure 1 : Overview of Flotation Module and Control Panel

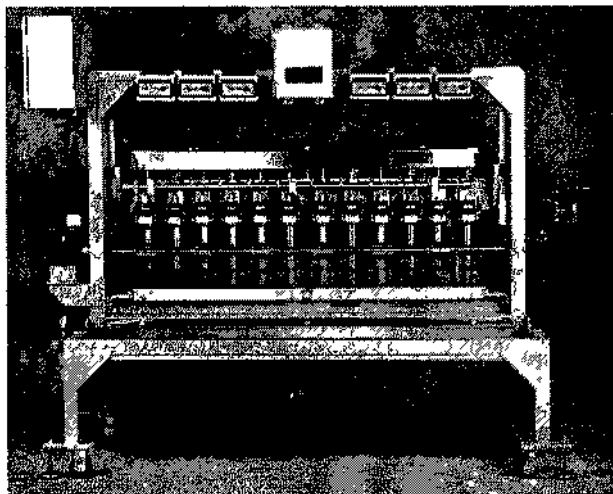


Figure 2 Front View Showing Pump Controllers and Air Flowmeters

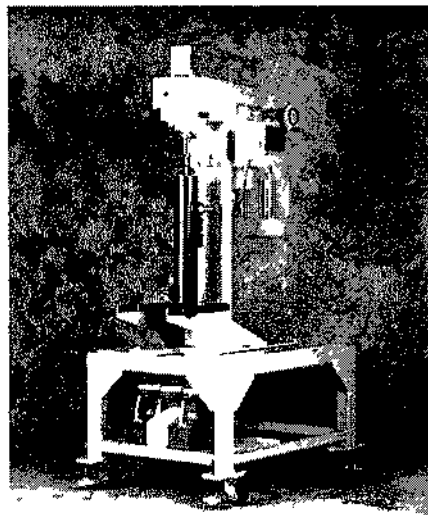
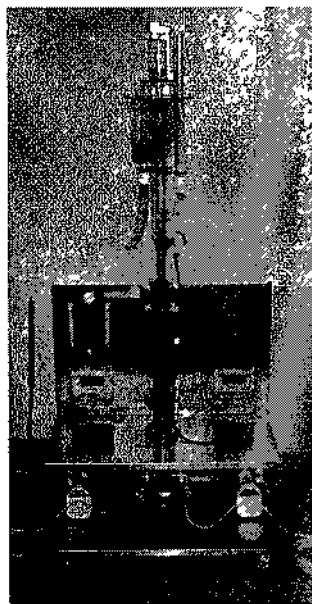


Figure 3 Column Cell Module and Regnnd Module

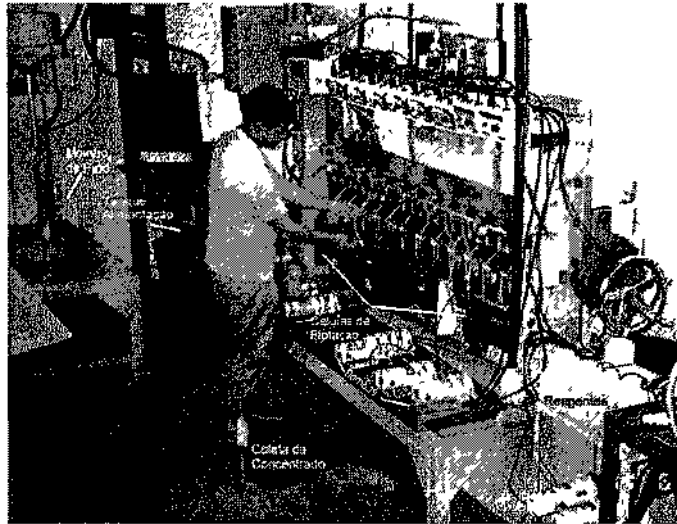


Figure 4 Mini Pilot Plant in Operation

### 3. TEST PROGRAM

#### Test Samples

Two different copper ores originating from the northern region of Brazil were selected for testing and evaluation. These samples were designated as Ore A and Ore B. Ore A is a mixture of bornite and chalcocite, with a very fine grain structure ( $P_{80} = 16 \mu\text{m}$ ). Ore B is primarily chalcopyrite and has a coarser grain size ( $P_{80} = 44 \mu\text{m}$ ).

#### Process Description

The ores were subjected to the following treatment stages:

- Grinding
- Rougher and Scavenger flotation
- Regrinding of the combined Rougher and Scavenger concentrates
- Cleaning of the «ground product (cleaner 1)
- Scavenging of the cleaner 1 tailings
- Recleaning of the concentrate (cleaner 2)

Figure 5 shows the basic flowsheet used in the tests.

For Ore A, two different flowsheets were tested to enable production of both a low grade concentrate

(25% Cu) and a high grade concentrate (38% Cu). The flowsheet shown in Figure 5 was used to produce the low grade concentrate. Two additional cleaning stages were added in order to produce the high grade concentrate. This test (high grade) was compared with a previous conventional pilot plant test campaign.

#### Bench Scale Tests

Bench scale flotation testing was performed in a Denver D12 laboratory cell with self aeration and rotational speeds of 900 and 1500 rpm depending on the flotation stage. The grinding was carried out in a ceramic mill using steel rods and the regrinding was carried out using a ceramic mill and steel grinding balls.

In order to determine the conditions to be used in the locked cycle tests and in the continuous flow test, bench scale testing was carried out only up to the first cleaner with a timed collection of products during the stage.

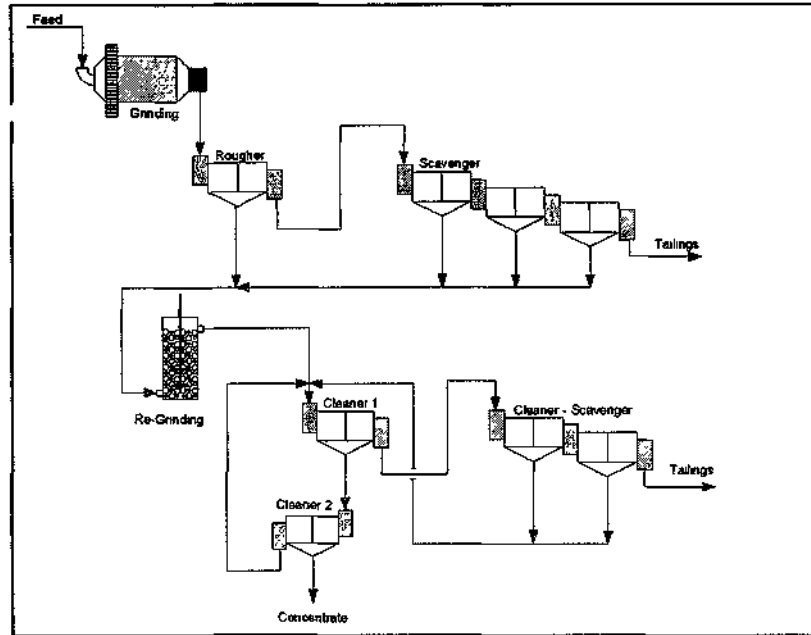


Figure 5: Simplified flowsheet for processing of Ores A and B

#### Locked Cycle Test (LCT)

In a continuous process, the concentrate of the cleaner scavenger and the tailings of second cleaner are recirculated to the feed of the first cleaner. In order to simulate this process as a series of bench scale tests, the tests are carried out in a closed circuit or "locked cycle" (LCT) test. An LCT comprises a sequence of flotation tests in which the intermediate products of a test cycle are added to the appropriate stage of the subsequent cycle. Therefore, the recirculation of the cleaner scavenger concentrate to the first cleaner is carried out by the addition of the cleaner scavenger concentrate from test (n-1) to the feed of the cleaner test (n). The test series is terminated when the circuit is stabilized, as verified by the mass and grade of the final products, which must remain constant between successive cycles, and the balance must match the initial sample data.

#### Mini Pilot Plant (MPP)

The initial grinding was carried out separately in 20 kg batches using a rod mill. The ground product was transferred to an agitated holding tank and then to the MPP feed tank. Feed slurry was pumped to the Mini Pilot Plant using a peristaltic pump.

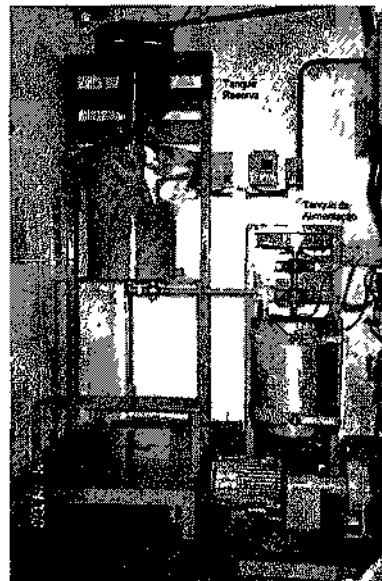


Figure 6: MPP feed system showing holding tank (L) and feed tank (R)

Tests were performed at a continuous feed rate of 5 kg/h using the circuit configuration shown in Figure 7

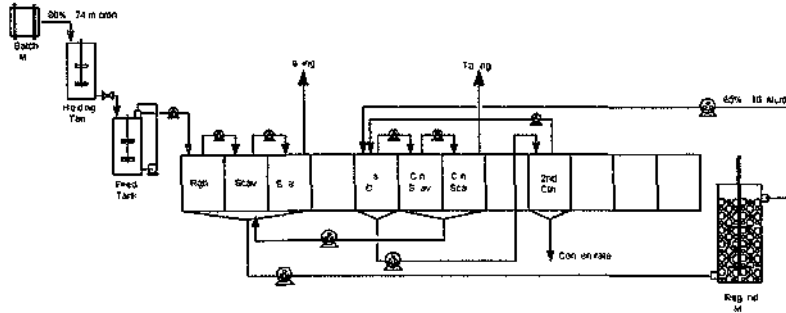


Figure 7 MPP Circuit Configuration

**Conventional Pilot Plant**

The grinding and flotation pilot plant circuits available at the CDM have a maximum capacity of 500 kg/h. The grinding section includes a variable speed transfer system and a primary ball mill operating in closed circuit with a spiral classifier. The flotation section is very flexible in terms of quantity of mechanical cells. Cells of 25, 50, 60, 150 and 500 liters are available.

Ore type B was extensively tested in the pilot plant in the past. The results obtained by the MPP were compared to the results obtained from the

conventional pilot plant

**4. RESULTS**

**Preliminary Tests**

It was necessary to conduct a series of preliminary tests to establish basic operating conditions and characteristics for the MPP. Specific tests were performed to evaluate the performance of the Rougher and Scavenger stages. Figure 8 shows a photograph of these stages.

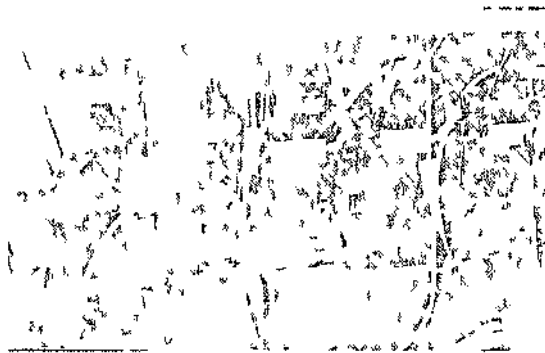


Figure 8 Rougher (1 to the left) and Scavenger Cells (2 and 3 to the right)

To evaluate these stages, a series of bench scale and Mini Pilot Plant tests was performed. The bench scale tests were done in a 2,500 mL Denver D12 flotation machine operating at 1,200 rpm. The products were collected in stages and timed accordingly. In the Mini pilot Plant, 3 flotation cells were used, the first operating as a rougher and the

other two operating as scavengers. Flotation conditions such as the percent solids and reagent addition rates were kept the same for both tests. Figure 9 shows the results of copper grade and recovery achieved in the bench scale test as well as from the Mini Pilot Plant.

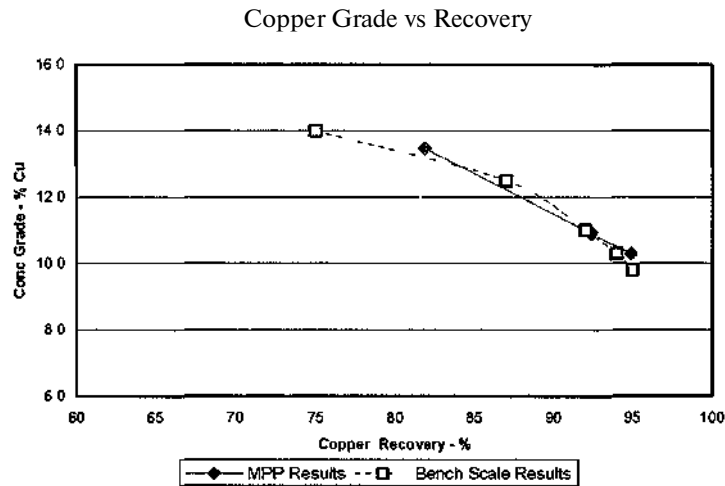


Figure 9 Copper Grade/Recovery Curves for the Bench and Mini Pilot Plant Tests

The results obtained from both tests were very similar, demonstrating that the values obtained from the standard bench scale test can be reproduced in the Mini Pilot Plant. Figure 10 shows the mass, water and copper balances obtained from the Mini Pilot Plant test.

This general balance was generated using software called Bilmat, and it shows that the calculated values have a very small deviation relative to the measured data. Most of the tailings values deviated by less than 3% with a maximum deviation of 7.5%, indicating that the process had stabilized prior to sampling.

Figure 11 shows some modifications which were done to the MPP to make operation easier. The

white circles indicate the feeding system into each cell. The hose on the left cell is supported only by a tube which feeds the material to the bottom of the cell. It was observed that the concentrate would flow on top of this tube thus displacing and losing some of the material. In order to solve this problem, a small funnel was fabricated and installed for the proper feed of this flow (as shown to the right of the picture). Any froth formed at the funnel would now flow into the interior of the flotation cell.

A flotation cell of smaller volume was also fabricated in order to guarantee the proper process for very small flow rates.

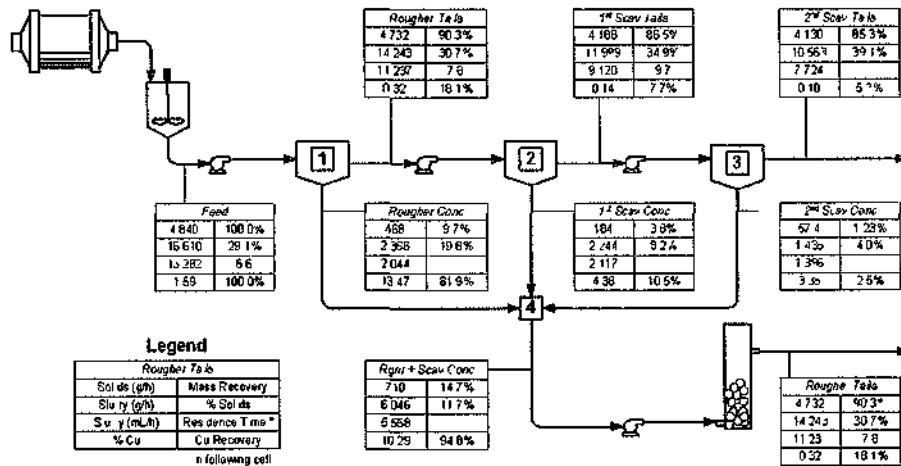


Figure 10 Simplified Flow Sheet Rougher and Scavenger Mass Balances



Figure 11 Cell Constructed at CMD and Cell Feeding SysLm (white circles)

The addition of water into the launders (fine white hoses in the picture) was customized. Recently, a froth crowder, circular in shape, was added to reduce cell surface area. This device is used in the

inside of the I mal cleaner cells

Comparative data for tests on Ore A are shown in Tables 2, 3 & 4 and for Ore B in Tables 5 & 6

Table 2 Comparative Data for Ore A

Flows	Mini Pilot Plant			Locked Cycle Test			Open Circuit Test		
	Wt. %	%Cu	Cu Rec.	Wt.%	%Cu	Cu Rec.	Wt. %	%Cu	Cu Rec.
Feed	100 0	141	1000	1000	142	100	100 0	132	1000
Rghr Cone	52	18 68	68 7						
Scav Cone	14 9	2 45	25 8						
Combined Cone	20 0	6 65	94 5	220	6 00	94 8	23 0	5 27	93 6
Scav Tails	80 0	0 10	57	78 0	0 09	49	77 0	0 11	64
1 ClnrFeed	30 3	6 83	146 6	410	5 00	142 8			
1 ClnrConc	77	20 09	110 2	17 0	10 40	1240	5.0	23.30	79.5
1 ClnrTail	22 5	2 28	36 4	240	1 11	18 4	190	0 92	13 2
Clnr Scav Cone	79	5 80	324	70	2 78	13 7	40	296	93
Clnr Scav Tail	147	0 39	41	170	042	49	15 0	0 35	39
2 Clnr Cone	5.4	23.74	90.5	6.0	22.00	90.1			
2 <sup>nd</sup> ClnrTail	24	1178	19 7	110	4 38	34 3			
Final Tail	94 6	0 14	97	94 0	0 15	99	910	0 15	10 4

Table 3 Comparative Stage Testing for Ore A

Stage	Copper Recovery - %			Enrichment Ratio		
	Open Circuit	Locked Cycle	MPP	Open Circuit	Locked Cycle	MPP
Rougher + Scavenger	93 6	94 8	94 5	40	42	47
1 <sup>st</sup> Cleaner	85 0	86 9	75 2	44	21	29
Cleaner Scavenger	70 2	74 1	88 9	32	25	25
2 Cleaner		72 7	82 1		21	12
Total Cleaner Circuit		95 1	95 8		37	36
Overall Circuit	79 5	90 1	90 5	17 7	15 5	16 8

1 Recirculating Load | 18.1 | 10.2

Table 4 Comparative Data from the MPP and the Conventional Pilot Plant for Ore A

	%Cu	Recovery (%)
Mini Pilot Plant	36 0	86 0
Full Pilot Plant	37 0	87 0

Table 5 Comparative Data for Ore B

Flows	Mini Pilot Plant			Locked Cycle Test			Open Circuit Test		
	Wt.%	%Cu	Cu Rec.	Wt.%	%Cu	Cu Rec.	Wt.%	%Cu	Cu Rec.
Feed	100 0	120	100 0	100 0	127	100 0	100 0	131	1000
Combined Cone	69	17 20	96 2	71	17 23	96 3	74	17 23	97 2
Scav Tails	93 1	0 10	38	92 9	0 05	37	92 6	0 04	28
1 ClnrFeed	94	1560	119 4	95	13 94	104 2	74	17 23	97 2
1 ClnrConc	51	26 40	109 6	46	27 37	99 4	4.0	30.59	92.9
1 ClnrTail	43	2 80	98	49	125	48	34	165	43
Clnr Scav Cone	13	8 60	92	17	2 99	41	07	6 86	39
Clnr Scav Tail	30	0 20	05	31	0 29	07	27	0 20	04
2 Clnr Cone	3.9	30.00	95.7	4.0	30.70	95.6			
2 <sup>nd</sup> ClnrTail	12	14 40	14 0	07	7 29	38			
Combined Tailings	96 1	0 05	43	96 0	0 06	44			

Table 6: Comparative Stage Testing for Ore B

Stage	Copper Recovery - %			Enrichment Ratio		
	Open Circuit	Locked Cycle	MPP	Open Circuit	Locked Cycle	MPP
Rougher + Scavenger	97.2	96.3	96.2	13.1	13.6	<b>14.0</b>
1 Cleaner	95.6	95.4	91.8	<b>1.8</b>	<b>2.0</b>	<b>1.7</b>
Cleaner Scavenger	4.6	85.0	94.5	4.2	<b>2.4</b>	<b>3.1</b>
2 Cleaner		96.2	87.2		<b>1.1</b>	<b>1.1</b>
Total Cleaner Circuit	95.6	99.3	99.4	<b>1.8</b>	<b>1.8</b>	<b>1.8</b>
Overall Circuit	92.9	95.6	95.7	23.3	24.2	24.5
Recirculating Load		2.4	2.5			

## 5. DISCUSSION OF RESULTS

Execution of the test work using different test methods permitted an evaluation of the type of data that can be obtained and reveals some of the limitations for each of the flotation processes tested.

### Open Test

The open circuit test allows basic process parameters to be obtained. These parameters include development of a preliminary flowsheet, kinetics of flotation, reagent types and dosages and grinding requirements. It is an easy test to perform and requires very little ore (1 to 4 kg). The time and effort required to conduct a test is also small. This test provides good information with regard to the grade of the final products and the recovery in the rougher stage. For example, for Ore A, copper recovery in the open test rougher stage was 93.6% and in the Mini Pilot Plant it was 94.5%.

However, since it is a test without the intermediate recirculating flows, an open test does not allow an acceptable prediction of the total circuit recovery. This would be the case for an ore with difficult liberation characteristics and high recirculating loads such as Ore A. The cleaner stage recovery for this ore, in open test, was 79.5%, while in the Mini Pilot Plant test it was 90.5%. For an ore like Ore B, which is easily liberated and has good flotation characteristics with small circulating loads, total recoveries achieved in open tests are similar to produced in a continuous test. In this case, the cleaner recovery in the open test was 96.3% while in the MPP, it was 99.4%.

Beyond this, the quality of the final concentrate does not reflect the possible contamination by impurities carried by the recirculating streams.

### Locked Cycle Test (LCT)

The LCT provides a good estimation of overall recovery for the rougher and cleaner circuits and

does take into account the effects of the recirculating streams. For Ore A, the global cleaner recovery was 95.1%, while in the MPP a recovery of 95.8% was achieved. For Ore B, the final circuit recovery obtained by the LCT was 95.6% and for the MPP it was 95.7%. The LCT can also offer a very good estimation of the circulation loads, depending upon the ore being tested. For Ore B, the values obtained by the LCT and MPP were 2.4% and 2.5%, respectively. On the other hand, for Ore A, a circulating load of 18% was obtained in the LCT compared to only 10% in the MPP.

The LCT is a more complex type of test, requiring a greater operational effort in relation to the open test and is similar to the effort required to run the MPP. The weight of sample required varies between 20 and 30 kg, which is also much greater than the weight required for the open test. A limitation of the LCT is its lack of operational flexibility, since the testing conditions of each cycle are pre-established and cannot be modified during the test procedure.

Since the LCT is operator dependent, the metallurgical difference between cycles, even though they are in equilibrium, may call results into question. Since the LCT must be carried out without interruption, the maximum number of cycles is normally between 10 and 15. When the ore is difficult and has a high recirculating load, this number of cycles may be insufficient to reach equilibrium.

### Mini Pilot Plant and Conventional Pilot Plant

The principle merit of these two types of tests is their ability to test the process on a continuous basis. This is of major importance to the investor. The test in the MPP allows great operational flexibility and therefore permits optimization of operating conditions during its execution. With this method, it is possible to obtain trustworthy engineering data such as grades and recoveries of the various stages,

as well as an evaluation of the influence of the recirculating load on the metallurgical performance

The MPP predicts, with sufficient confidence, the results obtained from a conventional Pilot Plant. For Ore A the recoveries and final grades obtained in the MPP were 86% and 36% respectively, which were very close to those obtained in the conventional Pilot Plant, at 87% and 37% respectively. The advantage of the MPP is even greater when one compares the ore requirements necessary to carry out both tests. The MPP requires about 200 kg of ore, while the conventional pilot plant requires at least 10 tonnes of ore.

With the MPP, the low sample requirement allows operation using drill core samples, which in turn allows a continuous circuit evaluation of the variability of the deposit without the need to develop underground adits. This is a major cost benefit, particularly for projects with uncertain economics.

While the MPP is able to reproduce flotation results obtained in a conventional pilot plant, there are many other reasons for running the larger conventional pilot plants. A conventional pilot plant allows generation of large quantities of products which can be given to potential clients for evaluation, for conducting grinding and filtration tests and so forth.

## 6. CONCLUSIONS

The information obtained from the different flotation tests, performed at the different scales and flow conditions, are complementary. As soon as the basic information is obtained in the bench scale tests, more complete and trustworthy information can be

obtained as the complexity and dynamics of the tests increases. In terms of evaluating flow recirculation and for obtaining a stable closed circuit operational regime, the LCT and MPP somewhat compete with each other, since the required effort to perform both types of test is very similar. The MPP, with its higher level of instrumentation, is easier to control and is less operator dependent. MPP testing requires a greater amount of ore than the LCT, which may be a determining factor in defining the type of test to be carried out with certain ore types at the initial phase of the project. However as the project develops and more detailed information is required for engineering studies, it will be necessary to carry out a series of tests in the MPP.

The data obtained demonstrates that the metallurgical performance of the MPP is equivalent to that of a conventional Pilot Plant. Since the MPP requires fewer personnel and significantly less ore, it can be concluded that the MPP is the equipment best suited to obtaining the data required for the engineering studies necessary to justify financial resources for the implementation of a new project.

## REFERENCES

- MULAR, Andrew L and BHAPPU, Roshan B, Mineral Processing Plant Design Symposium SME, New York, 1980
- WEISS, N.L. SME Mineral Processing Handbook, New York 1985
- FUERSTENAU, MC Flotation - Gaudin Memorial Flotation Symposium, New York, 1976
- OUNPUU, M Proceedings - 33<sup>rd</sup> Annual Meeting of Canadian Mineral Processors, Ottawa, 2001

## Breakage Properties of Porous Materials by Ball Milling

V. Deniz

*Department of Mining Engineering, Süleyman Demirel University, İsparta, Turkey*

**ABSTRACT:** This paper presents the breakage properties of five different porous materials based on a kinetic model, which was commonly used in the cement industry. For this purpose, firstly, standard Bond's grindability tests were made for five porous samples. Secondly, eight different mono-size fractions were ground between 1.7 mm and 0.106 mm formed by a V2 sieve series. Then,  $S$ , and  $B_j$  equations were determined from the size distributions at different grinding times, and the model parameters ( $S$ ,  $a$ ,  $a_y$  and  $\$$ ) were examined. Finally, relationship between the Bond's grindability and breakage parameters were compared for five different porous samples.

The validity of the relationships between Bond's grindability with breakage parameters ( $S$ ,  $a$ ,  $\$$  and  $y$ ) has been not confirmed with good correlation coefficients, through a regression analysis of samples. The reason of this negative result is the geological origin of porous materials which is not similar.

### 1 INTRODUCTION

Comminution is known to be a large consumer of the energy, which consumes 3-4% of the electricity generated world-wide and comprises up to 70% of all energy required in a typical mineral processing plant, and is one of the most important unit operations in mineral processing. The grinding process has many variables, some of which are difficult to understand.

Bond's grindability can be empirically related to the energy required for comminution and thus is useful for the design and selection of crushing and grinding equipment (Deniz et al., 1996).

In the recent years, matrix model and kinetic model, which are suggested by investigators, have been used in the laboratory and in the industrial areas. Kinetic model which is an alternative approach is considered comminution as a continuous process in which the rate of breakage of particles size is proportional to the mass present in that size (Deniz and Onur, 2002).

The analysis of size reduction in tumbling ball mills using the concepts of specific rate of breakage and primary daughter fragment distributions have received considerable attention in years. Austin has reviewed the advantages of this approach and the scale-up of laboratory data to full-scale mills have

also been discussed in a number of papers summarized by Austin et al. (1984).

The behaviour of porous materials in comminution processes differs substantially from that of non-porous materials. It is strongly affected by the type of porosity, which may be characterized by different void shapes and interconnection degrees.

This paper presents a comparison of the breakage parameters of five different porous materials under standard conditions in a batch laboratory ball mill, and relationships between Bond's grindability values with breakage parameter values of samples are investigated.

### 2 THEORY

When breakage is occurring in an efficient manner, the breakage of a given size fraction of material usually follows a first-order law (Austin, 1972). Thus, the breakage rate of material that is in the top size interval can be expressed as:

$$-\frac{dw_i}{dt} = S_i w_i(t) \quad (1)$$

Assuming that  $S_i$  does not change with time (that is, a first-order breakage process), this equation integrates to

$$\log(w_i(t)) - \log(w_i(0)) = \frac{-S_i t}{2.3} \quad (2)$$

where,  $w_i(t)$  is the weight fraction of the mill hold-up that is of size  $i$  at time  $t$  and  $S_i$  is the specific rate of breakage. The formula proposed by Austin et al (1984) for the variation of the specific rate of breakage  $S_i$  with particle size is

$$S_i = a_i X_i^\alpha \quad (3)$$

where,  $X_i$  is the upper limits of the size interval indexed by  $i$ , mm, and  $a_i$  and  $\alpha$  are model parameters that depend on the properties of the material and the grinding conditions

On breakage, particles of given size produce a set of primary daughter fragments, which are mixed into the bulk of the powder and then, in turn, have a probability of being re-fractured. The set of primary daughter fragments from breakage of size  $j$  can be represented by  $b_{i,j}$ , where  $b_{i,j}$  is the fraction of size  $i$  material, which appears in size  $j$  on primary fracture,  $n \geq i > j$ . It is convenient to represent these values in cumulative form

$$B_{i,j} = \sum_{k=i}^j b_{k,j} \quad (4)$$

where,  $B_{i,j}$  is the sum fraction of material less than the upper size of size interval  $i$ ; resulting from primary breakage of size  $j$  material  $b_{i,j} = B_{i,j} - B_{i+1,j}$ . Austin et al (1981) have shown that the values of  $B_{i,j}$  can be estimated from a size analysis of the product from short time grinding of a starting mill charge predominantly in size  $j$  (the one-size fraction BII method). The equation used is,

$$B_{i,j} = \frac{\log(1 - P_i(0)) / \log(1 - P_i(t))}{\log(1 - P_{j+1}(0)) / \log(1 - P_{j+1}(t))} \quad n \geq i \geq j+1 \quad (5)$$

where,  $P_i(t)$  is the fraction by weight in the mill charge less than size  $i$  at time  $t$ .  $B_{i,j}$  can be fitted to an empirical function (Austin and Luckie, 1972)

$$B_{i,j} = \phi_j [X_{i,j} / X_j] + (1 - \phi_j) [X_{i,j} / X_j]^\beta \quad n \geq i \geq j \quad (6)$$

where

$$\phi_j = \phi_1 [X_{i,j} / X_j]^{-\delta} \quad (7)$$

where,  $\delta$ ,  $\phi_1$ ,  $\beta$ , and  $\beta$  are model parameters that depend on the properties of the material. It is found

that,  $B_{i,j}$  functions are the same for different ball filling ratios, mill diameters, etc (Austin et al, 1984). If  $B_{i,j}$  values are independent of the initial size, i.e. dimensionally normalizable, then  $S_i$  is zero

### 3. MATERIALS AND METHOD

#### 3.1 Material

Five different porous samples taken from different region of Turkey were used as the experimental materials. The chemical properties of the porous samples are presented in Table 1

Table 1 Chemical composition of porous samples using in experiments

Oxides	Pumice I	Pumice II	Trass	Amorphous Silica	Diatomite
SiO <sub>2</sub>	63.50	57.37	58.82	90.91	89.58
Al <sub>2</sub> O <sub>3</sub>	14.56	18.74	17.78	0.13	1.77
Fe <sub>2</sub> O <sub>3</sub>	2.02	5.93	3.91	0.11	0.78
CaO	3.11	2.16	4.12	0.36	0.70
MgO	3.80	2.95	0.11	...	0.22
Na <sub>2</sub> O	4.62	4.25	-	0.07	0.12
K <sub>2</sub> O	4.50	3.66	...	0.06	0.21
SO <sub>3</sub>	0.10	1.23	...	0.27	1.61
LOI	2.80	1.75	3.66	4.95	4.99

#### 3.2 The test of standard ball mill Bond grindability

The standard Bond grindability test is a closed-cycle dry grinding and screening process, which is carried out until steady state condition is obtained. This test was described as follow (Bond and Maxson, 1943, Yap et al, 1982, Austin and Brame, 1983, Magdahnovic, 1989)

The material is packed to 700 cc volume using a vibrating table. This is the volumetric weight of the material to be used for grinding tests. For the first grinding cycle, the mill is started with an arbitrarily chosen number of mill revolutions. At the end of each grinding cycle, the entire product is discharged from the mill and is screened on a test sieve ( $P_i$ ). Standard choice for  $P_i$  is 106 micron. The oversize fraction is returned to the mill for the second run together with fresh feed to make up the original weight corresponding to 700 cc. The weight of product per unit of mill revolution, called the ore grindability of the cycle, is then calculated and is used to estimate the number of revolutions required for the second run to be equivalent to a circulating load of 250%. The process is continued until a constant value of the grindability is achieved, which is the equilibrium condition. This equilibrium condition may be reached in 6 to 12 grinding cycles

After reaching equilibrium, the grindabilities for the last three cycles are averaged. The average value is taken as the standard Bond grindability.

#### 4 EXPERIMENTS

Firstly, Standard Bond's grindability tests were made for five porous samples. Result of tests, Bond grindability values of porous samples were appeared 2.96 g/rev, 2.67 g/rev, 2.45 g/rev, 1.74 g/rev and 8.12 g/rev, respectively. Then, the standard sets of

grinding conditions used are shown in Table 2, for a laboratory mill of 6283 cm<sup>3</sup> volume. Eight mono-size fractions (-1.7+1.18, -1.18+0.850, -0.850+0.600, -0.600+0.425, -0.425 +0.300, -0.300+0.212, -0.212+0.150, -0.150+0.106 mm) were prepared and ground batch wise in a laboratory-scale ball mill for determination of the specific rate of breakage. Each sample was taken out of the mill and dry sieved product size analysis.

Table 2. The standard set of grinding conditions

Mill	Diameter	200 mm				
	Length	200 mm				
	Volume	6283 cm <sup>3</sup>				
Mill Speed	Critical	101 rpm				
	Operational (<math>\epsilon = 75\%</math>)	76 rpm				
Balls	Diameter (mm)	25.4 mm				
	Specific gravity	7.8				
	Quality	Alloy Steel				
	Assumed porosity	40 %				
	Ball filling volume fraction (J)	20 % (J = 0.2)				
Material	Powder gravity, g/cm <sup>3</sup>	Pumice 1 0.96	Pumice 2 1.15	Trass 1.35	Amorphous Silica 0.67	Diatomite 0.58
	Interstitial filling (U%)	52.5 % (U = 0.525)				
	Powder filling volume (f <sub>c</sub> %)	6.4 % (f <sub>c</sub> = 0.064)				

#### 4.1 Determination of the specific rate of breakage

The first-order plots for various feed sizes of porous samples are illustrated in Figure 1-5. The results indicated that grinding of all size fractions, five samples could be described by the first-order law. In additional, parameters of specific rate of breakage to supply by first-order plots are present in Table 3. The specific rates of breakage of each mono-size fraction that exhibited first-order grinding kinetic behaviour were determined from the slope of straight-line of first-order plots. Additional, Figure 6 shows the values of S, for grinding of the five different porous samples, as a function of size.

#### 4.2. Determination of B function

By definition, the values of B were determined from the size distributions at short grinding times. The parameters were determined according to the BII method (Austin et al, 1984), and show the graphical representation on Figure 7. Porous samples show a typical normalised behaviour, and the progeny distribution does not depend on the particle size, and it followed that the parameter 5 was zero. Model parameters supply by cumulative distribution and these parameters are presented in Table 3.

Table 3. Bond's grindability values and characteristic breakage parameters for samples of porous materials

Material	g/rev	S, (0.212-0.150 mm) (min <sup>-1</sup> )	ai- imin <sup>-1</sup>	a	r	*
Pumice-1	2.96	0.174	0.42	0.619	0.291	0.347
Pumice-2	2.67	0.182	0.88	0.998	0.597	0.389
Trass	2.45	0.315	1.11	1.458	0.299	0.234
Amorphous Silica	1.74	0.342	2.33	1.406	0.729	0.324
Diatomite	8.12	0.825	9.12	1.866	0.526	0.442

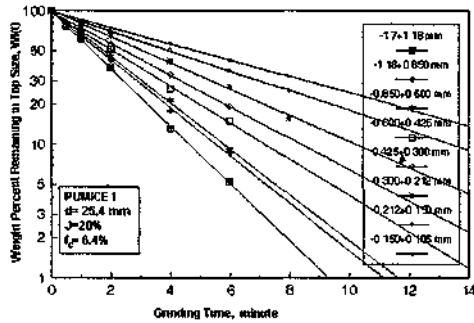


Figure 1. First-order plots for Pumice-I

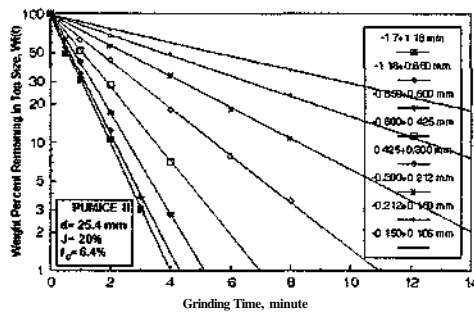


Figure 2. First-order plots for Pumice-II

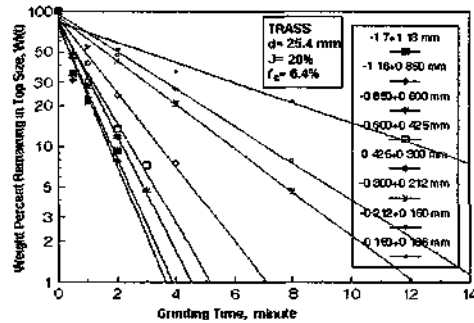


Figure 3. First-order plots for Trass

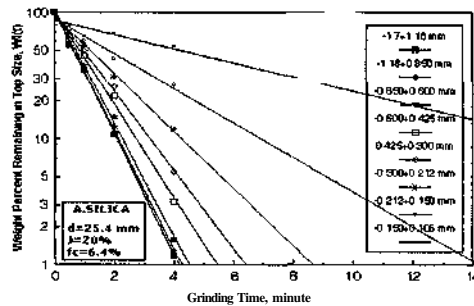


Figure 4. First-order plots for Amorphous silica

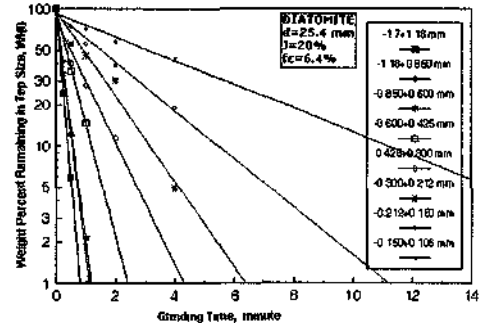


Figure 5. First-order plots for Diatomite

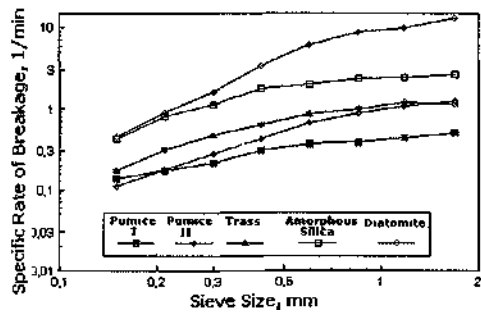


Figure 6. Variation of specific rates of breakage with particle size for samples of porous materials

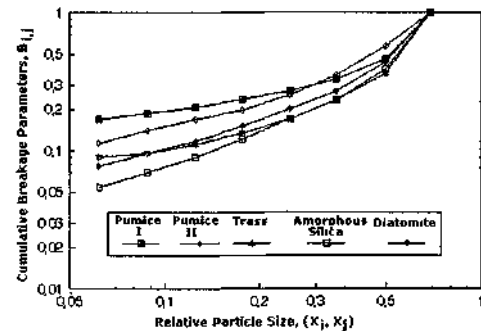


Figure 7. Cumulative breakage distribution functions for porous materials

## 5 THE RESULTS AND DISCUSSION

Further work was done Deniz (2004) to study relationships between Bond's grindability and breakage parameters of grinding kinetic on limestone. The results from the research were the validity of the obtained relationships parameters has been confirmed with good correlation coefficients.

In this study, a relationship between Bond's grindability and breakage parameters of grinding kinetic on porous samples was not obtained. Reason of this negative result, geological origin of porous materials is not similar.

This study showed that a relationship between breakage approaches with chemical analysis results, SiO<sub>2</sub> contents values, was not expressed. The experimental values show that diatomite and amorphous silica are higher porosity, however, diatomite is faster grinding, while amorphous silica is slowly grinding.

Furthermore, effect of porosity on breakage approach of porous materials is not clear. Therefore, it has appeared that the grinding kinetics for each material must be evaluated to lower the energy costs in the grinding process.

#### CONCLUSIONS

The dry grinding of size intervals of porous samples showed that these samples followed the first-order breakage law with constant normalized primary breakage distribution function.

The values of the primary daughter fragment distributions and the values of  $m$ ,  $S$ ,  $=arX^m$  are different in the samples of porous. As the amount of  $S$ , or  $\dot{U}T$  values increase, the effective breakage increases, and breaks as very fast in the undersize of original particle size. The lower  $y$  values, the fineness factor, contribute more for the large parameter values of the finer size fractions,  $\$$  values contribution mainly towards the coarser size fractions.

Although, diatomite is higher SiO<sub>2</sub> content than other samples, it is faster grinding of original particle size than other porous.

Pumice samples lesser than diatomite sample to respect to contain SiO<sub>2</sub>, pumice samples showed a slowing down of breakage rate fine dry grinding, while amorphous silica, more contain SiO<sub>2</sub>, showed deceleration of grinding rate.

From the Table 3, it is seen that diatomite is broken faster than amorphous silica in terms of the  $ar$  values. Similarly, the Bond's grindability value ( $G_b$ ) for diatomite is easier than other samples. On the contrary, the Bond's grindability value for amorphous silica is harder than these samples, while amorphous silica is broken faster than pumice-I, pumice II and Trass in terms of the  $ar$  and  $S$ , values.

Additional, pumice-I and trass samples produce finer material than diatomite by considering the  $y$

value of  $B_p$ , while diatomite easy grinding than pumice-I and trass samples.

The  $\$$  value (0.442) is higher for diatomite than other porous samples, indicated that breakage of the top size showed acceleration, and deceleration for trass (0.234).

#### REFERENCES

- Austin, L.G., 1972. A review introduction to the description of grinding as a rate process. *Powder Technology* Vol 5 1-7.
- Austin, L.G. and Luckie, P.T., 1972. Methods for determination of breakage distribution parameters. *Powder Technology* Vol 5 215-222.
- Austin, L.G. and Bagga, R., Çelik, M., 1981. Breakage properties of some materials in a laboratory ball mill. *Powder Technology* Vol 28 235-241.
- Austin, L.G. and Brame, K., 1983. A comparison of the Bond method for sizing wet tumbling mills with a size-mass balance simulation method. *Powder Technology* Vol 34 261-274.
- Austin, L.G., Khmpel, R.R. and Luckie, P.T., 1984. *Process Engineering of Size Reduction Ball Milling*. SME-AIME New York USA.
- Bond, F.C. and Maxson, W.L., 1943. Standard grindability tests and calculations. *Trans. SME-AIME*, Vol 153 362-372.
- Demz, V., Balta, G. and Yamık, A., 1996. The interrelationships between Bond grindability of coals and impact strength index (ISI), point load index (Is) and Friability index (FD). *Changing Scopes in Mineral Processing*. Kemal et al (Editors). AA Balkema, Rotterdam, Netherlands 15-19.
- Deniz, V. and Onur, T., 2002. Investigation of the breakage kinetic of pumice samples as dependent on powder filling in a ball mill. *Int. Journal of Mineral Processing* Vol 67 71-78.
- Demz, V., 2004. Relationships between Bond's grindability ( $G_b$ ) and breakage parameters of grinding kinetic on limestone. *Powder Technology* Vol 139 208-213.
- Horst, W.E. and Bassarear, J.H., 1976. Use of simplified ore grindability technique to evaluate plant performance. *Trans. SME AIME* Vol 260 348-351.
- Magdalmovic, N., 1989. A procedure for rapid determination of the Bond work index. *Int. Journal of Mineral Processing* Vol 27 125-132.
- Prasher, C.L., 1987. *Crushing and Grinding Process Handbook*. John Wiley & Sons, Chichester, England.
- Yap, R.F., Sepulveda, J.L. and Jauregui, R., 1982. Determination of the Bond work index using an ordinary laboratory batch ball mill. *Design and Installation of Comminution Circuits*. A.L. Mular (Co-Editor). Soc. Min. Eng. AIME, USA 176-203.



## Performance Evaluation Studies in Çayeli Grinding Circuit

L. Ergün, Ö. Y. Gülsoy, N.M. Can & H. Benzer

Hacettepe University, Department of Mining Engineering, Ankara, Turkey

**ABSTRACT:** The aim of the study is to investigate the performance of the grinding circuit of Çayeli Bakır İşletmeleri A.Ş. (ÇBİ) for higher tonnages and also to evaluate effect of hydrocyclone geometry on the performance, after installation of tertiary crusher in the crusher circuit. Seven sampling surveys were undertaken at varying feed rates and cyclone apex and vortex finder diameters. Mass balance studies were performed to calculate flowrates of streams. For all the feed rates examined, the target values for flotation feed, i.e. 70% passing 36 $\mu$ m and 40% solids by weight, were reached. Although, primary ball discharge became coarser with the increase in feed rate, top size of the product did not change significantly. On the other hand, the performance of 70 mm apex and 130 mm vortex finder combination was better than any other combination.

### 1 INTRODUCTION

The grinding circuit of ÇBİ flotation plant was originally designed to process 600,000 tpa ROM ore to produce a flotation feed containing 80% -36 micron. The circuit was reached to an annual throughput of 850,000 tons, after modifications during the years.

Further improvement was achieved by the use of single stage classification instead of double stage and annual capacity has reached to 1,000,000 tons. This has also improved control over classification and simplified the operation (Aksam and Mian, 2003).

A tertiary crusher was installed in crushing circuit to provide finer feed to the circuit and also increase the capacity to 1,250,000 tpa.

The aim of the study is to evaluate the performance of the grinding circuit after installation of tertiary crusher and at higher feed rates and varying cyclone apex and vortex finder diameters. These data were also used for the modelling aided optimization of the circuit (Ergün et al, 2005).

For this purpose seven sampling surveys were carried out around the grinding circuit. Four of them were used to evaluate the effect of feed rate on the performance and three sets of samples for the evaluation of the effect of cyclone apex and vortex finder diameter. Further samples were also taken from primary ball discharge which has a limited power.

### 2 SAMPLING STUDIES AT THE CIRCUIT

Sampling studies were focused to evaluate the effects of feed rate and hydrocyclone apex and vortex finder diameters on the circuit performance. A detailed sampling program has planned by communications with Plant Management. Seven sampling surveys were carried out in the circuit at different operating conditions which are given in Table 1. Six separate samples were also taken from primary ball mill discharge at various feed rates up to 165 tph (*all the tonnages reported are in dry basis*).

Table 1. Main operating conditions for the sampling surveys

	Feed rate (tph)	Number of Operating Cyclones	Vortex Finder Diameter(mm)	Apex Diameter (trim)
1	132	4	130	90
2	146	4	130	90
3	151	4	130	90
4	152	5	130	90
5	132	4	140	95
6	132	4	130	95
7	132	4	130	70

Simplified flowsheet and sampling points are shown in Figure 1.

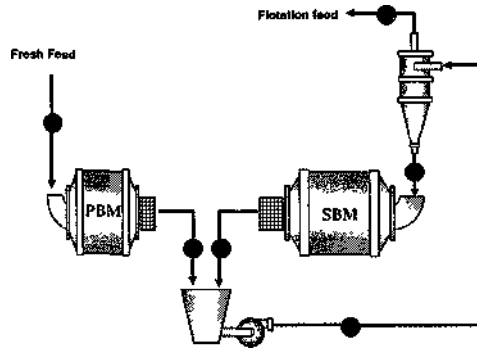


Figure 1. Simplified flowsheet of ÇBI grinding circuit and sampling points.

Prior to each sampling survey, steady state conditions were verified by examining the values of variables recorded in the control room. Each survey lasted in approximately two hours. During this period, samples were taken from each point with approximately 15-20 minutes intervals and combined in a separate bucket. Due to the physical difficulties, combined stream of hydrocyclone underflows were not sampled. Except Survey 3, samples were taken from all individual cyclone underflows. A stream cutter sampler was used for the hydrocyclone underflows; while a specially designed sampler was used for taking cyclone feed samples from sump. Cyclone feed samples were also taken from overflow pipe of one cyclone which was arranged for this purpose by blocking underflow discharge. The existing sampling system was used for taking samples from the cyclone overflow. For sampling the primary and secondary ball mill products, open channel chutes were intercepted by a shovel to create a well mixed zone at upstream. Then, a ladlelike sampling device with long handle and 1 liter volume was dipped into the zone and a sample was taken. The feed to circuit was sampled by stopping the conveyor belt and stripping the ore from a length of 1.5-2 m. Separate larger samples were also collected from fresh feed for the determination of Bond work index.

The dimensions and some operating parameters of the ball mills and hydrocyclones are given in Table 3 and 4. The ball loads within the mills were determined by measuring the free height between balls and mill shell during a shut down just before the surveys. The measured ball loads for primary and secondary ball mills were 43% and 35%, respectively. All cyclone dimensions were measured. For the Survey 5-7 cyclone apex and vortex finders were replaced.

Table 3. Design and some operating parameters of the ball mills.

	Primary Ball Mill	Secondary Ball Mill
Mill Outer Diameter (mm)	3200	4400
Mill Length (mm)	4300	7200
Liner Thickness (mm)	100	50
Mill Speed (rpm)	17.4	15.4
Critical Speed, Cs (rpm)	24.8	20.5
%Cs	70.0	75.1
Ball Size(mm)	100-80	40-26
Power (kW)	560	2160

Table 4. Design and some operating parameters of the hydrocyclones

Diameter (mm)	375
Inlet Diameter (mm)	152
VF diameter (mm)	130, 140
VF length (mm)	276
Apex diameter (mm)	70, 90, 95
Cylinder length (mm)	360
Cone angle °	10

### 3 LABORATORY STUDIES

The samples were first weighed wet. Then, they were dried and weighed again. Solids content of the samples were determined from wet and dry weights. All the samples were sieved from 13.2 mm to 0.85 mm. Approximately 600 grams of samples were taken from -0.85mm by using sample splitters. Then, samples were sieved wet using series of standard sieves down to 0.036 mm. The particle size distribution of -0.036 mm fraction was determined down to 8.8(J.m by a cyclosizer.

Bond grindabilities and work indices of the plant feed samples were determined using standard Bond test for 74 micron test sieve. Bond indices of the feed for Survey 1 and 7 feed samples were 9.70 kWh/t and 9.55 kWh/t, respectively.

### 4 MASS BALANCING

Using mass flow rate of the fresh feed, size distributions and percent solids, flowrates of each stream were calculated. During mass balancing, errors were distributed according to physical condition at any particular sampling points. For example, larger weighting of error was given to cyclone feed than the cyclone overflow stream.

Convergence limits in all iterations were chosen as  $10^{-5}$ . Mass balancing of the raw data was accomplished by using JKSimMet software. The measured and adjusted size distributions of the streams around the circuit for each survey are given in Figure 2-8.

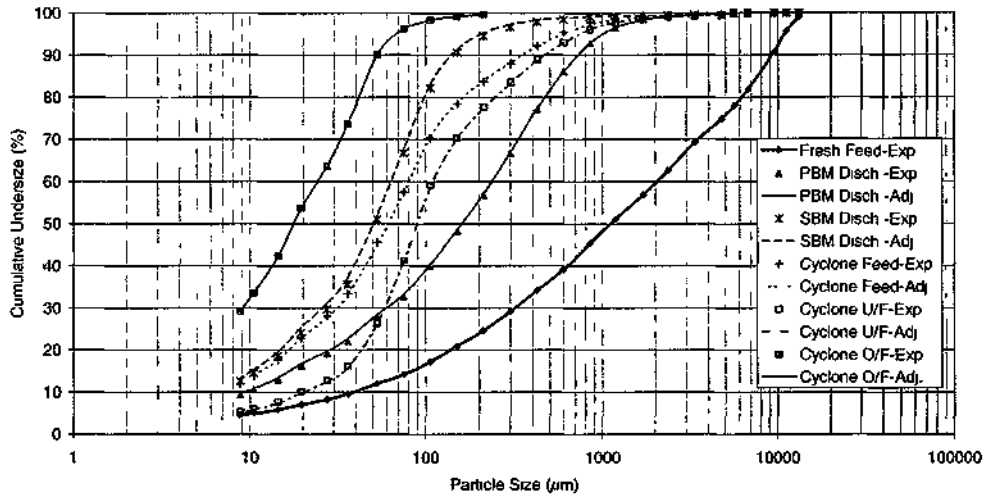


Figure 2. Expenmental and mass balanced size distributions for Survey 1.

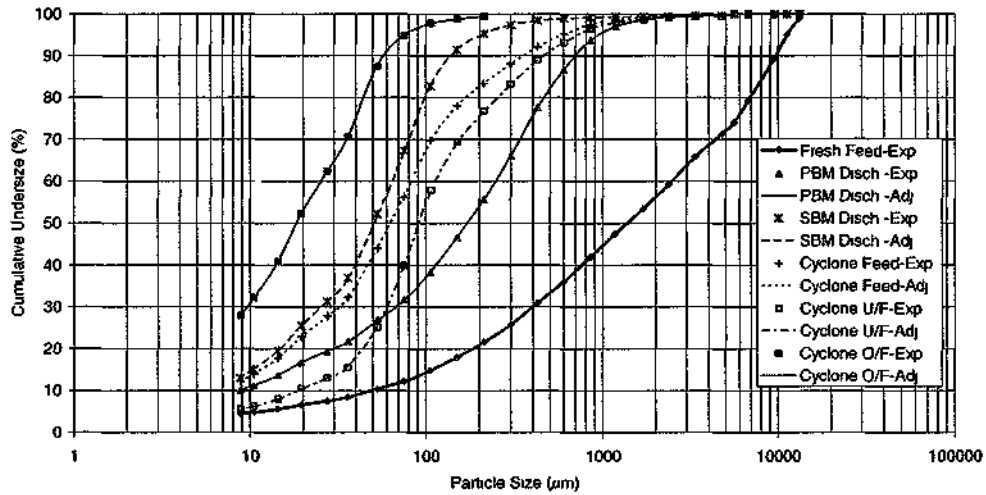


Figure 3. Expenmental and mass balanced size distributions for Survey 2.

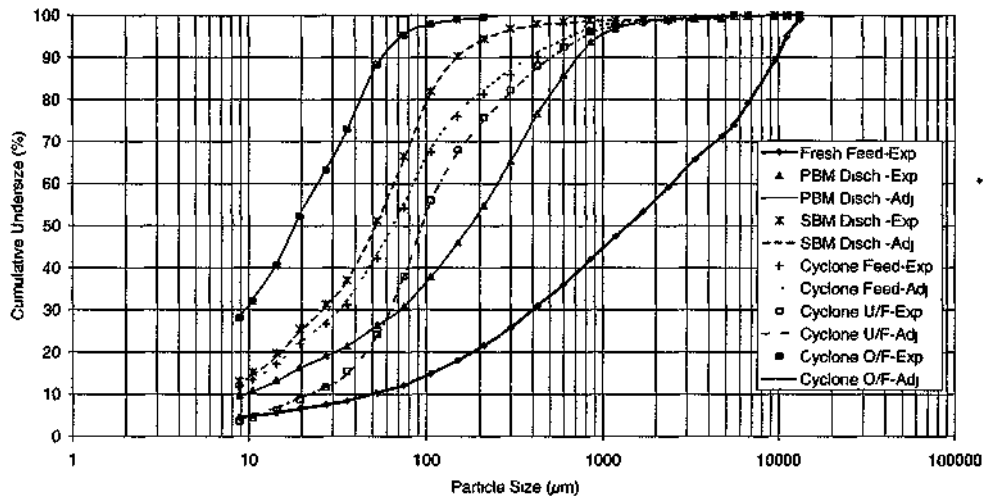


Figure 4 Experimental and mass balanced size distributions for Survey 3

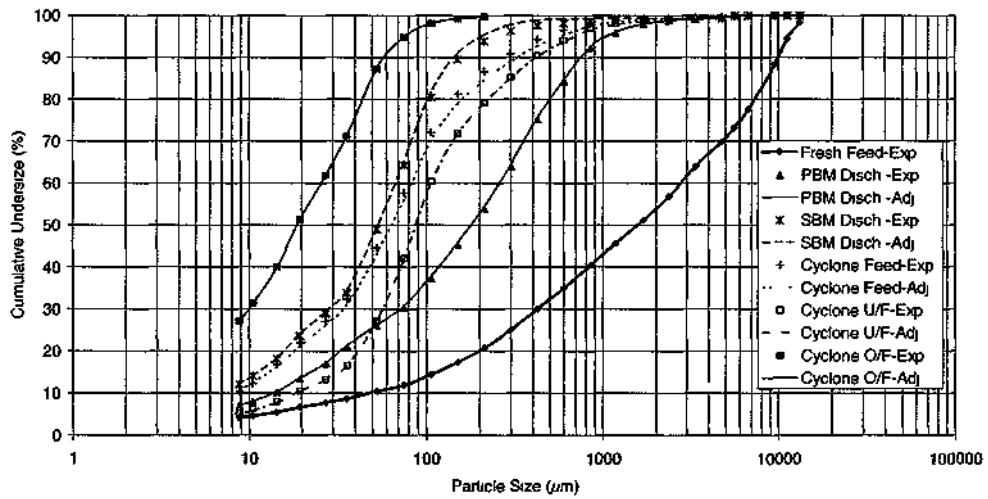


Figure 5 Experimental and mass balanced size distributions for Survey 4

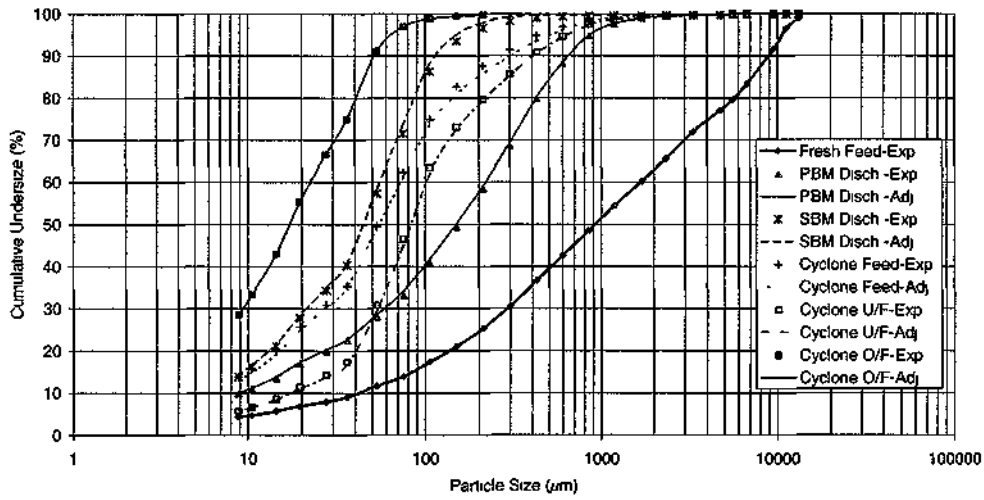


Figure 6 Expenmental and mass balanced size distnbtions for Survey 5

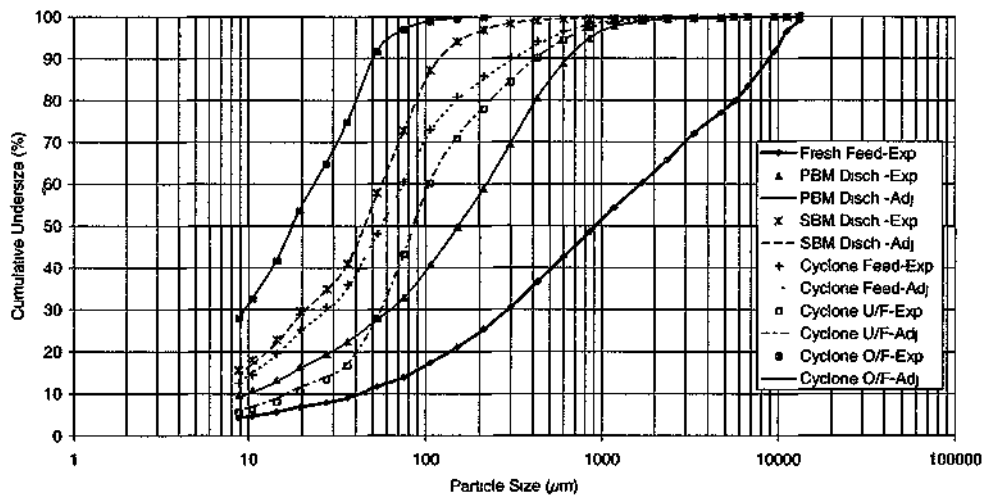


Figure 7. Expenmental and mass balanced size distributions for Survey 6

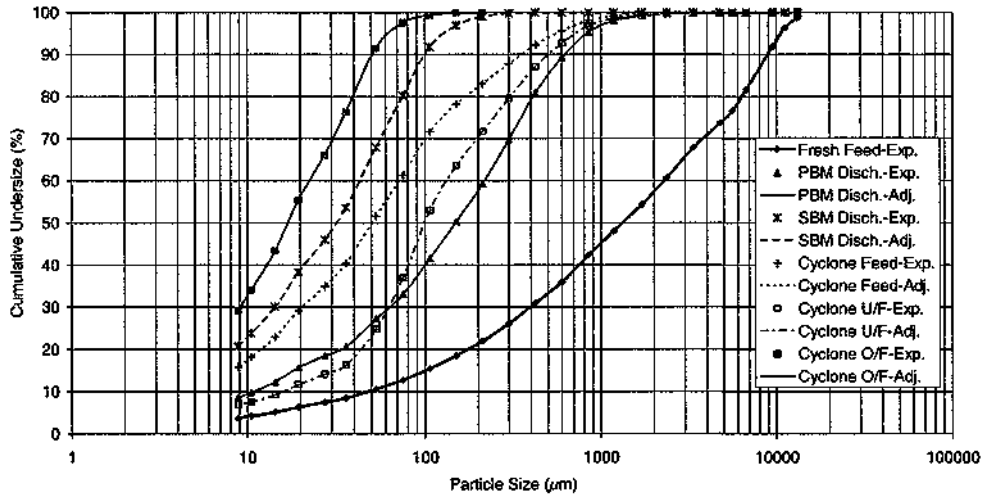


Figure 8. Experimental and mass balanced size distributions for Survey 7.

As can be seen from Figure 2-8, the measured and mass balanced the size distributions of the streams were close to each other showing that sampling studies were performed successfully. The flow rates of the streams calculated after mass balancing are given in Figure 9.

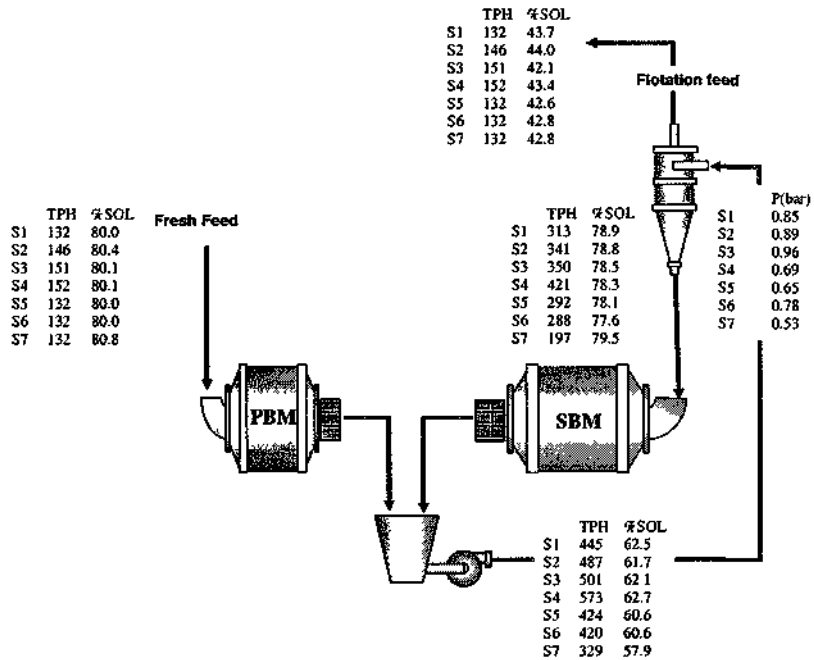


Figure 9. Flow rates of the streams for all surveys and cyclone pressures measured.

5 PERFORMANCE EVALUATION

5.1 Effect of feed rate on the performance

Surveys 1-4 were carried out to evaluate the effect of feed rate on the circuit performance. Four cyclones having 90 mm apex diameter and 130mm vortex finder diameter were used in surveys 1-3. In survey 4, the number of operating cyclones was increased to five.

In terms of flotation feed fineness and % solids, the performance of the circuit did not exhibit any deterioration with the increasing feed rate. For all the feed rates examined, the target values, i.e. 70% passing 36µm (Figure 10) and 40% solids by weight, were reached.

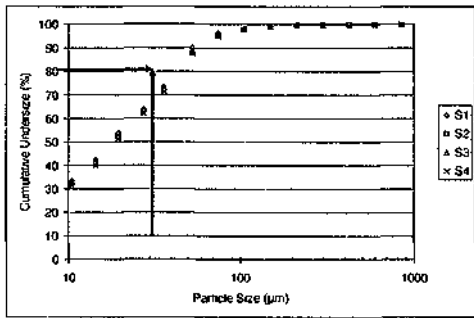


Figure 10. Size distribution of the hydrocyclone overflows for Survey 1-4.

Actual performance curves of the hydrocyclones for Survey 1-4 are given in Figure 11.

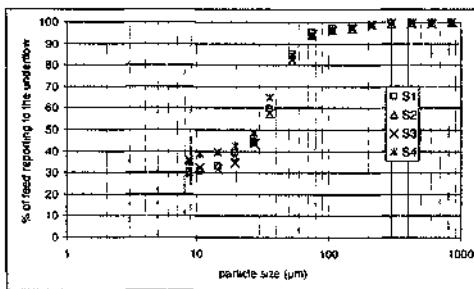


Figure 11. Actual performance curves for the cyclones for the Surveys 1-4.

For the Survey 1-3, the actual performance curves were found to be very similar. Surveys 4-5 were performed practically at the same flow rate. However, for Survey 5, as the number of operating cyclones was increased from four to five, the amount of material going to the underflow increased. This resulted in a higher bypass as shown in Figure 11 and also significant increase in circulating load (Figure 12).

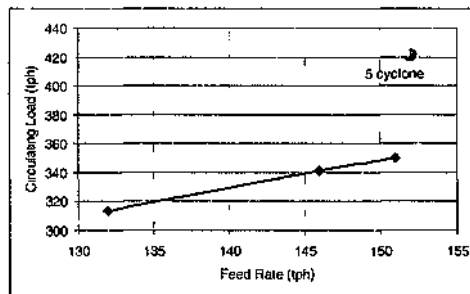


Figure 12. The effect of feed rate on circulating load tonnage.

As can be seen from Figure 12, an increase in feed rate resulted in a linear increase in circulating load tonnage when the number of operating cyclones was four. For the five cyclones, a higher increase was observed. The circulating load ratios were in the range of 232-237% for the Survey 1-3 and 276% for Survey 4.

This point was also verified by the operating pressure values. For the four cyclone case, the pressure increased with the increase in cyclone feed volumetric flow rate, however it drastically decreased for five cyclone case. It may be concluded that the four operating cyclones was better than five for the conditions investigated.

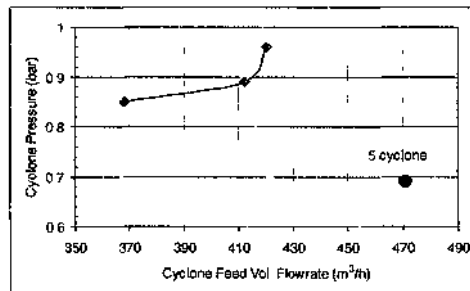


Figure 13. The relationship between cyclone volumetric feed rate and operating pressure.

### 5.2 Effect of apex and vortex finder diameters

The effect of cyclone apex diameter was evaluated between 70mm and 95mm using the data from Survey 1, 6 and 7. In these surveys vortex finder diameters were kept constant as 130 mm. Vortex finder diameter was tested only in two levels of 130 mm and 140 mm for 90 mm and 95 mm apex diameters using the data obtained from Survey 1 and 5. All of these studies were performed at constant feed rate of 132 tph.

Actual performance curves for these surveys are presented in Figure 14. Except for Survey 7, the cyclone performance did not change significantly. However, in Survey 7 the bypass of the separator significantly reduced. Actual  $d_{50}$  of the cyclones in Survey 7 was about 38  $\mu\text{m}$ , whereas it was about 30  $\mu\text{m}$  for the other surveys.

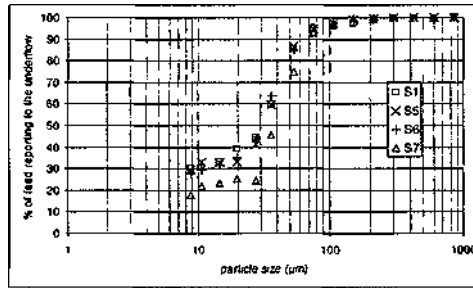


Figure 14. Actual performance curves for the cyclones for the Surveys 1 and 5-7.

Since 70 mm apex in Survey 7 was the minimum apex diameters tested, minimum water recovery to the underflow was expected. The percent solids of the cyclone underflow 79.5 % and was the highest, as expected.

As the apex diameter decreased, the size distribution of cyclone underflow became coarser. The size distributions of cyclone underflow streams for 90 mm, 95 mm and 70 mm apexes are given in Figure 15.

For the range studied, the performance of 70 mm apex was better than the others. The product was the finest among all surveys. The circulating load tonnage was 197 tph and circulating load ratio was 149%. Operating pressure for the cyclones was 0.53 bar. Although actual  $d_{50}$  of the cyclones is greater than the other, the tonnage going to secondary ball mill significantly reduced. Therefore, it was functioning much better. P80 of secondary ball mill

discharge was 74  $\mu\text{m}$ , while for the other surveys at the same feed rate varied between 98  $\mu\text{m}$  and 86  $\mu\text{m}$ . In other words, -36 $\mu\text{m}$  was about 54% for 70 mm apex, while varied between 37% and 41% for the other apex diameters.

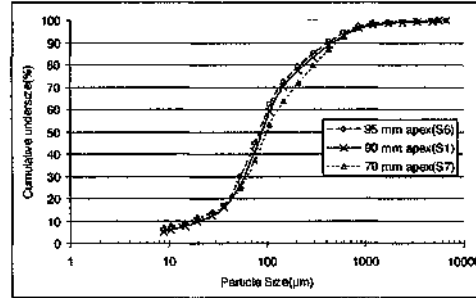


Figure 15. Size distribution of the hydrocyclone underflows for different apex diameters.

Changing vortex finder diameter from 130mm to 140 mm did not exhibit a discernible difference probably due to the differences in apex diameters.

Finally, for the all the surveys (1-7), reduced performance curve of the hydrocyclone is presented in Figure 16.

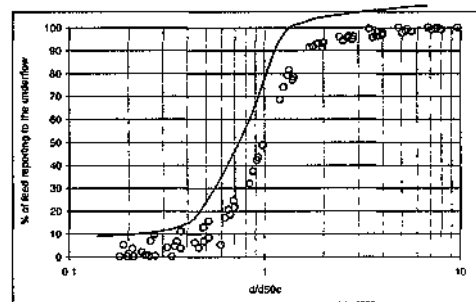


Figure 16. The reduced performance curve for the hydrocyclone

### 5.3 Effect of feed rate on primary ball mill performance

One of the constrain to increase the capacity of the circuit seemed to be the performance of primary ball mill. Therefore, apart from planned sampling surveys, separate samples were also taken from primary ball mill discharge to evaluate the performance of it at higher tonnages. Size

distributions of primary ball mill discharge samples at various feed rates are shown in Figure 17

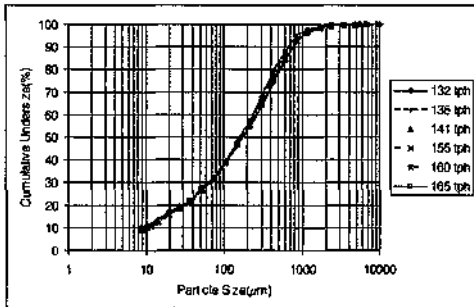


Figure 17 The size distributions of primary ball mill discharge at different feed rates

As can be seen from the figure, an increase in feed rate resulted in a coarser product. However, the top size of the product did not change significantly.

For a better demonstration, Figure 18 were drawn by modifying the Figure 17

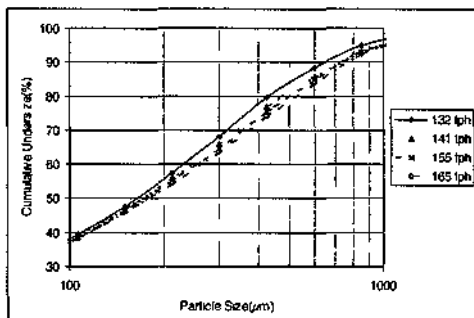


Figure 18 The effect of feed rate on primary ball mill performance (scales are adjusted)

## 6 DISCUSSION

Performance of the ÇBI grinding circuit was evaluated by the data obtained from detailed sampling surveys.

Since all the information extracted from the surveys maximum care must be taken for representative sampling. Although some general rules available (Napier-Munn et al, 1996), sampling procedures for each plant and particular sampling point must be developed.

Mass balancing studies provide the evaluation of the sampling procedures as well as calculation of flow rates and adjusted size distributions. Adjustments in the measurements are the indication of the quality of the sampling procedures. Mass balancing algorithms can not adjust erroneous data, however, help to identify where sampling method is not appropriate. With this respect, as shown in Figure 2 8, sampling in this study were performed successfully.

After mass balancing, the quantitative picture of circuit performance for each survey was obtained. The results showed that the capacity of the circuit could be increased to 150 tph and the performance could be improved by optimizing the cyclone parameters. However, it is extremely difficult to optimize the circuit by plant scale tests, due to the number of variables affecting the performance (Lynch, 1977, Napier Munn et al, 1996). Simulation is a very useful tool for optimization of the circuits by considering all the variables involved simultaneously. In an earlier study in ÇBI grinding circuit, the success of modelling and simulation has proven during conversion of double stage classification to single stage (Ergun et al, 2000, 2002, Aksam and Mian, 2003).

The studies for the optimization of the circuit will be presented in another study (Ergun et al, 2005).

## 7 CONCLUSIONS

The performance of the ÇBI grinding circuit was evaluated by the data obtained from several sampling surveys performed after installation of a tertiary crusher in crushing circuit.

The ÇBI grinding circuit can be operated at 150 tph without deterioration in flotation feed fineness and % solids. This would also provide 15% decrease in specific energy consumption of the circuit.

The performance of the circuit could be improved by optimizing cyclone parameters.

The primary ball mill discharge became coarser with increasing feed rate. However, the top size of the product did not change.

## Acknowledgment

The authors would like to thank ÇBI Management for the financial support and for the permission to publish this paper, and also to Mill Staff for their efforts during the studies at Çayeli.

REFERENCES

- Aksarı, B , Mian, M N , 2003, Comparison of one stage and two stage classification - A case study, *Proceedings of 8th Mill Operators' Conference*, Aus IMM, Townsville, 21-23 July, pp3-9
- Ergun, Ş L, Ersaym, S , Gulsoy, O Y , Ekmekçi, Z, Can, M, Aslan, A, 2000, Modelling and simulation of grinding circuit at Çayeli Bakır işletmeleri A Ş (ÇBI) flotation plant, *Mineral Processing on the Verge of the 21<sup>st</sup> Century*, Ozbayoğlu et al (eds), A A Balkema Publishers, pp65-70
- Ergun, Ş L, Gulsoy, O Y , Aksarı, B , Mian, N , 2002, Comparison of simulation results with the actual performance at the grinding circuit of Çayeli Bakır İşletmeleri A Ş , 9<sup>th</sup> *Int Min Pro Symposium*, Extended Abstracts, pp143-144
- Ergün, Ş L , Gulsoy, O Y , Can, M , Benzer, H , 2005, Optimization of çayeli grinding circuit by modelling and simulation, The 19th International Mining Congress and Fair of Turkey(accepted for presentation and publication)
- Lynch, A J 1977 *Mineral crushing and grinding circuits then simulation, optimisation, design and control* Elsevier 340pp
- Napier-Munn, T J, Morrell, S, Morrison, R D & Kojovic, T 1996 *Mineral comminution circuits then operation and optimisation* JKMC 413pp

## Granulometric and Gravimetric Separation of Microspheres Using Laminar Flow

I Nishkov

Mineral Processing Department, University of Mining and Geology "St Ivan Rilski", 1700 Sofia, Bulgaria

A Kalatzis

ATLAS, Thessaloniki, Greece

**ABSTRACT:** In this work we present the development of a method and the design of an apparatus for studying the behavior of solid microspheres dispersed in a laminar flow. The flows both in up- and down-direction in a vertical glass tube with a circular cross-section were examined. In the up-flow experiments rapid lateral migration of the particles was observed towards the tube axis. In the down-flow the spheres migrate in the opposite direction towards the wall of the tube. A significant dependence on the size of the particles and their relative speed versus the main flow speed was observed. This allows the flow to be used for particle separation by size (granulometric separation) and by specific gravity (gravimetric separation).

### 1 INTRODUCTION

Serge & Silberberg (1962) published their experimental investigations on the flow of suspension of small, freely floating spheres (i.e. with the same density as the surrounding liquid) in a tube. They found out the extraordinary fact that the spheres are not distributed uniformly across the cross section of the tube, but migrate across the current lines to a stable equilibrium at a position of 0,6 of tube's radius.

Many authors repeated and modified the experiments of Serge & Silberberg (modifying flow type, size and density of particles) obtaining similar result. For example, in a flow with a constant gradient (Couette) the particles gather in the middle between the two walls.

The theoretical studies suggested the following explanation of the physical nature of the migration force. The current of the main flow is Poiseuille's (with a parabolic velocity profile). Faxen (1922) found out that a solid sphere, which is in such a flow, is slow with regard to the surrounding liquid. The velocity of the lagging behind is proportional to the gradient of pressure along the tube's length and the square of the sphere's radius. The studies of Faxen (1922) and later calculations of Bretherton (1962) showed that for one direction external flow at comparatively small lagging out of the particle the interaction results only in increase of the resistance

force in the direction of the main flow. In this case no radial displacement along the section of the tube appears.

A significant contribution in studying the nature of the effect was performed by Saffman (1965). He demonstrated that at higher relative speeds of the particle, the disturbance which it introduces in the carrying flow spreads at a longer distance and creates a lateral force, which moves the particle perpendicularly to tube's axis. At the same time this force is viscosity inert - similarly to the interactions in a boundary layer.

$$F_L \sim \mu a^2 V (\gamma / v)^{1/2}, \quad (1)$$

where  $\mu$  is the viscosity of the carrying fluid,  $a$  - sphere's radius,  $v$  - relative velocity of the particle with regard to the flow,  $\gamma$  - speed gradient in the external current.

Of course, the presence of walls and other additional disturbances in the carrying fluid will modify the effect. It's considered that this is the reason for fixing the particles in the equilibrium position in the experiment of Serge & Silberberg (1962).

At present the theoretical and experimental investigations are concentrated on studying the nature of the migration mainly at neutral floating or for not very heavy particles (Jeffrey & Pearson 1965, Tachibana 1973, Cox & Vasseur 1976).

Regarding the movement of particles with a density significantly different from that of the fluid the theoretical description is not so complete and no experimental studies exist at all. Thus, many authors focused their efforts in this field. The aim of this work is the development of a method of Serge - Silberberg for heavier particles and the study of the migration direction in downstream and upstream laminar flow in a tube.

2 EXPERIMENTAL

The model studies were performed with apparatus presented in Figure 1 (downstream and upstream flow). A given volume of suspension with fixed particle concentration passes at constant speed through a vertical glass tube / with internal diameter  $2R = 10,10$  mm and length  $l_0 = 120$  cm. The tube is connected at both ends with two vessels: feeding vessel 2, where the stability of the suspension is kept by stirring with stirrer 3 at constant minimal speed and catcher 4 in which the suspension is collected after passing through the tube. The valve 7 switches

on/off between the two options I and II of the functioning of the apparatus. This determines the direction of the flow, vertically downward (downstream flow) or vertically upward (upstream flow). At option "downstream flow" the catcher is placed above the level of the feeding vessel in order to eliminate the additional influence of the hydrostatic pressure on the current speed. The movement of the suspension through the tube in both options is executed by applying negative pressure to the catcher. The negative pressure is provided by a vacuum pump and is preserved constant by a system of two buffers (10) - operative and additional - to compensate small changes in the negative pressure occurring during long periods of time. Using the three-way valve (8) the system may be connected to the atmospheric pressure. It is used to transfer back the suspension from the catcher to the feeding vessel due to the established very high-pressure gradient.

The flow velocity in the tube is set and kept constant by areometer 9 and is controlled by direct reading of the suspension's flow rate  $Q$ ,  $\text{cm}^3/\text{s}$

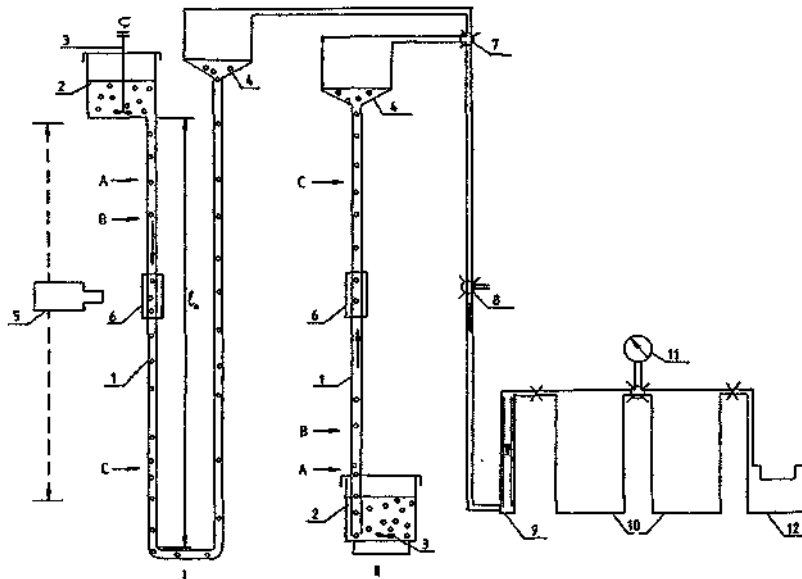


Figure 1 Principle scheme of the apparatus: 1- glass tube; 2 - feeding vessel; 3 - stirrer; 4 - catcher; 5 - horizontal microscope; 6 - cell with plane-parallel walls; 7 - three-way valve for switching on option I or II of the system; 8 - three-way valve for connection with the atmosphere; 9 - areometer; 10 - buffer system; 11 - vacuum meter; 12 - vacuum pump

The behavior of the particles at their movement in the current can be established by determining the particles' concentration distribution at different levels (sections A, B or C on Figure 1) along the length of the tube in points with coordinates  $r$  and  $z$ , where  $r$  defines the radial position and coincides with the direction of section's radius of the tube, perpendicularly to the walls, and  $z$  is the coordinate coinciding with tube's axis in direction parallel to the walls. By the ratio  $r/R$  is determined the position of the particles with regard to the axis  $z$ .

Certain minimal volume  $v$  of the interior of the tube with coordinates  $(r, z)$  can be focused using a horizontal microscope that can be moved in vertical direction. At a diameter of the vision field  $Ax = 1,2$  mm and at a maximal depth of the focus  $d_f = 0,05$  mm, this volume is

$$v = n(Ax/2)^2 dy = 0,018 \text{ mm}^2 \quad (2)$$

The number  $N$  of the particles that pass through the focused minimal volume is read per a unit of time. The obtained values are averaged for 20 measurements at the corresponding mean quadratic error ( $a = \pm 0.2 \cdot 52$  particles depending on  $r$ ). In this way the number of the particles  $N$  is determined for a fixed section of the tube ( $z = \text{const}$ ), as a function of  $r$ , and this allow a statistical information on the behavior of a set of particles to be obtained.

The corresponding concentration distribution of the particles  $C(r)$  is calculated by the dependence  $N(r)$  according to the formula:

$$C(r) = N(r)/Ax dy U(r)t, \quad (3)$$

where  $Ax dy U(r)$  is the volume of the suspension passed through the area  $Ax dy$  with speed  $U(r)$  for time  $t$  of reading the number  $N(r)$ .

It is assumed that the speed of the particles in  $z$  direction coincides with the speed  $U(r)$  of the laminar flow that is not affected by the presence of the particles.

According to Poiseuille's law:

$$U(r) = U_{max}(1 - r^2/B^2) \quad (4)$$

where  $U_{max}$  is the speed of the flow along the axis of the tube.

The measurements at two relatively perpendicular diameters of the section  $x$  and  $y$  and at the intermediate radial positions show symmetrical distribution of the particles around the tube's axis, i.e. the obtained results confirm the reference data for symmetry of the flow (Segre & Silberberg 1962, Jeffrey & Pearson 1965).

According to reference data, the main parameters determining the trajectory of a particle in a flow are the Reynolds's number of the tube  $Re$ , the ratio of particle's diameter to the diameter of the tube and the ratio of sedimentation speed of the particle by Stokes to the maximal speed of the flow. The physical variables defining the flow in any moment of time, which may be used in general for experimental studies are the radius of the tube  $R$ , the particle's radius  $a$ , the flow speed along the axis of the tube  $U_{,max}$ , the viscosity of the suspension  $\eta$ , the fluid density  $P/$ , the particle density  $pp$ , and the cylindrical coordinates  $(V, z)$ .

For laminar flow  $Re = PfU_{max} R/\beta < 23$

The model experiments were carried out under the following conditions. It was used a suspension of glass microspheres with dimensions  $2a = 50 \mu\text{m}$  and  $Pp = 2,38 \text{ g/cm}^3$  in a media of monodistilled water with initial concentration  $C_0 = 50 \text{ part/cm}^3$ . The behavior of the particles during their movement in the tube is observed at flow rate of the suspension  $Q = 4 \text{ cm}^3/\text{s}$ , average speed of the flow  $U = Q/nR^2 = 5 \text{ cm/s}$ , and corresponding maximal speed  $U_{mm} \sim 10 \text{ cm/s}$ . This maximal value of the flow's speed was confirmed by the introduction of colorant fine insoluble particles and reading the speed of movement at the top of the obtained profile of the laminar flow in the tube. Under these conditions  $Re$ , is 500.

The speed of the flow is set and maintained constant by negative pressure  $P_s = -83,4 \text{ kN/m}^2$ . The time for reading the number of ballots  $N$  passed through the envisaged minimal volume is 1 minute.

The suspension is stirred with minimal speed of the stirrer (350 rev/min) to achieve good dispersion of the particles in the volume without forming bubbles. The lack of bubbles in the system under these experimental conditions was proven by a zero experiment, where an observation of the flow without ballots was performed.

At flow of the suspension in the beginning of the tube it is observed a section with chaotically moving particles due to the stirring in the feeding vessel. The experimentally established length  $l$  of this section for the flow upwards is 13 cm, and for the flow downwards is 14,5 cm.

The registration of the passed ballots trough the observed minimal volume at both options of the model experiment - upstream and downstream is taken at levels A ( $z = 0$ ), B ( $z = 37 \text{ cm}$ ) and C ( $z = 77 \text{ cm}$ ), where  $z = l, -A$ , i.e. A corresponds to the end of the chaotic movement of the particles along the section of the tube.

3 RESULTS AND DISCUSSION

It was determined the dependence of the number of ballots passed through the minimal observed volume per unit of time as a function of the radial coordinate  $r$  at  $z = \text{const}$ , as well as the respective concentration distributions  $C(r)$ , calculated according to formula (3).

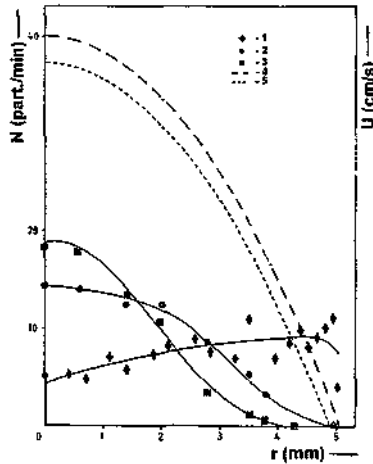


Figure 2. Dependence of the number  $N$  of passed particles as a function of radial coordinate  $r$  for an upstream flow: 1 - at level A ( $z = 0$  cm); 2 - at level B ( $z = 17$  cm); at level C ( $z = 11$  cm); 4 - profile of velocity of a flow  $U(r)$ ; 5 - relative speed of movement of ballots along the axis  $z: V_j(r) = U(r) - V_{s,d}$

Figure 2 shows the distribution of the particles at levels A, B and C for the upstream flow of  $N^A(r)$ ,  $N^B(r)$  and  $N^C(r)$ . On the same figure are presented the profile of speed of the flow  $U(r)$  and the profile of the speed of movement of the ballots in the flow considering the speed of lagging behind according to Stokes:  $V = U(r) - V_{s,d}$ . In this way it is determined the width of the zone free of particles next to the tube wall formed only due to sedimentation ( $Ar = 0,2$  mm).

If the concentration  $C$  of the particles at their flow through the tube is constant along  $r$ , the number of particles  $N$  passed through a given point per unit of time is proportional to the speed of the suspension flow at the same point. As the speed  $U(r)$  has a parabolic distribution across the section of a tube for a laminar flow, the number of the particles passed  $N(r)$  is also distributed according to a parabolic law.

For neutrally floating particles ( $Ap = 0$ ) such parabolic distribution was located at a small distance above the inlet of the tube, after which many

different distributions are observed till forming a peak at  $r/R = 0,6$  (Segre & Silberberg 1962).

For heavy particles ( $Ap > 0$ ) the place  $z$  of even distribution of the concentration along  $r$  is more difficult to be established. Due to the need of more intensive stirring in the feeding vessel, the concentration of the particles at their entering into the tube is higher near the walls and they have some non-rectilinear movement there, influenced by the direction of rotation of the stirrer. For this reason  $C(i,r)$  has the trend shown on Figure 3. In addition the speed of the cross migration is comparatively high and the particles near the tube's axis start to migrate more rarely (at lower value of  $z$ ) than those next to the wall.

At level B the function  $N_B(r)$  has the nature of a parabola near the axis, but next to the walls, even after determining the width of the free zone due to particle sedimentation is formed a zone with decreased concentration of particles because of migration. The effect is even more expressed at level C- $N^C(r)$ .

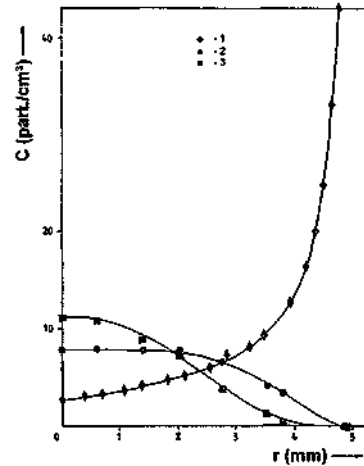


Figure 3. Distribution of the concentration  $C$  as a function of the radial position for an upstream flow: 1 - for level A ( $z = 0$  cm); 2 for level B ( $z = 17$  cm); for level C ( $z = 77$  cm)

In Figure 3 are presented the concentration distributions of the microspheres at levels A, B and C -  $C_A(r)$ ,  $C_B(r)$  and  $C_C(r)$  for an upstream flow. The obtained distributions of ballots as a function of  $r$  definitely prove the cross migration of heavy particles ( $Ap = 1,38$  g/cm<sup>3</sup>) under the conditions of upstream laminar flow in direction to the tube axis.

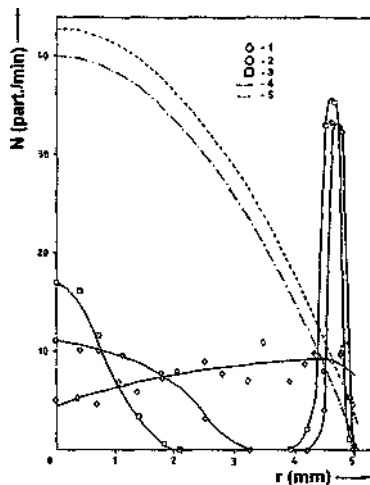


Figure 4. Dependence of the number  $N$  of passed particles as a function of the radial coordinate  $r$  for downstream flow: 1 - for level A ( $z = 0$  cm); 2 for level B ( $z = 17$  cm); for level C ( $z = 77$  cm); 4 - flow's velocity profile  $U(r)$ ; 5 - relative velocity of ballots' movement in the current along the axis  $z$   $V_z(r) = U(r) - V_{sed}$

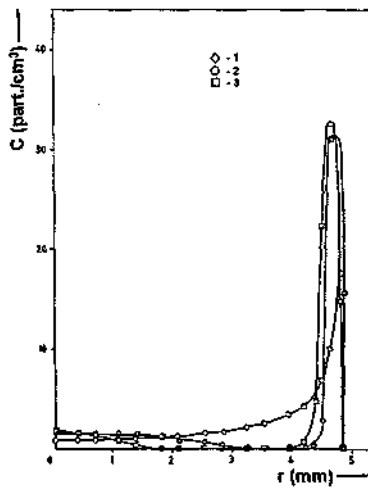


Figure 5. Distribution of the concentration  $C$  as a function of the radial position  $r$  for a downstream flow; 1 - for level A ( $z = 0$  cm); 2 for level B ( $z = 17$  cm); for level C ( $z = 77$  cm)

Figure 4 shows the distributions of ballots  $N(r)$  at levels A, B and C for downstream flow and on Figure 5 are shown the respective concentration distributions  $C_{fr}$ ,  $C_e(r)$  and  $C_{cir}$ .

The cross migration of the particles in direction to the walls of the tube is clearly visible. At distance between 0,1 and 0,5 mm from the walls (level B) and between 0,2 and 0,6 mm (level C) is observed highly increased particle concentration. A zone free from particles is formed with a width of 0,9 mm at level B ( $r/R = 0,65$  to  $0,83$ ), which increases with 1 mm ( $r/R = 0,4$  to  $0,77$ ) when the length of the travel increases to level C.

The results obtained here for downstream and upstream flows are in agreement with the observations of Jeffrey & Pearson (1965). An attempt for quantitative evaluation is made by Cox & Vasseur (1976), but the calculations were done at heavy initial assumptions, which in the investigated case are not met. The form of the solutions obtained there does not present a clear physical idea for the mechanism of the phenomena. This is a specific combination of the effect of the walls, the difference in the density of the particles and the fluid  $\Delta\rho$  and the character of the main flow.

It is forth a further investigation of the displacement of the maximum in the concentrations distribution across the cross section depending on  $\Delta\rho$ .

Near the tube axis at downstream flow is observed some increasing of ballots concentration, which according to the reference data hasn't been observed until now. This effect is not predicted by the theory and has no explanation at the moment.

#### 4 CONCLUSIONS

1. A method and apparatus for studying the behavior of heavy particles under the conditions of laminar flow in a tube with circular cross section were elaborated.
2. The conducted model investigations with glass microspheres demonstrate definitely the presence of comparatively fast cross migration. Under the conditions of upstream flow this migration is in the direction to the tube axis. Under the conditions of downstream flow it is established a strongly increased concentration along the walls, the formation of a free of particles zone at  $r/R = 0,4$  to  $0,8$  and a particle concentration around the tube axis.
3. The study performed in this work might have significant practical application. The observed dependence on the size of the particles and on

their relative speed with regard to the main flow allows its application to classification of materials by size (granulometric separation) and by specific weight (gravimetric separation).

## 5 REFERENCES

- Bretherton, F., 1962,/. *Fluid Mech*, 14, 284.  
Cox, R., P.Vasseur, 1976, *J. Fluid Mech.*, 78, 385.  
Faxen,H., 1922, *Ann. der Physik*, 68, 101.  
Jeffrey, R., J.Pearson, 1965, *J. Fluid Mech.*, 22, 721.  
Saffman, P., 1965, *J. Fluid Mech.*, 22, 285.  
Segre,G., A.Silberberg, 1962,/. *Fluid Mech.*, 14, 115.  
Tachibana, M, 1973, *Reol.Acta*, 12, 58.

## A New Model on Breakage Behaviour of A Laboratory Impact Mill

V. Deniz, Y. Akkurt & Y. Umucu

*Department of Mining Engineering, Süleyman Demirel University, İsparta, Turkey*

**ABSTRACT:** In this study, the breakage behavior of three different limestones in impact crushers using common in quarry and mineral processing plants was investigated. The laboratory horizontal shaft impact mill used in the experiments is rotating at 2840 rpm, which driven by a 1.1 kW motor, carries three rows of hammers. In the evaluation of crushers, *t-family* curves obtained used from weight drop test method are frequently used. It is known fact that there are many difficulties and problems in this test. A new model is developed by *t-family* value evaluation and Bond work index approach, and this model is tested. As a result it is determined that the limestone properties are important in crushing and the validity of the model is proved by a high regression value ( $r^2=0.88$ ).

### 1 INTRODUCTION

Energy necessity is very high in crushing and grinding process. There are many crusher manufactures and many varieties of machines made for crushing minerals. The correct selection between all alternative is a difficult problem.

Impact-induced rock fragmentation is relevant for many fields of science and technology. Impact mills have been applied in mineral, coal and cement industries for a long time. The literatures show that substantial effort has been expended in understanding the impact mill performance in relation to machine configuration and operational conditions through experimental work and mathematical modelling. However, due to lack of detailed knowledge on velocity and energy distributions of collision inside a milling chamber, the mechanisms are still not clear (Djordjevic et al, 2003).

Single particle tests to determine the comminution behaviour of ore can be separated into pendulum and drop weight based tests. Twin pendulum test relies on the particle being broken between an input pendulum released from a known height and a rebound pendulum. The drop weight test differs in that the particles are placed on a hard surface and struck by a falling weight. Both these approaches have been used extensively in field of comminution. In recent years, the drop weight

apparatus are being replaced by twin pendulum. The standard drop weight device is fitted with a 20 kg mass, which can be extended to 50 kg. The effective range of drop heights is 0.05 to 1.0 m, which represents a wide energy range from 0.01 to 50 kWh/t (based 10-50 mm particles). Following sample preparation the mean mass of each set of particles to be broken is calculated. The results from the drop weight tests provide an energy/input size/product size relationship. This relationship is analysed using a set of curves to describe the size distribution produced from breakage events of increasing size reduction or energy input (Bearman et al, 1997).

Narayanan and Whiten (1998) have widely used a novel procedure for estimation of breakage distribution functions of ores from the so-called *t-family* of curves. In this method, the product size distribution can be represented by a family of curves using marker points on the size distribution defined as the percentage passing( $f$ ) at a fraction of the parent particle size. Thus,  $h$  is the percentage passing an aperture of half the size of the parent particle size,  $U$  is one quarter and  $t/10$  is one-tenth of parent particle size. They have proposed empirical equations for relating the reference curve data  $t/10$  with the impact energy.

The  $t_m$ , versus  $t_{ig}$  relationships can then be used to predict the product size distributions at different grind times (Sand & Subasinghe, 2004).

The  $t_{jo}$  value is related to the specific comminution energy by the equation:

$$t_m = A[1 - e^{-bE^n}] \quad (1)$$

where,

$t_{jo}$  = percentage passing 1/10 of the initial mean size,

Ecs = specific comminution energy (kWh/t)

A, b = ore impact breakage parameters

In the drop weight test, a known mass falls through a given height onto a single particle providing an event that characterisation of the ore under impact breakage. Although, the drop weight test has advantages in terms of statistical reliability and the potential use of the data from the analysis, it has a number of disadvantages, particularly the length of time taken to carry out a test. For each drop weight test, 15 samples are tested in 5 size fractions at 3 levels of energy input (Kingman et al, 2004).

In this study, breakage behavior of three different limestones in a laboratory impact crusher was investigated. It is known fact that there are many difficulties and problems in drop weight test method. A new model is developed by *t-family* value evaluation and Bond work index- approach, and this model is tested.

## 2 MATERIALS AND METHOD

### 2.1 Material

Three different limestone samples taken from different region of Turkey were used as the experimental materials. The chemical properties of the limestone samples are presented in Table 1.

Table 1. Chemical composition of limestone samples used in experiments

Oxides (%)	Limestone I	Limestone II	Limestone III
CaO	31.03	46.85	48.99
SiO <sub>2</sub>	0.05	8.45	10.60
Al <sub>2</sub> O <sub>3</sub>	0.90	1.02	1.07
Fe <sub>2</sub> O <sub>3</sub>	0.00	0.35	0.59
MgO	22.42	0.92	1.11
SO <sub>3</sub>	0.02	0.07	0.09
Na <sub>2</sub> O	0.07	0.02	0.04
K <sub>2</sub> O	0.10	0.06	0.08
L.O.I	45.24	36.50	38.72

### 2.2 The test of Standard ball mill Bond grindability

The standard Bond grindability test is a closed-cycle dry grinding and screening process, which is carried out until steady state condition is obtained. This test was described as follow (Bond and Maxson, 1943; Yap et al., 1982; Austin and Brame, 1983; Magdalinovic, 1989):

The material is packed to 700 cc volume using a vibrating table. This is the volumetric weight of the material to be used for grinding tests. For the first grinding cycle, the mill is started with an arbitrarily chosen number of mill revolutions. At the end of each grinding cycle, the entire product is discharged from the mill and is screened on a test sieve ( $P_i$ ). Standard choice for  $P_i$ , is 106 micron. The oversize fraction is returned to the mill for the second run together with fresh feed to make up the original weight corresponding to 700 cc. The weight of product per unit of mill revolution, called the ore grindability of the cycle, is then calculated and is used to estimate the number of revolutions required for the second run to be equivalent to a circulating load of 250%. The process is continued until a constant value of the grindability is achieved, which is the equilibrium condition. This equilibrium condition may be reached in 6 to 12 grinding cycles. After reaching equilibrium, the grindabilities for the last three cycles are averaged. The average value is taken as the standard Bond grindability ( $Q_g$ ).

The products of the total final three cycles are combined to form the equilibrium rest product. Sieve analysis is carried out on the material and the results are plotted, to find the 80% passing size of the product ( $P_i$ ). The Bond work index values ( $W_i$ ) are calculated from the equation below.

$$W_i = 1.1 * \frac{44.5}{P_i^{0.23} * G_b^{0.82} * \left[ \left( \frac{10}{\sqrt{P_{80}}} \right) - \left( \frac{10}{\sqrt{F_{80}}} \right) \right]} \quad (2)$$

$W_i$  : Bond's work index, (kWh/1)

$P_i$  : screen size at which the test is performed (106 Uni)

$G_b$  : Bond's standard ball mill grindability, net weight of ball mill product passing sieve size  $P_i$  produced per mill revolution, (g/rev)

$P_{80}$  and  $F_{80}$  - sieve opening which 80% of the product and the feed passes, (xm)

## 3 EXPERIMENTS

Firstly, Standard Bond's grindability tests were made for three limestone samples. Results of tests, Bond grindability values of limestone samples were

appeared 6.14 g/rev, 1.69 g/rev and 1.54 g/rev, Bond work index values were calculated 4.44 kWh/t, 10.10 kWh/t and 13.53 kWh/t, respectively. Then, the laboratory horizontal shaft impact mill, rotating at 2840 rpm, driven by 1.1 kW motor, carry three rows of hammers, were used in the experiments. One kilogram sample of six mono size fractions (-6.7+4.75, -4.75+2.8, 2.8+1.7, -1.7+1.18, 1.18+0.600, -0.600+0.355 mm) were prepared and crushed in a laboratory scale impact mill for determination of the *t*-family curves. Each sample was taken out of the impact mill and sieved product size analysis.

Results of *t*-family curves versus mean size fraction for three different limestone are shown in Figure 1-3.

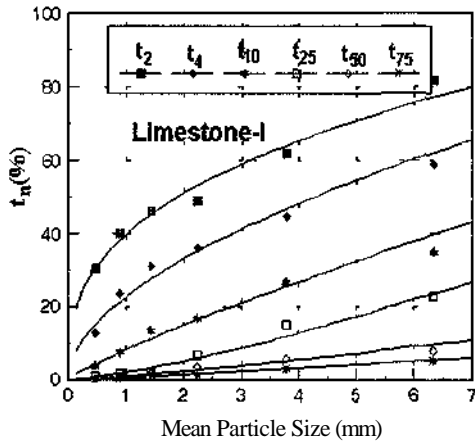


Figure 1 *t<sub>n</sub>*, versus mean size fraction for limestone-I

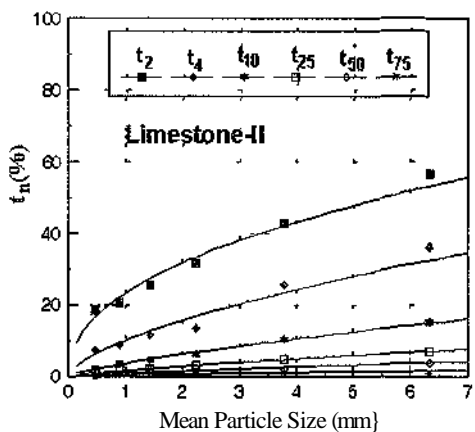


Figure 2 *t<sub>n</sub>*, versus mean size fraction for limestone-II

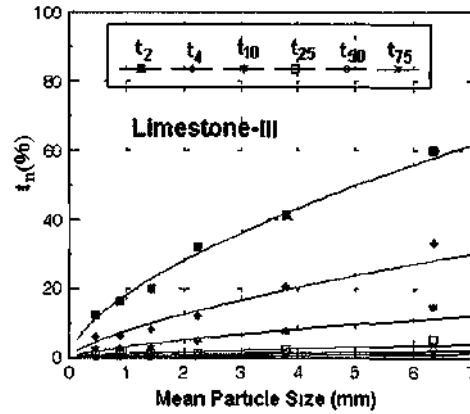


Figure 3 *t<sub>n</sub>*, versus mean size fraction for limestone-III

#### 4 PROPOSED MODEL

Narayanan and Whiten (1998) that the cumulative fraction of products passing  $1/n^*$  of the mean size was denoted by  $t_n$ . It was also reported that this relationship was applicable to different ore types tested under different impact loading conditions. A similar relationship has been observed  $t_n$  values for crushing products in the direct laboratory impact mill and forms the basis of the proposed model.

In this work, the relationship between the cumulative percentage passing ( $t_n$ ) with Bond's work index ( $W_i$ ) and mean feed size ( $X$ ) was empirically described by Eq. (3).

$$t_n = \frac{406.35}{W_i^{0.921} * n^{1.1}} X^{0.108 W_i^{0.663} * n^{2.47 W_i^{-1.184}} \quad (3)$$

where,

$t_n$ , the cumulative percentage passing ( $1/n^*$ ) of the mean particle size (%)

$W_i$ , Bond's work index of limestone (kWh/t)

$X$ , Mean particle size (mm)

The experimental values and the calculated results obtained by Eq. (3) were compared in Figure 4. Eq. (3) mostly satisfies the experimental values in a wide range of feed size, and Eq. (3) is useful especially when evaluating the particle size proportion in the actual operation by a high regression value ( $r^2=0.88$ ).

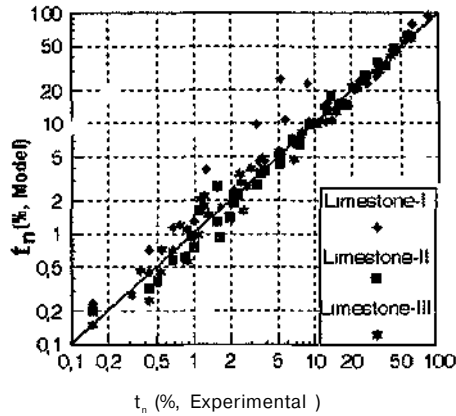


Figure 4 Comparison of experimental and calculated  $t_n$  value for limestone

#### CONCLUSIONS

In this study, laboratory crushing tests of three different limestones with an impact mill were carried out. The effects of mean particle size and Bond's work index of limestones on product size distribution were investigated.

The results showed that limestone-I sample was more friable than limestone-II, which was more friable than limestone-III. A set of  $t$ -curves were calculated from the laboratory impact mill, and a new model was developed.

Obtaining  $t$ -family values from drop weight apparatus is time consuming and difficult. The mathematical model based on impact crusher results, is found to be more appropriate in determining  $t$ -family values than drop weight apparatus.

There are not many studies on the effects of rotor speed, lining design, hammer design and feed dose of limestone in impact crushers, which are used in quarries and mineral processing plants. For this

purpose, similar mathematical models should be developed for different work parameters for various materials and various crusher types.

#### REFERENCES

- Austin, L G and Brame, K, 1983 A comparison of the Bond method for sizing wet tumbling mills with a size-mass balance simulation method *Powder Technology* Vol 34 261-274
- Bearman, RA, Bnggs, CA, Kojovic, T, 1997 The application of rock mechanics parameters to the prediction of comminution behaviour *Minerals Engineering* Vol 10 255-264
- Bond, FC and Maxson, WL, 1943 Standard grinding tests and calculations *Trans SME-AIME* Vol 153 362-372
- Djordjevic, N, Shi, FN, Morrison, RD, 2003 Applying discrete element modelling to vertical and horizontal shaft impact crushers *Minerals Engineering* Vol 16 983-991
- Kingman, S W, Jackson, K, Cumbane, A, Bradshaw, S M, Rowson, N A, Greenwood, R, 2004 Recent developments in microwave assisted comminution *Int J Mineral Processing* Vol 74 71-83
- Magdalinovic, N, 1989 A procedure for rapid determination of the Bond work index *Int J Mineral Processing* Vol 27 125-132
- Narayanan, S S, Whiten, WJ, 1988 Determination of comminution characteristics from single particle breakage tests and its application to ball mill scale-up *Trans Inst Min Metall (Section C)* Vol 97 115-124
- Sand, G W, Subasinghe, G K N, 2004 A novel approach to evaluating breakage parameters and modelling batch grinding *Minerals Engineering* Vol 17 1111-1116
- Yap, R F, Sepulveda, J L and Jauregui, R, 1982 Determination of the Bond work index using an ordinary laboratory batch ball mill *Design and Installation of Comminution Circuits* A L Mular (Co-Editor) Soc Mm Eng AIME, USA 176-203

## Performance Evaluation of ÇBİ Flotation Plant Using Mineralogical Analysis

Z. Ekmekçi, M. Can, Ş.L. Ergiın, Ö.Y. Gülsoy, H. Benzer & İ. B. Çelik  
*Hacettepe University, Mining Engineering Department, Beytepe - Ankara*

**ABSTRACT:** Performance evaluation of ÇBİ Cu-Zn flotation plant was presented based on size-by-size materials balance and mineralogical analysis. Mineralogical analysis was performed mainly by using Clemex image analysis system and for some critical streams QemSCAN system. Although, the performance evaluation was performed for all of the streams in the plant, in this paper only the results of main streams were given for simplicity. The results revealed that finer grinding to prevent the loss of copper at +50 /ım fraction in combination with modification of flotation conditions to minimize the loss of valuables at -9 /ım size fraction would improve the performance of the flotation plant.

### 1. INTRODUCTION

Çayeli complex Cu-Zn sulphide ore deposit is situated in the North-East of Turkey. The concentrator treats a complex base metal ore having typical feed composition of 4.32 % Cu and 4.51 % Zn. The flotation feed is a mixture of yellow ore with high Cu content and black ore with high Zn content mined in the same region. The major sulphide minerals are pyrite, chalcopyrite and sphalerite associated with minor amounts of bornite, tennantite and galena (Akçay and Arar, 1998).

Performance of flotation concentrators need to be assessed both routinely and periodically to obtain maximum recoveries. Routine assessments are performed to monitor operations, and periodic assessments to evaluate performance and to identify processing problems. The assessment process involves collecting and analyzing representative samples and interpreting the data. The techniques used to analyse the samples are chemical and quantitative mineralogical analyses. Elemental recoveries are determined by materials balance performed throughout a circuit. When problems are indicated by the chemical assays and materials balance, a quantitative mineralogical analysis is needed for detailed interpretations (Petruk, 1992). Quantitative mineralogical data include mineral quantities, size distributions of free and locked

mineral grains, percentage of minerals that is liberated and locked.

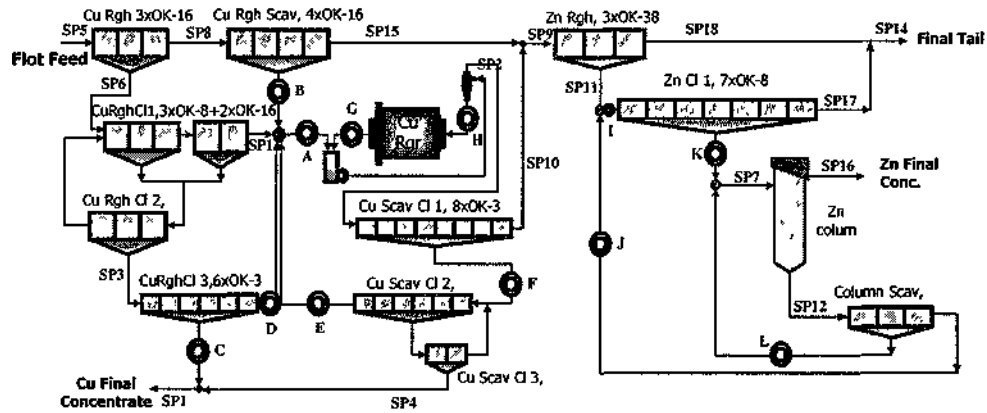
Performance of evaluation of the ÇBİ Cu-Zn flotation plant was performed by using chemical and quantitative mineralogical analyses. For this purpose a detailed sampling survey was performed in the copper and zinc flotation sections in the plant. Pulp samples from almost all of the streams were taken to determine performance of every stage in the flotation plant. However, in this paper, only the main streams were used in the performance analysis.

### 2.SAMPLING SURVEY

The sampling survey was undertaken at 148 dtph feed rate. The locations of the sampling points are illustrated in Figure 1. In the circuit, many streams were sampled by an automatic sampling system called multiplexer. The other flows were sampled by a specially designed sampling device. Before the sampling survey the operational parameters were monitored for 4-5 hours to ensure steady state operation during the survey. The sampling was performed sequentially four times over a period of two hours to obtain an adequate amount of representative samples.

Size distributions of the samples were determined by the combination of wet sieving and

cyclosizer down to 9  $\beta m$ . The size fractions of +50  $\mu m$ , -50+36  $\beta m$ , -36+20  $\mu m$ , -20+9  $\mu m$  and -9  $\beta m$  were prepared for chemical and mineralogical analysis.



SP : Samples from Multiplexer

Figure 1. Location of the sampling points.

### 3. MINERALOGICAL ANALYSIS

The bulk work was done using the Clemex optical image analysis system. Mineralogical analysis of the samples (excluding -9  $\mu m$  fraction) were performed for all of the streams using Clemex image analysis system at Hacettepe University, Mining Engineering Department. In addition to that some of the critical samples were also analysed by the QemSCAN system at CSIRO, Australia.

#### 3.1. Clemex System

Polished sections were prepared using 50 gr of representative samples. The samples were mounted in cold mounting resins and ground on the SiC discs with 400-, 600-, 1000- and 1200- mesh grain size. The ground samples were polished in three different steps by using the diamond abrasives with 3, 1 and 0.25  $\mu m$  grain size.

Clemex Vision PE is the software program used for quantification of the images taken by an optical microscope equipped with a high resolution camera and motorized stage. Following image acquisition from polished sections, suitable algorithm instructions (a routine) are brought together in order to describe an image. A routine consists of a sequence of operations that are performed on each

image or field of analysis. The goal is to produce a representative binary detection of the microstructure and obtain meaningful measurements of a particular feature. The routine is built once on a typical field, and then it is repeated automatically by a motorized stage on any number of fields, generating results for the total area covered in the analysis. So it makes possible to perform the analysis on many numbers of features or particles.

#### 3.2. Assay Reconciliation

As a check of the reliability of the measurements a comparison was made between the true chemical assay and the assays calculated from mineral modal analysis. QemSCAN identifies minerals on a chemical basis and accepted as the most reliable quantitative image analysis method. Comparison of the assays is shown in Figure 2. The excellent agreement shown confirms that QemSCAN is accurately identifying the mineral phases in the samples.

Comparison of the assays for Clemex system is shown in Figure 3. The results showed that the mineral phase identification is quite good, but not as accurate as QemSCAN. This was related to the segmenting of the optical image, which is always

more difficult than a SEM image. But in general the results are reasonable for sound interpretation.

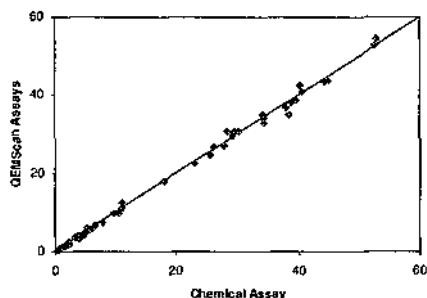


Figure 2. Comparison of the chemical assays performed with standard Atomic Absorption Spectroscopy (AAS) and QEMScan methods.

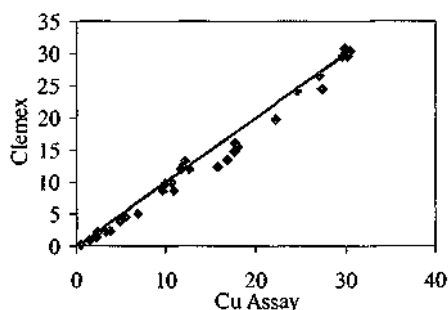


Figure 3. Comparison of Cu assay measured by standard AAS method and calculated from Clemex system.

#### 4. MASS BALANCING

In any sampling operation, some errors are inevitable due to dynamic nature of the system, the physical conditions at a particular point, random errors, measurement errors and human errors. Mass balancing involves statistical adjustment of raw data to obtain the best fit estimates of flowrates.

During sampling surveys, excess data were collected in some points to obtain reliable solution in mass balancing. After having Cu, Zn and Fe assays of the samples, mass balancing studies were commenced. Using mass flow rate of the fresh feed and chemical assays of the streams, flowrates and recoveries of copper, zinc and pyrite in each stream were calculated. Mass balancing studies were carried out by using a step by step approach around various nodes and finally for the whole flotation plant. Therefore, the calculations were checked and verified for different routes (Convergence limits in

all iterations were chosen as 10'. Mass balancing of the raw data was performed by using JKSimMet software). The accuracy of the mass balancing is shown in Figure 4 by plotting raw assays vs adjusted assays.

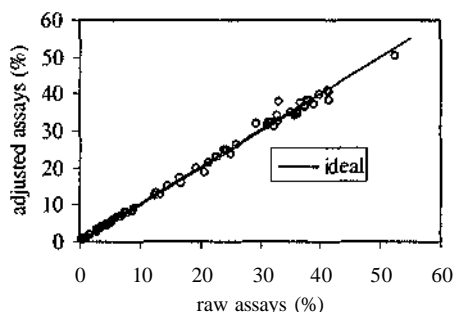


Figure 4. Overall comparison of the raw and adjusted assays.

#### 5. RESULTS AND DISCUSSION

In spite of mineralogical evaluations have been done for all of the streams in the flotation plant, in this paper only the results of the main streams are discussed due to complexity of the circuit.

##### 5.1. Size by Size Recovery and Metal Distribution

In this section, the overall flotation performance of the entire circuit is discussed based on the characteristics of the flotation feed, copper final concentrate, zinc final concentrate and final tail. The mass flow rate, recovery and assays of copper, zinc and pyrite are illustrated in Figure 5.

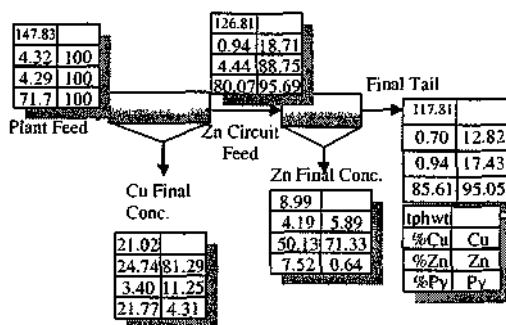


Figure 5. Overall performance of the flotation operation.

For the whole copper circuit, it is not possible to calculate size by size recovery based on the plant feed, the copper final concentrate and the zinc rougher feed, due to the copper regrinding (Figure 1). Therefore, using mass flowrates and mass balanced size by size data for the copper final concentrate and copper circuit tail (zinc rougher feed), a reconstituted feed (virtual feed) for the copper circuit was calculated. Then, size by size recovery in the copper circuit was calculated using the virtual feed. The comparison of Cu metal distribution in the plant feed and the virtual feed is shown in Figure 6. As expected, copper exists in +36µm decreased in the virtual feed, and the amount of copper increased in -20/µm. Therefore, using virtual feed in place of plant feed provided real recovery figures.

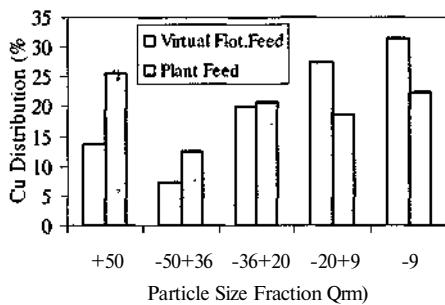


Figure 6. Comparison of Cu distribution between the virtual feed and the plant feed.

The size-by-size recovery of copper and copper distribution of the streams is presented in Figure 7. The copper recovery and grade of the copper final concentrate are 81.29 % and 24.74 % Cu, respectively (Figure 5). However, size-by-size copper recoveries to the copper final concentrate showed that the recovery values in +50/µm and -50+36/µm were as low as 29% and 65%, respectively. As can be seen from Cu metal distribution data, +50/µm fraction contained 46% of the copper loss to the Zn circuit feed and 41% of the copper in the final tail. Therefore, considering the 18.71% total copper loss to the final tail and zinc concentrate (Fig. 5), it was found that 8.6% of the total copper loss was in the +50/µm fraction. Most of the copper lost to the zinc circuit feed at this size fraction reported to the final tail.

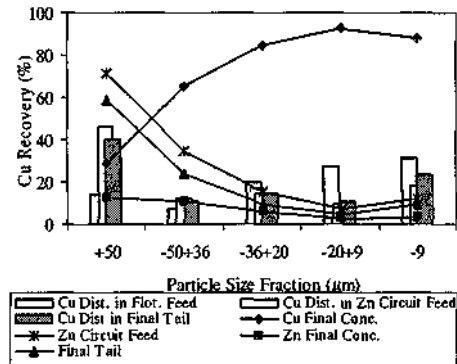


Figure 7. Size-by-size copper recovery of the main streams and Cu metal distribution in the plant feed and Zn circuit feed in ÇBI flotation plant.

The size-by-size recovery of zinc and zinc distribution of the streams are presented in Figure 8. The recovery and grade of the zinc final concentrate were 71.33 % and 50.13% respectively (Figure 5). Figure 8 shows that the recoveries in the coarse (+50 µm) and fine (-9 µm) particle fractions are substantially lower than the medium size range. The majority of zinc loss occurred at these size fractions. Zn distribution in the final tail showed that these fractions contained 2/3 of the Zn. The zinc lost to the copper concentrate increases as the particles size decreases. Considering the total 11.25 % Zn loss to the copper final concentrate (Fig 5), 10.65% of the Zn lost was due to -36µm fractions.

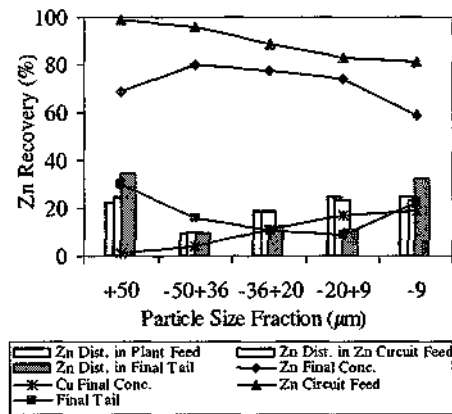


Figure 8. Size-by-size zinc recovery of the main streams in ÇBI flotation plant.

## 5.2. Mineralogical Evaluations of the Main Streams

### Plant Feed

The results of mineralogical analysis of the plant feed are given in Figure 9 as a function of particle size fractions. It must be noted that mineralogical analysis of -9 *fm* fraction has not been performed and hence this fraction is not included in the graph. However, liberation state of -9 *fm* fraction was assumed to be similar to the -20+9 *fm* fraction. Figure 9 shows that about 55 % of the plant feed is composed of liberated pyrite particles, mainly at -36 *fm* fraction. The total liberation of both chalcopyrite and sphalerite was about 75% (liberation of -9 /*tm* fraction assumed as the same with -20+9/*tm* fraction). The locked chalcopyrite particles are mainly found with pyrite rather than sphalerite. Besides, the locked chalcopyrite/pyrite particles are mostly accumulated in -36 /*tm* fraction. Similar behaviour is also observed with sphalerite/pyrite particles.

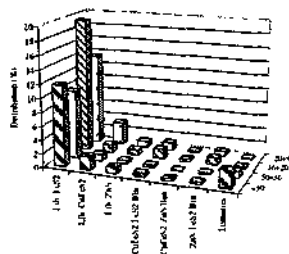


Figure 9. Modal analysis of the flotation feed for different size fractions.

The amount of ternaries in the +50 *fm* and -50+36 /*tm* fractions is considerably higher than the finer fractions. In spite of that the amount of chalcopyrite/pyrite, chalcopyrite/sphalerite and sphalerite/pyrite binary particles is very low compared to the ternaries in these fractions. Mineral distribution of the ternary particles in +50 *fm* and -50+36 *fm* fractions are also calculated and illustrated in Figure 10. The results show that the amount of pyrite in both fractions is higher than chalcopyrite and sphalerite, particularly in -50+36 *fm* fraction. Chalcopyrite occupies larger area than sphalerite, indicating that majority of these particles may be considered as chalcopyrite/pyrite binary particles with small inclusions of sphalerite. Considering the higher percentage of pyrite and

coarse size, these particles can be liberated by finer grinding of the flotation feed.

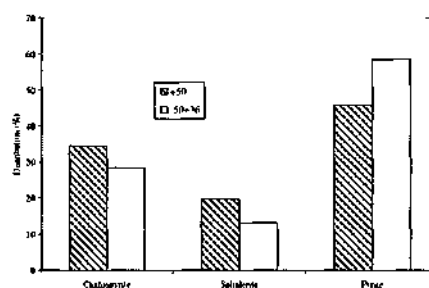


Figure 10. Mineral distribution of the ternary particles at +50 /*im* and -50+36 *fm* fractions of plant feed.

### Copper Final Concentrate

The fine sphalerite particles are considered to be recovered mainly by entrainment and the coarse particles in the form of locked particles with chalcopyrite, as the flotation conditions were not suitable for flotation of sphalerite. Di-isobutyl dithiophosphinate, a selective collector for copper minerals, was used as collector in strongly alkaline condition (>pH 11.5). In these conditions liberated sphalerite and pyrite particles were considered to report to the copper concentrate by entrainment.

Mineralogical analysis of the copper final concentrate showed that liberation of the chalcopyrite was 81.55% (liberation of -9 *fm* fraction assumed as the same with -20+9/*tm* fraction) (Figure 11). More than 30 % of these particles are found at -36 *fm* fraction. In addition to that considerable amount of chalcopyrite-pyrite and chalcopyrite-sphalerite binary particles are also recovered to the copper final concentrate. Therefore, the large portion of pyrite and sphalerite recovered to the concentrate are in the form of locked particles. Besides, very fine pyrite particles (-20 *fm*) are also recovered most probably by entrainment. The mineralogical analysis of the copper final concentrate clearly shows that finer grinding is required to decrease the amount of pyrite and sphalerite at -36 /*tm* fraction. However, it must be noted that in the case of fine regrinding, the flotation conditions must be suitable for fine particle flotation, in terms of both improving flotation of -9 *fm* chalcopyrite particles and minimizing entrainment of fine pyrite and sphalerite particles.



in the existing chemical conditions. As the particle size decreases the percentage of pyrite in the ternary particles increases. Pyrite is mainly recovered with the locked particles and to some degree at very fine size due to entrainment.

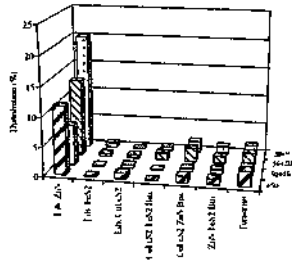


Figure 15. Modal analysis of zinc final concentrate.

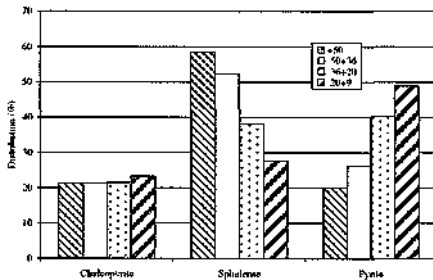


Figure 16. Mineral distribution of the ternary particles at various fractions of zinc final concentrate.

The mineral distributions of chalcopyrite/pyrite and chalcopyrite/sphalerite binary particles at 36+20 /tm and -20+9 /im fractions are given in Figures 17 and 18 respectively. The area percentage of chalcopyrite in chalcopyrite/pyrite binary particles is about 20 % for both size fractions. This value increased to about 30 % in the chalcopyrite/sphalerite particles. It must be noted that these binary particles are mainly in fine size range and these particles must be removed in the copper circuit, possibly by regrinding and more efficient fine particle flotation.

*Final Tail*

When pyrite was included, the liberation state of the other minerals is not clearly illustrated due to large amount of pyrite in the final tail. More than 70 % of the tailing stream (-9 fixa is not included) consists of liberated pyrite particles mainly at -36 /tm fraction.

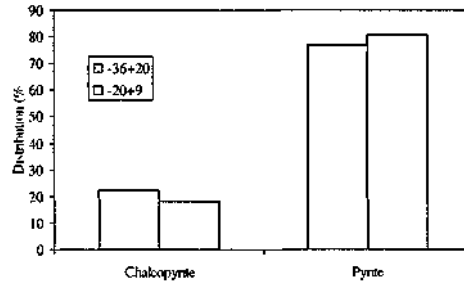


Figure 17. Distribution of chalcopyrite and pyrite in chalcopyrite/pyrite binary particles in -36+20 /im and -20+9 /im fractions of zinc final concentrate.

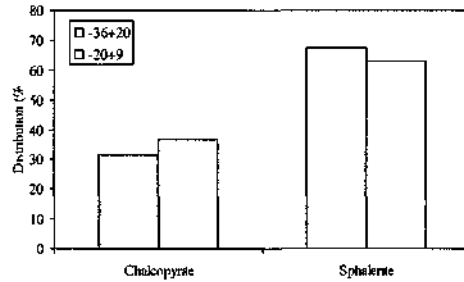


Figure 18. Distribution of chalcopyrite and pyrite in chalcopyrite/pyrite binary particles in -36+20 /un and -20+9 am fractions of zinc final concentrate.

Therefore, the liberation state of chalcopyrite and sphalerite are illustrated without liberated pyrite in Figure 19. The liberation of chalcopyrite and sphalerite were 28.32 and 46.28%, respectively (liberation of -9 /tm fraction assumed as the same with -20+9/im fraction). The coarse particles reported to the tailings are generally in the form of locked particles with slow floatability. The copper loss is mainly in the form of chalcopyrite/pyrite binary particles at -36+20 /im and -20+9 /im fractions and ternary particles at +50 /im and -50+36 /im fractions. As it was explained above, the reason for the measurement of high percentage of ternary particle in the coarse size fractions may be due to the high sensitivity of QemScan, which has the ability to detect very small inclusions of either sphalerite or chalcopyrite. However, it appears from Figure 20 that the ternary particles contain mainly pyrite. The chalcopyrite and sphalerite contents are higher in +50 /im fraction than the finer fraction. Therefore, the zinc loss to the final tailing from +50 /im fraction (Figure 9) is mainly from the ternary

particles and to a lesser degree from sphalerite/pyrite binary particles.

difficult and are reported to the final tail. But they are suitable to liberate by finer grinding due to very high content of one mineral (pyrite) (Petruk, 1992).

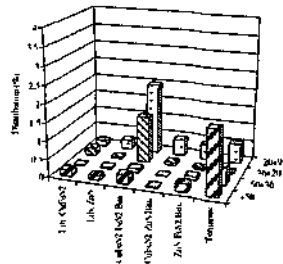


Figure 19. Modal analysis of the final tail in the absence of pyrite.

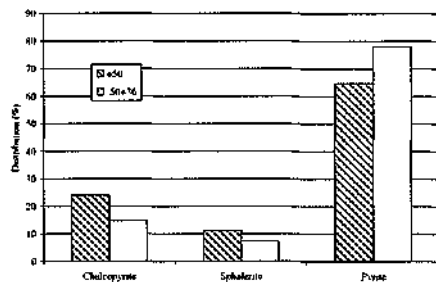


Figure 20. Mineral distribution of the ternary particles at +50 μm and -50+36 μm fractions of final tail.

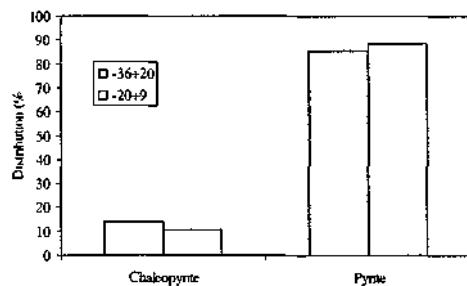


Figure 21. Distribution of chalcopyrite and pyrite in chalcopyrite/pyrite binary particles at -36+20 μm and -20+9 μm fractions of final tail.

Chalcopyrite is also lost with chalcopyrite/pyrite binary particles finer than 36 μm. Distribution of chalcopyrite and pyrite in these particles is given in Figure 21. These particles contain even less than 10 % chalcopyrite which makes their flotation very

## 6. CONCLUSIONS

The main copper loss was from +50/μm fraction. The recovery of +36/μm fraction was significantly lower than the others. Therefore, it can be concluded that finer flotation feed would improve the performance of the copper circuit. Zinc reported to the copper final concentrate is in the fine size ranges and recovered mainly by entrainment. For the locked particles, very fine regrinding is necessary. This should be applied with caution due to possibility of losing copper through very fines.

In the zinc circuit, the losses were from -9/μm and +50/μm fractions. Finer flotation feed would also decrease losses through +50/μm. However, further studies to improve -9/μm recovery are required.

## Acknowledgement

The authors gratefully acknowledge technical and financial support of Çayeli Bakır İşletmeleri A.Ş.

## REFERENCES

- Akçay, M and Arar, M., 1998; Geology, mineralogy and geochemistry of the Çayeli massive sulphide ore deposit, Rize, NE Turkey. *Mineral Deposits: Processes to Processing*, (Ed. Stanley et al.), Balkema, Rotterdam, 459-462.
- Petruk, W., 1992; Applied mineralogy and materials balancing procedures. Evaluations of flotation concentrators. *Innovations in Flotation Technology*, NATO ASI Series, Vol 208, Kluwer Academic Publishers, 125-148.

## Utilization of Sandy Clay "Kosarno" for other Raw Materials Production

D. Skendzic, S. Jugovic & B. Todorovic

*Keramika, 11400 Mladenovac, P.O.B. 44, Serbia and Montenegro*

M. Djuricic

*ITNMS, 11000 Belgrade, P.O.B. 390, Serbia and Montenegro*

**ABSTRACT:** The paper shows following: the derivation procedure, material balance and the results of physical and chemical qualities of the quartz, quartz-feldspar sand and clay concentrate.

Using the procedure of moist sorting we can get the concentrate of: quartz (92,6% SiO<sub>2</sub>), quartz-feldspar sand (64,5% quartz, 25,6% feldspar, 8,5% mica) and clay (62% kaolin, 22,3% quartz and 10,35% microklin). The kaolin has been concentrated in the class -0.063 mm, the feldspar in the class -0.8+0.09 mm, and most of all in the class -0.09+0.063mm. The type of the clay is ball clay, chemical composition (%): SiO<sub>2</sub> 52.02, Al<sub>2</sub>O<sub>3</sub> 27.78, Fe<sub>2</sub>O<sub>3</sub> 2.82, CaO 0.65, MgO 0.54, K<sub>2</sub>O 1.75, Na<sub>2</sub>O 0.2 and L.O.I. 14.06 of great plasticity, good workable, and sensitive to drying.

### 1. INTRODUCTION

There are several kinds of quality raw materials; kaolin, clay, feldspar and quartz sand which have been used individually for the production of the sanitary ware, porcelain and the tiles. Depending of their own physical and chemical qualities they can be mixed in an appropriate relation to reach the necessary physical, chemical and mechanical attributes of the final product. As a replacement for the pure feldspar and quartz sand it can be used quartz-feldspar sand (Bornioli et al. 1995, Mandt 1977), pegmatite, mica (Radford et al. 1985), porphyry (Ociepa et al. 1988), etc.

There have been used lately the purposely made composites, i.e. homogeneous mixtures of the single clays or raw materials in an appropriate relation and with appropriate physical and chemical attributes.

Using the composites and feldspar and quartz sand replacements, the production costs are reduced.

The mine "Kosarno" clays belong genetically to a tertiary miopliocene deposit of the basin in Mladenovac. The deposit consists of three parts. For the production of the ceramics the most interesting is the second deposit part, which consists of four layers of ceramic and fireproof clays. The fourth layer (K-2) round 2 m great, is a fireproof sandy (rest on the sieve 0.1 mm 17-30%) plastic clay, dark gray

colored, with feldspar fractions. It has a contact with the third deposit part.

The third deposit part is a round 20 m great layer of a sandy gray clay (rest on the sieve with 0.1 mm is 25-55 %), a mixture of quartz, clay, feldspar, kaolinised granite and mica. The composition of a layer is no homogeneous. With a deep decreases the clay content and the sand and feldspar content increases. It has been used in the production of tiles as a cheap feldspar, quartz and clay source.

Considering the K-2 and K-5 clay layer thickness, the exploitation technology with an excavator does not secure the permanent quality, and mostly is the mixture with a dominant content of the K-5 clay exploited.

### 2. EXPERIMENTAL WORK

#### 2.1 Procedure

The clay K2 has been comminuted -5mm, dried on 105 °C, blunged in the water (S:L=1:2), without adding of deflocculant and disseminated on the sieves (d) 2.5, 1.6, 0.8, 0.2, 0.091 and 0.063 mm.

The chemical and rational analyses are determined for each sieving rest as well as the presence of minerals (microscope analysis).

From underflow of the sieve 0.063 is the clay (K2-63) vacuum filtration isolated. It has been

determined the particle size distribution for hydrocyclons in the class -63+0 jxm, and the clay in the class -11+0 /im (K2-11 /tm) isolated

The physical and chemical attributes of the clay are determined, as well as its rational content and the reaction during the diyng (Bigot curve) and heating (DTA, TG)

The rational analysis remainder on sieve has been calculated according to the chemical analysis of each class, and hypothesis that the loss of ignition arises from the mica type muscovite  $KAl_2(Si_3Al)O_{10}(OH)_2$

## 2.2 Results

The physical attributes of the clay K2 are bending strength 154.1 N/cm<sup>2</sup>, shrinkage (105/1240°C) 6.1/6.5%, remainder on sieve 0.091 mm 24.8%, and water plasticity 27% (Pfeferkom 3.3) The chemical analysis has been shown in Tables 1 The Bigot curve has been shown on the Figure 1

Particle size distribution and the chemical analysis of the remainder on sieve has been shown in Tables 2 and 3 The chemical and rational analysis has been shown in Table 3 and 4 The mineralogical analysis has been shown in the Table 5

The physical qualities of the clay K2-63 urn are bending strength 79.7 N/cm<sup>2</sup>, shrinkage (105/1240°C) 6.1/9.5%, and water plasticity 39% (Pfeferkorn 3.3) The chemical analysis and partial size distribution of the clay in the class -0.063+0.00 mm has been shown in the Table 6 and 7

The DT and TG of the K2-63 um and K2-11 um clay has been shown on the Figure 3 and 4 The DT and TG of the K2-63 um and K2-11 um clays has been shown on the Figure 4

Table 1 The chemical analysis of the clay K2 (%)

SiO <sub>2</sub>	Al <sub>2</sub> O <sub>3</sub>	Fe <sub>2</sub> O <sub>3</sub>	CaO	MgO	K <sub>2</sub> O	Na <sub>2</sub> O	IL
63	47	21	67	2	34	105	0
52	15	0	2	9	33		

Table 2 The particle size distribution of the sieve residue (%)

d (mm)	0.063	0.091	0.20	0.80	1.60	2.50
%	14.7	21.6	29.7	25.4	7.1	3.3

Table 3 The chemical analysis of the sieve residue

d /mm	S.O.	AUO.	FcO.	CaO	MgO	K <sub>2</sub> O	Na <sub>2</sub> O
63	82.76	9.05	0.60	0.35	0.20	5.00	1.55
91	88.18	4.84	0.21	0.34	0.18	4.55	0.78
200	90.02	5.23	0.46	0.28	0.12	3.63	0.22
800	92.60	3.69	0.83	0.07	0.05	2.22	0.24

Table 4 The rational analysis of the sieve residue

d(um)	Quartz	K-feldspar	Na-feldspar	Mica
63	54.30	22.79	13.10	7.73
91	65.66	14.04	6.59	14.64
200	74.82	18.73	1.69	3.14
800	82.66	6.61	1.69	7.41
200.63	64.93	18.55	7.05	8.50

Table 5 The mineralogical analysis of the sieve residue

d (mm)	Description
2.54	The corns of quartz (85%) are racily large, partly rotund, with the parts of the mica granular to uniform forms, and with perceived breach of the twins The corns of the feldspar (15%) are bited into by the transformation, but they retained the primarily form with perceived parts of a fine corn quartz The look of a corn indicates that they originated as an effect of the mountain rock morphs
150	The quartz and feldspar corns are identical with the 2.54 mm sieve corns They differ because of parts of quartz with sphen parts and the presence of a black-gray quartz There are also some ferrihydroxide corns
D.80	The quartz appears in fragments It is mostly limpid, sharp edged and wiui shelly break The feldspar corns are bited into by the transformation, they lose their primarily form, they are extremely mat There is some free mica
0.20	The quartz is limpid, in fragments, rarely uniform, with eroded surfaces The feldspar appears once as fresh, and partly bitted into by the transformation The content of the feldspar rises in regard to quartz

Table 6 The chemical analysis of the K2-63 um clay

SiO <sub>2</sub>	Al <sub>2</sub> O <sub>3</sub>	Fe <sub>2</sub> O <sub>3</sub>	CaO	MgO	Na <sub>2</sub> O	K <sub>2</sub> O	IL
52.02	27.78	2.82	0.65	0.54	1.75	0.27	1.41

Table 7 The particle size distribution of me K2.63 |um clay (%)

d(nm)	63-44	44-33	33-23	23-15	15-11	11-0
%	7.76	5.93	4.38	4.76	3.16	74.18

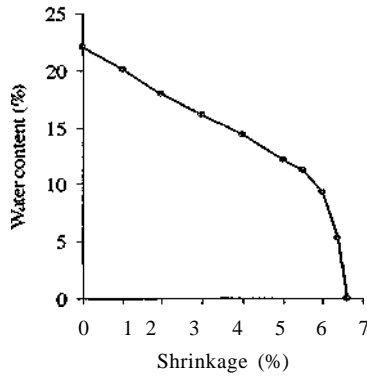


Figure 1 The Bigot curve of the K2 clay

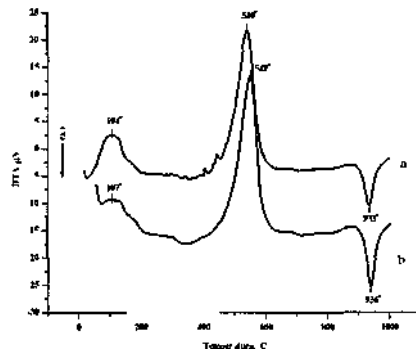


Figure 4 DTA and TG curves of the K2-63 (a) and K2-11 um (b) clays

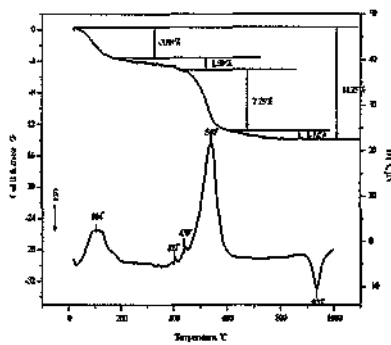


Figure 2 DTA and TG curves of the K2-63 um clay

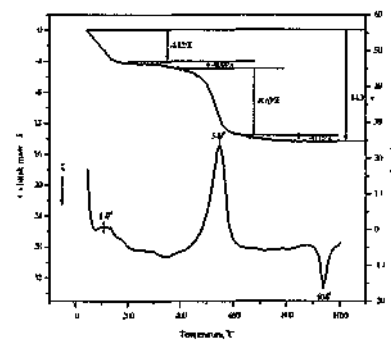


Figure 3 DTA and TG curves of the K2-11 um clay

### 3. DISCUSSION

Making categories using the moist sorting procedure on the control sieve 0.8 mm, 0.063 mm from a sandy clay, has for its result three products as follows

- a) 9.5 % sand (-2.5+0.8 mm)
- b) 17.5 %, quartz-feldspar sand (-0.8 +0.063 mm) and
- c) 63 % clay (-0.063+0.00 mm)

In the sand the quartz corns are limpid, racily large, partly rotund, with parts of the granular to uniform forms of mica, and with perceived breach of the twins, the parts of sphe. Some of them are from black corns. There are also some ferrohydroxide corns (Tab 5)

In the quartz-feldspar sand the quartz is limpid, appears in fragments, sharp edged and with shelly break. The corns of a feldspar are extremely mat as a result of transformation. It is concentrated in the class -0.2+0.063 mm in regard to reduced content of the quartz.

According to its physical and chemical qualities as well as its reaction during drying and heating (Tab 6, 7, Fig 1-4) the clay belongs to the sediment type with a high content poorly orientated kaolinite. The water content to the critical point is 9.45%. The drying shrinkage is 6.38%, and water plasticity 35% (Pfeferkorn 3.3). According to the form of a Bigot curve (Fig 1) the clay is sensitive to drying (K=1.33). If it has been accepted that Fe and Mg were in the structure of the mica the clay contents (%), kaolinite 61.99, ortoklas 10.35, mikrokh 1.7, quartz 27.26, mica 2.5 and anorthite 1.16.

The K2-63 urn and K2-11 jam clays are similar, but according to the magnitude of the effect during dehydration of kaolinite and originating of

*D. Skendzic, S. Jugovic, B. Todorovic & M. Djurtic*

metakaolinite the clay K2-11 fin contents more kaolinite than the clay K2-63  $\mu\text{m}$  (Fig 4)

#### 4. CONCLUSION

In the sorting procedure there have been abstracted 27% of sand (-2.5+0.063mm) and 73% of clay (-0.063 mm)

The sand can be parted into

- the concentrate of a quartz sand (9.5% in class -2.5+0.080 mm) which contents (%)  $\text{SiO}_2$  92.6,  $\text{Al}_2\text{O}_3$  3.62, 0.8  $\text{Fe}_2\text{O}_3$ , and,

- the concentrate of a quartz-feldspar sand (17.5% in class -0.80+0.063 mm) which contents (%) quartz 64.93, orthoclase 18.55, microcline 7.05 and mica 8.5,

The clay which contents (%) kaolinite 62, quartz 27.3, and feldspar 10.35 belongs to a ball clay type

It is fireproof, plastic, good workable and sensitive to drying

#### REFERENCES

- Bomioh R, Cau P, Manm C, Medici C, (1995) "Raw Ceramic Materials in Sardinia (Italy)", *Industrial Ceramics*, (15), 3, p 163-167
- Mandt P, (1977) „Feldspate und Feldspatsand-Bedeutung in der Keramik", *Keram Z*, (29), 5, p 227-228
- Ociepa Z, Slosarczyk A, (1988) "Porphyry Tuff as a Raw Material for the Ceramics Industry", *Interceram*, (8), 6, p 9
- Radford C, Keating R J, (1985) "The Use of Coarse Micaceous China Clay Fraction as Fluxing Material in Whiteware Bodies", Part I, Earthenware, *Interceram*, (5), 5, p 45-48

## Evaluation of Refractory Behaviour of Kaletaş (Turkey) Gold Ore

I Alp, O Celep, H Deveci, T Yilmaz & C Duran  
*Karadeniz Technical University Trabzon, Turkey*

**ABSTRACT:** In this study, the refractory behavior of Kaletaş ore was investigated within a diagnostic approach. Pretreatment of the ore via roasting and ultrafine grinding prior to cyanide leaching was also examined to enhance the gold recoveries. No significant improvement in the extraction of gold by roasting of the ore at 450-600 °C was observed despite the decrease in the cyanide consumption. Two-stage cyanidation of ultrafine ground ore was found to improve the extraction of gold to 93% with the implication of presence of readily recoverable gold and slowly dissolving gold in the ore. Diagnostic leaching provided an insight into the refractoriness of the ore, which could be attributed to the very fine gold particles locked up largely within the carbonates, oxides and sulfides and, to a small extent, within silicates present in the ore matrix.

### 1 INTRODUCTION

Gold ores can be broadly categorized as "free milling" and "refractory" depending on their response to cyanide leaching (La Broy, 1994, Gunyanga et al, 1999). A gold recovery of >90% can be readily achieved with a conventional cyanide leaching of free milling ores (Rubisov et al, 1996). However, refractory gold ores are often characterized by the low gold extractions (<50-80%) in cyanide leaching. The refractoriness of gold ores and concentrates stems primarily from the inherent mineralogical features with reference to the mode of presence and association of gold, and carbonaceous matter present. In practice, the refractoriness has been reported to be caused by (Petruk, 1989, Dunn and Chamberlain, 1997, Browner and Lee, 1998)

- Very fine dissemination (<10 µm) or presence of gold particles as solid solution within mostly pyrite and arsenopyrite
- Association and presence of gold with tellurides and base metal sulfides of lead, copper and zinc
- Carbonaceous matter and silicate minerals present
- Ultrafine gold locked up in the gangue matrix (mostly quartz) or complexes with manganese oxides

A suitable pre-treatment process is often required to overcome the refractoriness and render the gold accessible to the oxidative action of cyanide and oxygen (Gunyanga et al, 1999, Ubaldini et al, 1994, Lehman et al, 2000). Ultrafine grinding, modified cyanidation, roasting, pressure oxidation and bacterial oxidation are the pretreatment methods currently practiced for refractory gold ores and concentrates (Smadmovic et al, 1999, Costa, 1997, Iglesias and Carranza, 1994). Roasting, simple stage process using fluidized bed roaster at around 650°C, is one of the most common methods for the treatment of gold bearing pyrite/arsenopyrite and pyrrhotite concentrates to produce porous calcine and hence to increase the amenability to cyanidation (Roshan, 1990, Long, 2000, La Broy, 1994). Pressure oxidation and biooxidation methods have gained importance in recent years mainly due to the environmental problems (e.g. SO<sub>2</sub> emissions) associated with the roasting process (Smadmovic et al, 1999, La Broy, 1994, Long, 2000, Costa, 1997).

The selection of a particular pretreatment method is based primarily on the economics of gold recovery. However, the determination of the mode of occurrence and association of gold is of fundamental importance to identify the nature of refractoriness and then to manipulate and modulate the process variables to maximize gold recovery within a given pretreatment method. Diagnostic

leaching can provide an insight into the department of gold within ore (Lorenzen and TumiSty, 1992; Henley et al., 2000). It is essentially an analytical tool based on the selective removal of the phases at stages with each stage followed by cyanide leaching step to extract the gold exposed (Lorenzen, 1995; Lorenzen and Van Devender, 1993).

Kaletaş gold ore offers an estimated resource of 362 000 tonnes ore with an average grade of 6.8 g/t Au (Tüysüz et al., 1994). The Kaletaş disseminated gold occurrence, hosted by thin-bedded, silty to sandy limestones, consists of siliceous lenses developed along permeable zones such as fault, fracture and bedding planes. Gold is enriched in silicified limestones, especially along zones of extensive carbonate removal. The gangue minerals are composed of calcedonic quartz, calcite, dolomite, illite and halloysite (Tüysüz et al., 1994, Çubukçu & Tüysüz, 2000).

In previous studies (Alp et al., 2003; Gönen, 1999), in cyanide leaching tests, the gold recovery from Kaletaş ore has been reported to be limited to 50-67%. Roasting (at 550°C) as a pretreatment step before cyanidation was shown to improve the recovery of gold only to 80% (Oktay, 2001).

In this study, the application of roasting, ultrafine grinding and flotation to increase gold recovery from the ore was investigated. Diagnostic leaching procedure was also employed to identify the reason for the low gold recoveries and hence refractory behavior of the ore.

## 2 MATERIAL AND METHOD

### 2.1 Material

A total amount of 150 kg ore sample was obtained from Kaletaş (Gümüşhane) gold deposit. A number of hand-picked pieces of the ore were separated for the mineralogical analysis. The polished sections prepared from the hand-picked pieces for mineralogical examination were examined under an ore microscope (Leitz Wetzlar).

The remaining bulk of the samples was reduced to -4 trim, using jaw and roll crushers, and riffled to obtain 2 kg representative sub-samples. These were then ground in a laboratory rod mill for experiments at different grinding time (Table 1).

Table 1. Changing of particle size of ore versus grinding time.

Grind Time, min	10	20	30	40	50,60,70,80
Passing 38/tm,%	25	40	60	98	100

The chemical composition of the ore sample is presented in Table 2. The ore sample was determined to contain 6.8 g/t Au and 1.2 g/t Ag.

Table 2. Chemical composition of the ore sample

Compound	Content (%)	Element	Content (ppm)
SiO <sub>2</sub>	54.89	Au	6.8
Al <sub>2</sub> O <sub>3</sub>	4.88	Ag	1.2
Fe <sub>2</sub> O <sub>3</sub>	2.38	Cu	281.0
CaO	17.86	Zn	242.0
As	3.88	Pb	359.0
MgO	0.30	Zn	242.0
Na <sub>2</sub> CO <sub>3</sub>	0.09	Sr	223.7
K <sub>2</sub> O	0.14	Sb	101.9
TiO <sub>2</sub>	0.09	Ni	46.0
P <sub>2</sub> O <sub>5</sub>	0.52	V	42.0
MnO	0.03	Co	16.1
Cr <sub>2</sub> O <sub>3</sub>	0.02	Zr	17.9
LOI	16.30	U	6.6
Tot. C	3.75	Cd	2.1
Org. C	0.18	Ga	3.3
		Mo	7.0

The chemical and mineralogical analysis of the samples used in this study indicated that the ore consisted of predominantly quartz, calcite and, to a less extent, silicates and sulphides of Pb, Fe, Zn, As and Cu. Pyrite, realgar, orpiment, marcasite and native sulphur were identified as sulphide phases (Fig. 1-2). Quartz and calcite were the most abundant non-sulphide phase (Fig. 1-3). Pyrite were commonly present as particles of 3-75 µm in size and as finely disseminated within quartz (Fig. 3). Gold were present as native and electrum form (Fig. 1-2). Organic matter was also identified to be present in the ore.

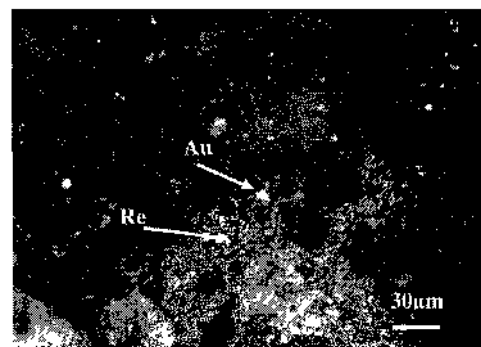


Figure 1. A view of a Au particle (9 µm) as electrum and realgar gram (Re) in quartz matrix.

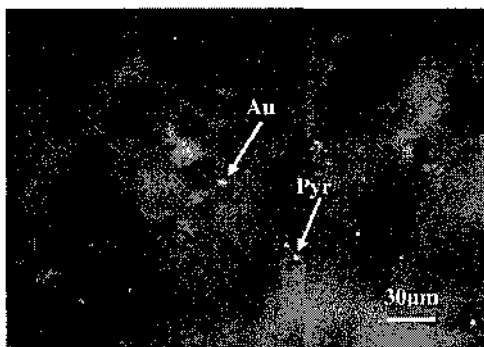


Figure 2. A view of Au (3,5/ım) and pyrite (Pyr) grains in quartz matrix.

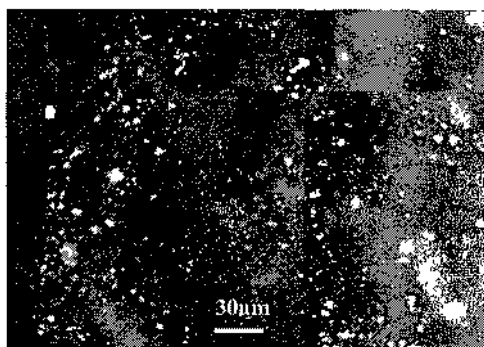


Figure 3. A view of pyrite grains (1-15fıra) disseminated within quartz matrix.

## 2.2 Method

The cyanide leaching tests (24 h) were performed in a glass reactor equipped with a pitched blade turbine impeller rotating at 1400 rpm (Figure 4). NaCN concentration was maintained at 1.5 g/l over the leaching period and the consumption of cyanide was recorded. Roasting of the ore samples (1 h) in 250 g batches were carried out in a furnace set to the predetermined temperature. The calcines produced at different temperatures (450-600 °C) were subjected to cyanide leaching. The experimental conditions for cyanide leaching and flotation tests are shown in Table 3-4.

Diagnostic leach tests involved a series of acid leaching stages aimed to destroy specific minerals, followed by cyanidation of the residue from each stage. Table 5 shows the sequence and conditions of acid leaching steps in diagnostic leach tests. Conditions for two-stage cyanide leaching of ultrafinely ground ore to determine the gold available to cyanidation are presented in Table 6.

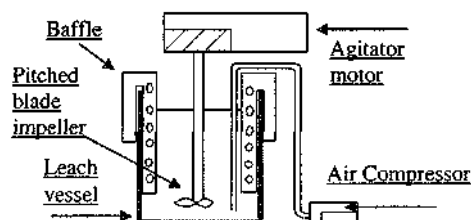


Figure 4. Experimental set-up for cyanide and diagnostic leaching of the ore.

Table 3. Experimental conditions for cyanide leaching of the ore and calcine.

Sample weight, g	250
Water	Tap water
Girind time, min.	10-20-30-40-50-60-70-80
Pulp density, w/w%	25
pH (NaOH)	10-10,5
Agitation, rpm	1450
NaCN, g/l	1,5
Leach time, h	24
Temperature, °C	20±3

Table 4. Experimental conditions for the flotation of the ore

Sample Weight, g	= 1000
Pulp density, w/w %	36
pH	7-7.4
Grind time, min.	10-15-20-30
Aerofloat 208, g/t	100
MIBC, g/t	20
CuSO <sub>4</sub> , g/t	1000
Na <sub>2</sub> SiO <sub>3</sub> , g/t	1000
Agitation, rpm	1250
Flotation time, min.	5

Table 5. Sequence and conditions of diagnostic leaching of the ore sample (80% passing 37 /ım) (Lorenzen and Van Devanter, 1993; Lorenzen, 1994; Henley et al. 2000).

Treatment Stage	Leach Parameter	Minerals likely to be destroyed
NaCN, 1,5 g/l	24 h, pH 10.5	Gold
HCl (12%)	L/S=2:1, 8h 60°C	Calcite, Dolomite, Galena, Pyrrhotite, Hematite
H <sub>2</sub> SO <sub>4</sub> (48%)	L/S=2:1, 5h 80°C	Cu-Zn sulphides, Labile pyrite
HNO <sub>3</sub> (33%)	L/S=2:1, 6h 60°C	Pyrite, Marcasite Arsenopyrite,
HF (20%)	L/S=2:1, 6h	Silicates
Acetonitrile elution (40%)	L/S=2:1, 6h 10 g/l NaCN	Gold adsorbed on carbon

Table 6 Conditions for two-stage cyanidation of ultrafinely ground (6 h) ore

Conditions	Stage	Gold
NaCN (1.5 g/l) 24h, pH 10 >	Stage I	Native, electrum and metastable gold
NaCN (2 g/l), 96 h, pH 12, 1kg/tPb(NO <sub>3</sub> ) <sub>2</sub>	Stage II	Gold tellurides
Remaining gold	Invisible gold, Au selenide-metalloid-sulfides	

Analysis of gold in the samples removed at predetermined intervals was carried out using an AAS. Leach residues at the end of each stage were also analyzed for gold to establish mass balance and determine the gold recovery. CN concentration was determined by titration with silver nitrate using rhodamine as the indicator.

### 3 RESULTS AND DISCUSSIONS

#### 3.1 Cyanide Leaching of the Ore

Figure 5 shows the extraction of gold and cyanide consumption at different grinding times. Decreasing the particle size of the ore appeared not to produce the desired effect. This could indicate the refractory nature of the ore in agreement with the findings of mineralogical analysis. These low gold recoveries suggested the presence of encapsulated gold particles which did not come into contact with cyanide solution. The cyanide consumption was observed to increase with decreasing particle size as illustrated in Figure 5.

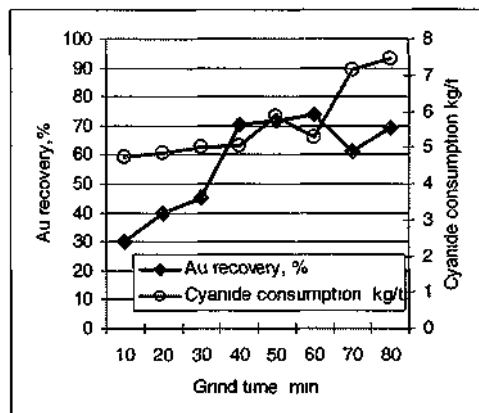


Figure 5 Gold recovery and cyanide consumption versus grind time

#### 3.2 Cyanide Leaching after Roasting of the Ore

In an attempt to decompose the sulfide phases such as pyrite and As-sulfides and hence to expose the locked-up gold in these minerals roasting of the ore as a pretreatment step prior to cyanidation was carried out at different temperatures. As the temperature increased only a limited improvement in the extraction of gold was noted to occur as shown in Figure 6. Highest gold recovery was obtained in the cyanide leaching of the calcine produced at 550°C.

Compared with the untreated ore there was no beneficial effect of roasting (Figure 7) apart from the decrease in the cyanide consumption (Figure 6). It is relevant to note that over an initial leaching period of 1 h -60% of gold was dissolved whilst over the following 23 h the extraction of gold was negligible.

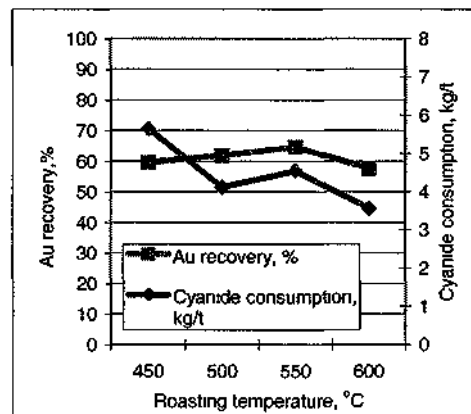


Figure 6 Au recovery and cyanide consumption versus roasting temperature

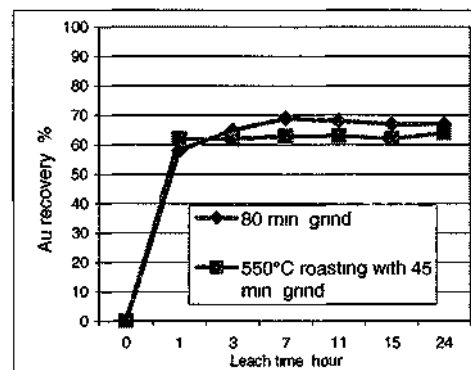


Figure 7 Au recovery leach kinetic with/without roasting

### 3.3 Flotation Tests

Preliminary flotation tests were undertaken to evaluate the recovery of free and sulfide-associated gold (Figure 8). Apart from zinc, consistently unsatisfactory recoveries for gold, copper and iron was obtained despite the production of concentrates with a gold content of 20-37 g/ton. Further detailed tests appeared to be required to improve the recovery of gold.

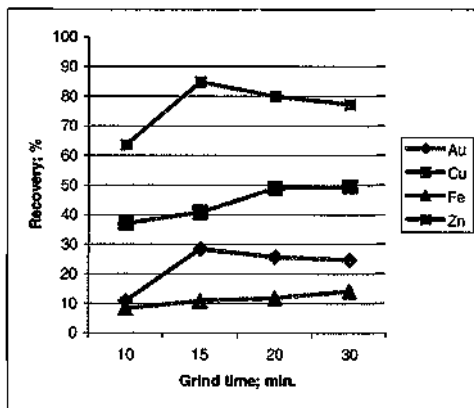


Figure 8. Gold and other metal constituents recovery versus grind time by flotation

### 3.4 Two-Stage Cyanide Leaching of Ultrafine Ground Ore

Figure 9 shows the results of two-stage cyanidation after ultrafine milling of the ore. These tests were designed to clarify whether the low gold extraction was due to the incomplete "liberation" of gold particles for cyanidation. The findings indicated that 74% of gold could be recovered in Stage I using standard cyanidation procedure adopted in this study. Compared with the earlier findings (Figure 5-6) only a limited enhancement with ultrafine milling was apparent.

In Stage II, the residues from Stage I was subjected to extended cyanide leaching using stronger cyanide solution over 96 h. A cumulative extraction of 93% Au was obtained in two-stage process. The gold extraction in Stage I could indicate the readily cyanidable gold content of the ore while the result of Stage II showed the presence of gold with slow dissolution characteristics.

The findings also revealed that 7% of the gold present in the ore was inaccessible gold.

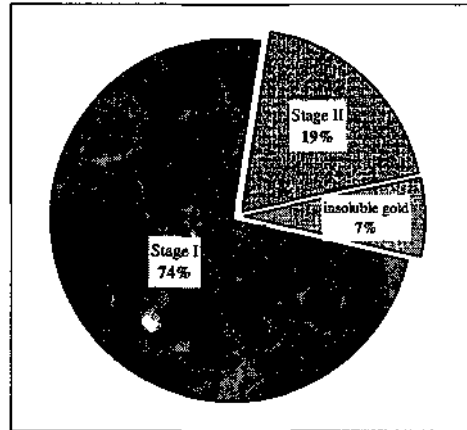


Figure 9. Extraction of gold from the ultrafine milled (6 h) ore in two-stage cyanidation.

### 3.5 Diagnostic Leaching Tests

Figure 10 illustrates the results of the diagnostic leaching of the ore which involves stepwise acid treatment followed by standard cyanide leaching after each stage. Initial cyanide leaching of untreated ore resulted in a gold extraction of 72%, this indicating the cyanide recoverable gold consistent with the findings reported in the previous sections. The remaining portion of the gold appeared to be refractory in character presumably due to the inaccessibility of gold particles to the action of cyanide. A sequence of acid treatment (HCl, H<sub>2</sub>SO<sub>4</sub>, HNO<sub>3</sub>, HF) was shown to improve the extraction of gold to 100% (Figure 10).

It has been reported that sequential acid leaching using HCl, H<sub>2</sub>SO<sub>4</sub> and HNO<sub>3</sub> would destroy a variety of mineral phases (Lorenzen and Van Devanter, 1993). It is extremely difficult to quantify the decomposed phases and hence draw firm conclusion from the data due to the non-selective nature of acid treatment expected i.e. partial removal of sulfides by HCl and H<sub>2</sub>SO<sub>4</sub> prior to HNO<sub>3</sub> treatment. Notwithstanding this, in the first stage of acid leaching by HCl, the oxides and carbonates would be completely destroyed to expose the gold associated. Further acid treatment with H<sub>2</sub>SO<sub>4</sub> and HNO<sub>3</sub> would be expected to remove the sulfides present. It could be estimated from the diagnostic leaching data that the refractoriness of the ore is caused by fine dissemination and association of gold particle within carbonates and oxides (-13%), sulfides (-13%) and silicates (-2%). The results of

acetonitrile elution stage suggests that no preg-robbing activity of carbonaceous material present

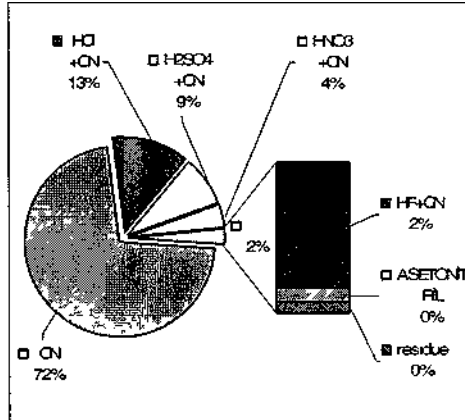


Figure 10 Extraction of gold following each stage of acid treatments with in diagnostic leaching of the ore

#### 4 CONCLUSION

In this study, the reasons for the low gold recoveries from the refractoriness of Kaletaş ore were investigated by adopting a diagnostic procedure. Pretreatment of the ore by roasting and ultrafine grinding was also examined to overcome the refractoriness and to improve the recovery of gold. Roasting was shown to produce no positive effect on the extraction of gold. Preliminary flotation tests failed to produce a gold/sulfide concentrate at acceptable recoveries.

The findings of the diagnostic leaching tests and two-stage cyanide leaching of ultrafine milled ore provided invaluable information on the refractory behavior of the ore. It was deduced that the occlusion of very fine gold particles within mineral phases such as carbonates, oxide and sulfides appeared to be the main reason for the refractoriness. Furthermore, the presence of alloyed gold with slow dissolution character could also contribute to the refractory behavior of the ore.

#### 5 REFERENCES

Alp, I, Celep, O , Tuysuz, N , Vieil, M , Lermi, A , 2003, Effect on Ore Processing of Mineralogical Structure Model Study on Mastra and Kaletaş Gold Ores, Proc of 18<sup>th</sup> International Mining Congress and Exhibitions of Turkey, 10-13 June, Antalya, Turkey, (in Turkish)  
 Browner, R.E, Lee, K H, 1998, Effect of Pyrrhotite Reacivity on Cyamation of Pyrrhotite Produced By

Pyrolysis of A Sulphide Ore, *Minerals Engineering*, Vol 11, No 9, pp 813-820  
 Costa, M C, 1997, Hydrometallurgy of gold New perspectives and treatment of refractory sulphide ores, *Fizikoc hemik zne Problemj Mmeralurgu*, Vol 63, pp 63-72  
 Çubukçu, A, Tuysuz, N, 2000, Kaletaş (Gümüşhane) Epitermal Altın Cevherleşmesinin Kökeni, Yerbilimleri ve Madencilik Kongresi, MTA, Ankara, (in Turkish)  
 Dunn, J G , Chamberlain, A C, 1997, The recovery of gold from refractory arsenopyrite concentrates by pyrolysis-oxidation, *Minerals Engineering*, Vol 10, No 9, pp 919-928  
 Gönen, N, 1999, Gumüşhane-Kaletaş Cevherinden Siyanürleme Yöntemiyle Altın Kazanımı, MTA Rap No 1324, Ankara, (in Turkish)  
 Gunyanga, F P , Mahlangu, T , Roman, R J , Mungoshi, J , Mbeve, K , 1999, An acidic pressure oxidation pretreatment of refractory gold concentrates from the Kwekwe Roasting Plant-Zimbabwe, *Minerals Engineering*, Vol 12, No 8, pp 863-875  
 Henley, K J , Clarke, N C , Sauter, P , 2000, Evaluation of A Diagnostic Leaching Technique for Gold in Native Gold and Gold+Silver Tellurides, *Minerals Engineering*, Vol 14, No 1 pp 1-12  
 Iglesias, N , Carranza, F, 1994, Refractory gold-bearing ore a review of treatment methods and recent advances in biotechnological techniques, *Hydrometallurgy*, Vol 34, pp 383-395  
 La Brooy, S R , Linge, H G , Walker, G S , 1994, Review of Gold Extraction from Ores, *Minerals Engineering*, Vol 7, No 10, pp 1213-1241  
 Lehman, M N , O'leary, S , Dunn, J G , 2000, An Evaluation of Pretreatments to Increase Gold Recovery from a Refractory Ore Containing Arsenopyrite and Pyrrhotite, *Minerals Engineering*, Vol 13, No 1, pp 1-18  
 Long, H, 2000, A fundamental study of the acidic pressure oxidation of orpiment and pyrite at high temperature, PhD Thesis, The University of British Columbia  
 Lorenzen, L, 1995, Some Guidelines to the Design of A Diagnostic Leaching Experiment, *Minerals Engineering*, Vol 8, No 3 pp 247-256  
 Lorenzen, L , Tumilty, J A , 1992, Diagnostic Leaching as an Analytical Tool for Evaluating the Effect of Reagents on the Performance of a Gold Plant, *Minerals Engineering*, Vol 5, No 3 pp 503-512  
 Lorenzen, L , Van Devender, J S J , 1993, The Identification of Refractoriness in Gold Ores by the Selective Destruction of Minerals, *Minerals Engineering*, Vol 6, No 8 pp 1013-1023  
 Oktay, C , Özşuca, D , Saklar, S , 2001, Gümüşhane - Kaletaş Cevherinden Kavurma ve Siyanürleme Yöntemi ile Altın Kazanımı, MTA, Ankara, (in Turkish)  
 Petruk, W, 1989, Recent progress in mineralogical investigations related to gold recovery, *Minerals Engineering*, Vol 32, pp 37-39  
 Roshan, B B , 1990, Hydrometallurgical Processing of Precious Metal Ores, *Mineral Processing and Extractive Metallurgy Review*, Vol 6, pp 67-80  
 Rubisov, D H , Papangelakis, V G , Kondos, P D , 1996, Fundamental Kinetic Models for Gold Ore Cyanide Leaching, *Canadian Metallurgical Quarterly*, Vol 35, No 4, pp 353-361  
 Smadmovic, D , Kamberovic, Z ve Vakanjac, B , 1999, Refractory Gold Ores, Characteristics and Methods of

- Their Procession, VIII Balkan Mineral Processing Conference Proceedings, pp 411-418
- Tuysuz, N , Ozdoğan, K , Er, M , Yılmaz, Z , Ağan, A , Pontid Adayayı'nda Carim Tıpi Kaletas (Gümüshane) Altın Zuhuru, *Tukiye Jeoloji Bülteni*, 37, 41-46 1994 (in Turkish)
- Ubalım, S, Massidda, R, Abbruzzese, C, 1994, Factorial experiments m the study of a biooxidatwe preatment for a conventional cyanidation of a Turkey arsenical gold ore, Proc of the 5<sup>th</sup> Int Mineral Processing Symposium, 6-8 September, Cappadocia, Turkey, pp 403-410



## Mineralogical Examination and Acidic Ferric Leaching of Kayabaşı (Trabzon) Massive Sulphide Ore

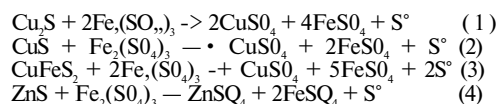
T Yılmaz, I Alp, H Deveci & O Celep

Karadeniz Teknik Üniversitesi, Trabzon, Turkey

**ABSTRACT:** In this study, the mineralogical characteristics and the acidic ferric leaching of Trabzon-Yomra-Kayabaşı Massive Sulphide ore were investigated. Mineralogical analysis of the ore samples has shown that the ore contains a variety of copper sulphides (12.5% Cu) including covellite, chalcocite, enargite, bornite, chalcopyrite, sphalerite (4.9% Zn), pyrite (29.9% Fe) and galena (0.7% Pb). Copper bearing minerals were found to occur as closely associated with pyrite and sphalerite. In the leaching tests, the effect of ferric iron concentration (0.0625-0.5 M), leaching temperature (25-80°C) and particle size (<106 µm) on the extraction of copper and zinc were examined at 0.5% w/v pulp density. The results indicated that the temperature exerts a strong effect on the rate and extent of extraction of copper and zinc that tended to increase exponentially with increasing temperature and over 90% Cu and 54% Zn recoveries were obtained at 80°C. The decrease in the particle size and the increase in the ferric iron concentration under the test conditions did not produce the desired effect on the metal extraction.

### 1. INTRODUCTION

High grade copper sulphide ores are mostly treated suitably within pyrometallurgical processes involving the production of flotation concentrates followed by smelting and refining. Mainly due to the ever increasing environmental concern and high energy costs associated with smelting and refining operations, hydrometallurgical process have gained importance for the treatment of sulphide ores (Davenport et al, 2002). Due to the low solubility of most base metal sulphides in acidic environments, the presence of an oxidizing reagent such as ferric iron and oxygen is required to engender their dissolution (Dutrizac and McDonald, 1974). Ferric salts with a standard electrode potential of 770 mV can effectively oxidise sulphide minerals including copper sulphides (Arslan et al, 2003, Burkin, 2001). The dissolution of some copper minerals and sphalerite in acidic ferric sulphate medium can be presented by the following reactions



As can be seen from the reactions above, ferric leaching of sulphides results in the formation and accumulation of elemental sulphur on the mineral surface, which can adversely affect the progress of the dissolution process (Dutrizac and McDonald, 1974).

Carranza et al (2004) reported that the concentrates containing mainly secondary copper sulphides could be leached successfully using acidic ferric sulphate media with a copper extraction of 92% at 8 h and 70°C. The authors also observed that the extended leaching periods and addition of catalyst were required to achieve high copper extractions from the concentrates with high chalcopyrite content. Smalley and Davis (2000) demonstrated the technical viability of atmospheric ferric leaching of a secondary copper ore at pilot scale.

Yomra-Kayabaşı copper ore deposit is located in Trabzon, Black Sea Region of Turkey (Figure 1). Yılmaz (2004) reported that Yomra-Kayabaşı ore did not respond well to the flotation concentration with very poor separation efficiency for copper minerals. The presence of penalty elements such as As and Hg in the ore would also make the flotation and smelting less attractive process route. Hydrometallurgical treatment of Yomra-Kayabaşı ore should therefore be examined.

In this study, the mineralogical properties and the acidic ferric sulphate leaching of Yomra-Kayabaşı ore for the extraction of copper and zinc were investigated. The effect of ferric iron concentration, particle size and temperature on the metal extraction was studied.

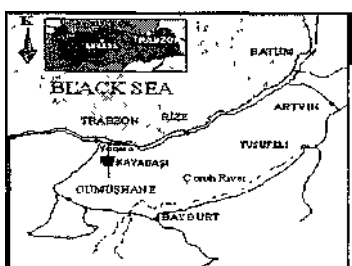


Figure 1. Location of Kayabaşı copper ore deposit.

## 2. EXPERIMENTAL

### 2.1. Material

Massive sulphide ore samples were obtained from Trabzon-Yomra-Kayabaşı (Turkey) ore deposit. For the ferric leaching studies samples were prepared as follows: Sub-samples of 1000 g were obtained from the bulk sample and these were then ground in a laboratory rod mill operating at a mill speed of 75 rpm corresponding to 73% of the critical speed. Hand-picked pieces and ground ore samples were used for mineralogical analysis. Chemical composition of the massive ore (Table 1) was determined using standard wet chemical analysis methods and an AAS (Atomic Adsorption Spectrometer).

### 2.2. Method

For the detailed mineralogical analysis of the ore, thin-sections and resin mounts were prepared, polished and examined under the microscope (Yılmaz, 2004; Alp et al., 2003). A total of 650-700 mineral particles were, on average, studied from each polished section. The mineral proportions were also determined.

Leaching experiments were carried out in a glass vessel placed in a water bath controlled within  $\pm 1^\circ\text{C}$  at the predetermined temperature. Acidified ferric sulphate solution (300 ml, 0.0625-0.5 M  $\text{Fe}^{+3}$  + 0.25 M  $\text{H}_2\text{SO}_4$ ) at the desired strength was poured into

the reaction vessel prior to the addition of the ore sample. In all the leaching tests, pulp density was kept constant at 0.5% w/v (-106  $\mu\text{m}$ ). Stirring of the reactor contents was performed using an IKA-RW20 overhead stirrer equipped with a pitched blade turbine impeller operating at a constant speed of 600 rpm. One ml samples were removed from the vessel at the predetermined time intervals and then used for the analysis of Cu, Fe and Zn in solution by an AAS. Evaporation losses were compensated for by the addition of de-ionised water. pH and Eh were also monitored during the leaching tests.

The effects of  $\text{Fe}^{+3}$  iron concentration in the range of 0.0625-0.5 M, leaching temperature in the range of 25-80°C and particle size in the range of -106+90  $\mu\text{m}$  to -38  $\mu\text{m}$  on the dissolution of Cu and Zn were examined.

Table 1. The chemical composition of the massive copper ore sample used

Element	%	Element	ppm
Cu	12.5	Au	2.7
Pb	0.7	Ni	27.1
Zn	4.9	Ag	117.7
Fe	29.94	Hg	26.48
As	0.9		
SiO <sub>2</sub>	22.08		

## 3. RESULTS AND DISCUSSION

### 3.1. Mineralogical characteristics of the ore

Detailed microscopic examination of the ore samples showed the presence of a wide variety of copper sulphide minerals; covellite, chalcocite, digenite, enargite bornite and chalcopyrite (Table 2). Chalcocite was found to be the most abundant copper sulphide mineral in the ore. Sphalerite, pyrite, and galena were identified as the other sulphide phases while quartz and silicate minerals were present as the important non-sulphide phases in the ore samples examined. Copper bearing minerals were found to occur as finely disseminated and closely associated with pyrite and sphalerite (Figures 2-3).

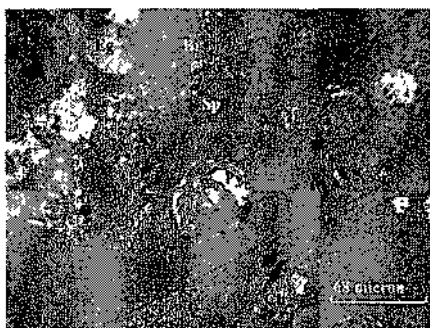


Figure 2. View of massive ore by ore microscope. (Sp: sphalerite, Py: pyrite, Ch: chalcocite, Eg: enargite, Br: bornite) (25x16).

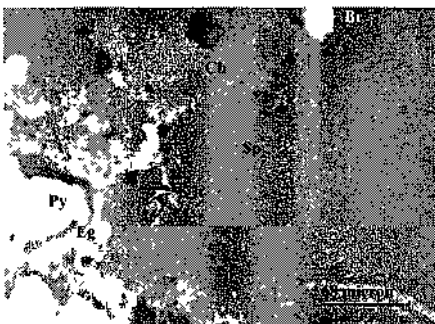


Figure 3. View of massive ore by ore microscope. (Sp: sphalerite, Py: pyrite, Ch: chalcocite, Eg: enargite, Br: bornite) (25x16).

Table 2. Copper sulphide minerals present and their relative abundance in the ore samples examined

Mineral	Amount (%)
Chalcocite (Cu <sub>2</sub> S)	40
Digenite (Cu <sub>9</sub> S <sub>5</sub> )	20
Bornite Cu <sub>5</sub> FeS <sub>4</sub>	20
Covellite (CuS)	10
Enargite (Cu <sub>3</sub> (As, Sb) <sub>2</sub> S <sub>4</sub> )	6
Chalcopyrite (CuFeS <sub>2</sub> )	4
Total	100

### 3.2. Acidified ferric leaching of the ore

#### 3.2.1. Effect of Fe<sup>3+</sup> iron concentration on the dissolution of Cu and Zn

Figures 4-5 show the effect of Fe<sup>3+</sup> iron concentration on the dissolution of Cu and Zn respectively from the ore at 0.5% w/v and 70°C. There appeared no significant influence of ferric iron concentration in the tested range on the metal extraction (Figure 6). The dissolution of copper was rapid during the initial leaching periods of 0.5 h; thereafter the dissolution rate slowed down (Figure 4). This could be due to the formation and accumulation of a diffusion barrier such as elemental sulphur on the mineral surface (Dutrizac and McDonald, 1974) and to the depletion of more reactive mineral phases leaving behind the recalcitrant phases such as enargite and chalcopyrite. A similar leaching trend was also observed for zinc (Figure 5).

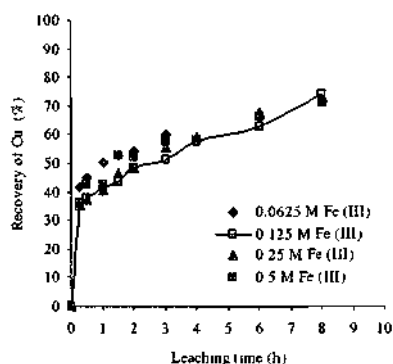


Figure 4. Effect of Fe<sup>3+</sup> iron concentration on the dissolution of Cu (Temperature 70°C; Stirring speed 600 rpm; Pulp density 0.5% w/v)

At the end of leaching time of 8 h, approximately 74% of copper and 45% of zinc was extracted using 0.125 M Fe<sup>3+</sup> solution (Figure 6). Copper seems to be solubilised more readily than zinc indicating the presence of more reactive copper phases than sphalerite. This could be consistent with the earlier reports that the rapid release of copper into the media adversely affected the flotation recovery of copper phases leading to the activation pyrite and particularly sphalerite (Yilmaz, 2004).

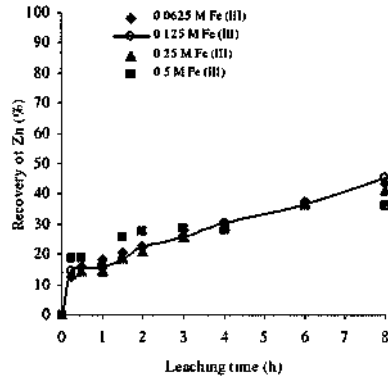


Figure 5 Effect of Fe<sup>3+</sup> iron concentration on the dissolution of Zn (Temperature 70°C, Stirring speed 600 rpm, Pulp density 0.5% w/v)

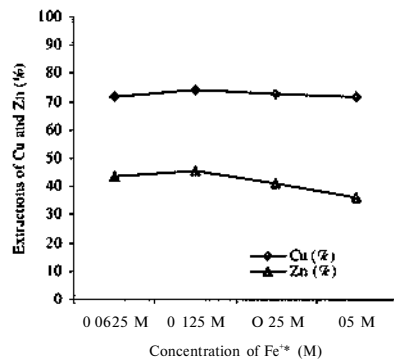


Figure 6 The plot of ferric iron concentration vs final metal extraction after 8 h

3.2.2 Effect of temperature on the dissolution of Cu and Zn

Figures 7-8 illustrate the influence of increasing temperature from 25°C to 80°C on the rate and extraction of copper and zinc respectively from the ore. Figure 9 depicts temperature versus the extraction of copper and zinc at the end of leaching period. Over a leaching period of 8 h approximately 91% of copper was solubilised at 80°C compared with 42% at 25°C (Figure 7). A similar trend of enhancement in the extraction of zinc with increasing temperature was also noted to occur. It was also observed that after 8 h the release of copper severely reduced despite the prolonged leaching period. This could be attributed to the poor accessibility of the leaching reagent to the remaining

portion of copper or the slow dissolution characteristics of refractory copper sulphides.

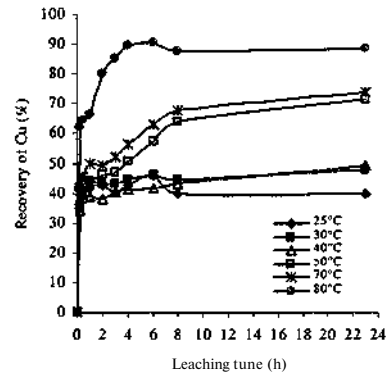


Figure 7 Effect of temperature on the dissolution of Cu (0.125M Fe<sup>3+</sup>, Stirring speed 600 rpm, Pulp density 0.5% w/v)

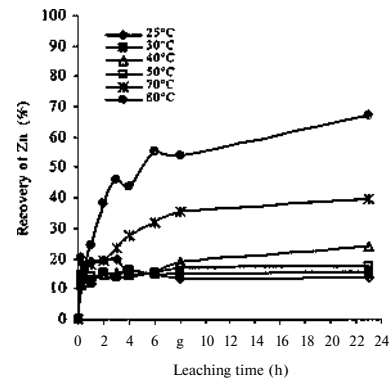


Figure 8 Effect of temperature on the dissolution of Zn (0.125M Fe<sup>3+</sup>, Stirring speed 600 rpm, Pulp density 0.5% w/v)

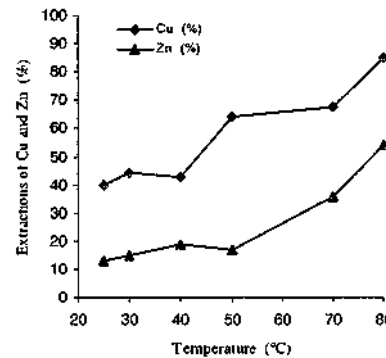


Figure 9 The plot of temperature vs final metal extraction

Carranza et al, (2004), Palencia et al, (2002) also observed the significant improvement in the extraction of copper and zinc from a secondary copper sulphide ore with increasing temperature to 90°C. They also noted the increase in the precipitation of iron as jarosite at high temperatures. In the current study, pH was controlled consistently below 1, which presumably curbed the formation of iron precipitates.

### 3.2.3 Effect of particle size on the dissolution of Cu and Zn

Surface area is an important variable in the leaching systems since the dissolution reactions occur on the mineral surface. The rate and extent of leaching generally tend to increase with increasing reactive surface area. Figures 10-11 show the effect of increasing surface area using the different size fractions obtained from the ground ore on the extraction of copper and zinc. The extraction of copper varied in the range of 78-93% with a general tendency of increasing with decreasing the particle size.

## 4. CONCLUSIONS

The mineralogical properties and the acidic ferric leaching of Trabzon- Yomra-Kayabaşı massive sulphide ore were studied. A wide range of copper sulphides with chalcocite as the most abundant copper phase were identified to be present in the ore. Copper sulphides were found to occur as finely disseminated within pyrite and sphalerite. Leaching tests have shown that the rate and extent of extraction of copper and zinc significantly increase with increasing temperature with over 90% Cu and 54% Zn recoveries at 80°C. The extraction of copper and zinc appeared to be independent of ferric iron concentration in the range of 0.0625-0.5 M at 0.5% w/v. A limited improvement in the rate and extent of dissolution of copper and zinc was found to occur with the increase in the surface area via size reduction.

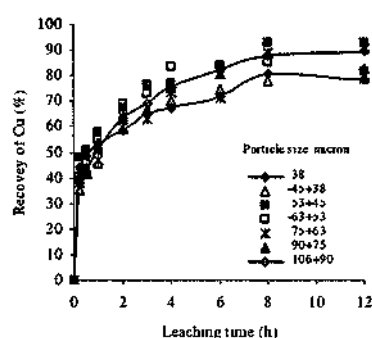


Figure 10 Effect of particle size on the dissolution of Cu (Temperature 70°C, 0.125 M Fe<sup>3+</sup>, Stirring speed 600 rpm, Pulp density 0.5% w/v)

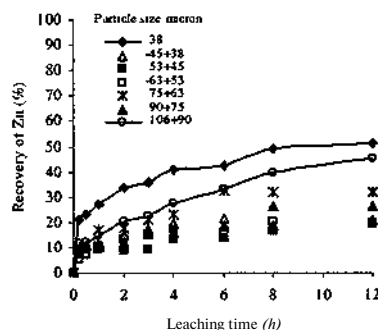


Figure 11 Effect of particle size on the dissolution of Zn (Temperature 70°C, 0.125 M Fe<sup>3+</sup>, Stirring speed 600 rpm, Pulp density 0.5% w/v)

## REFERENCES

- Alp I, Yılmaz T, Yazıcı E, Celep O, 2003, Determination of the Degree of Liberation and Optimum Grind Time of Kayabaşı-Trabzon (Turkey) Cu-Pb-Zn Massive Ore, 3<sup>rd</sup> International Conference "Modern Management of Mine Producing, Geology and Environmental Protection" SGEM, pp 39-44, Bulgaria
- Arslan F, Kangal M O, Bulut G, Gui A, 2004, Leaching of Massive Rich Copper Ore with Acidified Ferric Chloride, *Mineral Processing & Extractive Metall*, 25 143-158
- Carranza F, Iglesias N, 2004, Treatment of Copper Concentrates Containing Chalcopyrite and Non-Ferrous Sulphides by The BRISA Process, *Hydrometallurgy* 71 413-420
- Burkin A R, 2001, Chemical Hydrometallurgy, *Imperial College Press*, London

- Davenport, W G, King, M, Schlesinger, M, Biswas, A K, 2002, Extractive Metallurgy of Copper, Pergamon, UK
- Dutrizac, J E, McDonald R J C , 1974, Ferric ion as a leaching medium, *Mineral Sei Engng* 6 No2 59-95
- Palencia I, Romero R, 2002, Treatment of secondary copper sulphides (chalcocite and covellite) by the BRISA process, *Hydrometallurgy* 66 85-93
- Smalley, N , Davis, G , 2000, Operation of the Las Cruces Ferric Sulphate Leach Pilot Plant, *Minerals Engineering*, 13 599-608
- Yılmaz, T , 2004, Yomra-Kayabaşı Masif Sulfid Cu-Pb-Zn Cevherinin Flotasyon Yöntemi ile Zenginleştirilmesi, Yüksek Lisans tezi, KTU Muh Mim Fakültesi, Trabzon

## The Use of Raw and Calcined Diatomite in Art-Tile Bodies

N. Ediz

*Dumlupınar Unnemtü Ceramic Engineering Department, Main Campui, Kütahya TURKEY*

I Tatar

*Yurtbay Ceramic San A S, Inonu Eskişehir TURKEY*

I Bentli

*Dumlupınar Unvei uty, Mining Engineering Department, Main Campus, Kutahya-TURKEY*

**ABSTRACT:** In this study, the changes in the physical and mechanical properties of the art-tile bodies with high silica content were investigated after raw and calcined diatomite addition. For this purposes, raw and calcined diatomite were added at 18% to the traditional art-tile bodies having high silica content, the bodies were than pressed and fired at 900°C which is an accepted firing temperature for traditional art-tile bodies. The changes in the bodies were determined by some physical and mechanical tests while the mineralogical variations were examined by the XRD patterns. As a result, the fired strength of the bodies with 18% raw and calcined diatomite addition was increased by 2.5 and 3 times, respectively. Another interesting result obtained with such an addition was that the density of the bodies was decreased by 9.42% compared to the reference body.

### 1 INTRODUCTION

Art-tile and ceramic industry have played a very important role in the formation of Turkish culture and in enhancing the traditional arts. Izmir and Kütahya have become the major centers for the production of ceramic ware during the Ottoman term. At the end of the 18<sup>th</sup> Century, the production at Izmir had stopped and Kütahya became the only centre of this art and has survived until the present day. In 16<sup>th</sup> century, the ceramic industry has reached a flourished point both in technique and in art. In this period, there has been an important development in under-glazing technique which enabled the preservation of the figures, colours for a long time and provided a better appearance for the figures (Gyozo 1986). 16<sup>th</sup> century Izmir and Kütahya art-tile bodies contain silica, glass frit and bentonite with 80% montmorillonite. In this period, quartz, quartz sand and flintstone were used as the silica source (Atasoy, 1989).

As well known, diatomite is also an important silica source in the nature which is a fossil type of sedimentary rock, occurred by the accumulation of siliceous shells of diatoms (Onem 2000, Bozkurt 2000, Karaman&Kıbırcı 1999). The most important property of the diatomite is its low density. Although the wet density varies between 1.9-2.4 gr/cm<sup>3</sup>, it can

decrease down to 0.4 gr/cm<sup>3</sup> after drying. Another important property of the diatomite is that it has an average particle size of 50-100 *µm* (Breese 1994, Harben 1995). Therefore, diatomite is used mainly as a filtration, filler and insulation material (Bentli 2002, Kocurk 1997, Karadeniz 1996, Mete 1988). The research on diatomite and its industrial use has recently been increased in Turkey. Bentli et al (2004) has studied the physical and chemical properties of Kütahya Alayunt diatomite together with its processing possibilities. Aruntaş et al (1998) investigated the properties and the industrial use of Çankırı and Ankara diatomites while Mete (1985) searched the beneficiation of Kütahya-Alayunt diatomites and their use in insulating brick production. Ozbey and Atamer (1987), on the other hand, have made some proposals on the production and utilization of commercial diatomites.

High silica wall tiles currently produced in Kütahya are thicker and larger than traditional Kütahya tiles. One tile with 25x25 cm size weights about 1550-1560 gr and this causes some problems both in transportation and in mounting to the building since it increases the total weight of the structure. In this research, the modification in the physical and mechanical properties of the art tile bodies produced by the addition of raw and calcined diatomite was investigated.

2 EXPERIMENTAL STUDIES

2.1 Material

The quartz sand, Clay-1, Clay-2 and diatomite samples used in this research were collected from Istanbul, Eskişehir and Kütahya, respectively. In order to obtain calcined diatomite, raw diatomite was first dried at 110°C for 12 hours. The dried diatomite was then fired in an electrical chamber furnace at 1000°C for 1 hour. Furnace temperature was increased as 1°C per minute to the final level. Calcination temperature was determined by examining the TG-DTA curve of the raw diatomite (Bentli vd 2004). Chemical analysis of the raw and calcined diatomite was made using the ICP equipment (Perkin Elmer Optima 3000). However, an XRF instrument was used for the analysis of quartz sand, Clay-1 and Clay-2, the result was given in Table 1. Characterization of raw and calcined diatomite was made by Rigaku Mimflex diffractometer with CuK $\alpha$  radiation and XRD diffractograms are given in Figure 1. As seen from Figure 1, diatomite is in an amorphous state and there are cristobalite peaks due to the calcination temperature of the calcined diatomite. The densities of the raw, calcined and silica sand and their residues of sieve 63  $\mu$ m are given in Table 2.

Table 1 Chemical composition of the raw materials

Parameter (%)	Raw Diatom.	Calcined Diatom.	Quartz Sand	Clay-1	Clay-2
SiO <sub>2</sub>	89.86	93.60	87.02	50.12	68.12
Al <sub>2</sub> O <sub>3</sub>	1.62	1.24	7.12	6.76	14.98
Fe <sub>2</sub> O <sub>3</sub>	0.40	0.61	0.65	2.64	1.12
TiO <sub>2</sub>	0.05	0.05	0.32	0.42	0.10
Na <sub>2</sub> O	0.77	0.55	1.02	5.22	1.00
K <sub>2</sub> O	0.18	0.20	0.77	1.46	1.62
CaO	1.28	1.17	0.49	3.53	2.58
MgO	0.18	0.22	0.12	14.60	1.67
Firing Loss	5.66	0.51	2.49	11.41	6.46

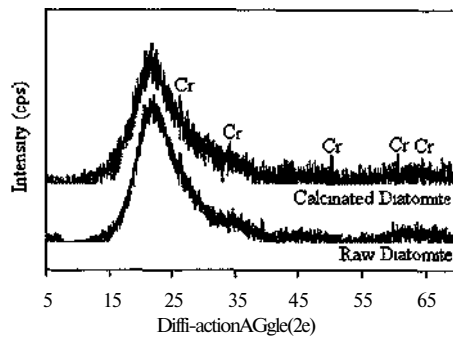


Figure 1 XRD Diffractograms of the raw and calcined diatomites (Cr Cristobalite)

Table 2 The densities of the raw, calcined diatomites and silica sand, their residues of sieve 63  $\mu$ m.

Property	RawDia	Calcined Dia	Quartz
Wet Density (gr/cm <sup>3</sup> )	2.01	2.01	~
Dry Density (gr/cm <sup>3</sup> )	0.374	0.384	2.65
63 $\mu$ m residue (%)	6	6	72.9

2.2 Method

In this research, new wall tile recipes were prepared by replacing the quartz sand in the original recipe (R) with raw and calcined diatomite at 18% (Tatar et al 2004). The prepared recipes are given in Table 3. In these recipes, the SiO<sub>2</sub> content was arranged so as to be 72%.

Table 3 Wall tile recipes (%)

Raw Material	R	D	KD
Quartz Sand	62	42	42
Raw Diatomite	-	18	-
Calcined Diatomite	-	-	18
Clay-1 + Clay-2 + Fluxes	38	40	40

The raw materials prepared according to the recipes given above were comminuted in a ball mill for 30 minutes. The comminuted materials were then dried at 105°C for 24 hours and undergone size reduction. The crushed material was sieved through 1500  $\mu$ m screens to obtain granules. These granules were then dry pressed at 160 kg/cm<sup>2</sup> pressure and finally fired in an electrical chamber furnace at 900°C for 1 hour. Furnace temperature was arranged to increase as 3°C per minute.

2.2 Physical tests

Total shrinkage, porosity, water absorption and density tests were carried out in order to determine the physical properties of fired art tile bodies.

2.2.7 Strength tests

The variation in the fired strength of the bodies with raw and calcined diatomite addition compared to the reference body is seen in Figure 2. As seen from the figure, the fired strength of the reference body was increased to 159 kg/cm<sup>2</sup> and 196.4 kg/cm<sup>2</sup>, respectively after 18% raw and calcined diatomite addition. This result can be explained by the finer particle size of the diatomite than quartz sand which causes more compact structure during sintering by filling the pores. Sintering of the materials with high silica content is accomplished by liquid-phase sintering method. Liquid phase wets the solid particles and capillary pressures of up to 0.007 kg/cm<sup>2</sup> are created in fine channels between the particles. Capillary pressures in fine materials are higher and sintering occurs easily (Geçkinli 1991).

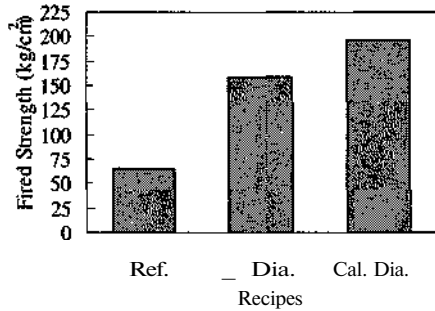


Figure 2. The variation in the fired strength of the bodies.

When XRD diffractograms are examined (Figure 3), anorthoclase development was found to be higher in the bodies with raw and calcined diatomite addition than the reference body. This is seen to be the main reason for the increase in the fired strength (Strnad, 1986). Therefore, diatomites when used, affect the property and the performance of the final product positively (Bozkurt, 2000).

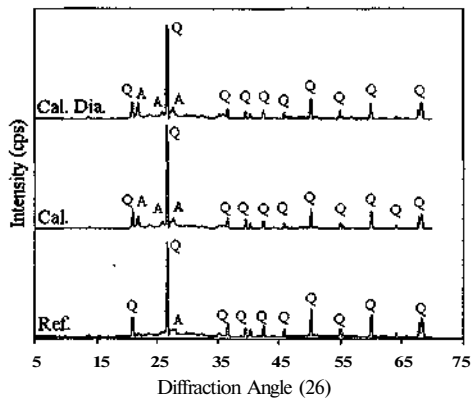


Figure 3. XRD diffractograms of the bodies (Q: Quar., A: Anorthoclase).

### 2.2.2 Shrinkage tests

Total shrinkage variations in the art tile bodies are seen in Figure 4. When the figure is examined, it is seen that the raw and calcined diatomite addition increases the total shrinkage of the bodies.

The increase in the total shrinkage and in the fired strength values of the bodies reflects better sintering conditions. The other explanation for the increased shrinkage is that diatomite has a firing loss of 5.59%, while the quartz sand has a firing loss of 2.15%.

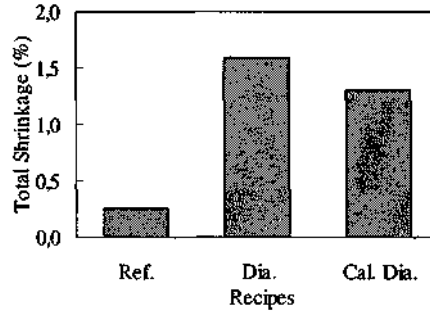


Figure 4. Total shrinkage variations for the bodies.

### 2.2.3 Water Absorption-Porosity Tests

Apparent porosity measurements of the art tile samples were made by using the Archimed weighting instrument. Water absorption-porosity values of the samples are given in Figure 5. Water absorption-porosity values of the bodies were increased compared to the reference body after diatomite addition since diatomite has more porous structure. However, this increase is in the acceptable range according to the Standard, TS EN 159.

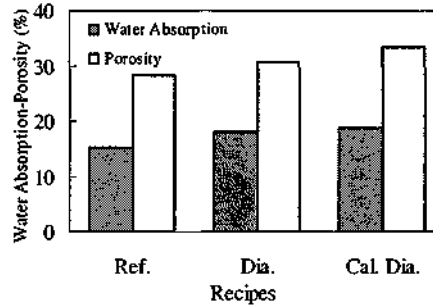


Figure 5. Variation in the water absorption-porosity values of the bodies.

### 2.2.4 Density Tests

The variation in the density of the high silica art tile bodies is given in Figure 6. As seen from Figure 6, the density of the bodies with raw and calcined diatomite addition were found to be 1.75 gr/cm<sup>3</sup> and 1.73 gr/cm<sup>3</sup>, respectively, while the density of the reference body was 1.91 gr/cm<sup>3</sup>. This result was explained by the lower density of both raw and calcined diatomite used than quartz sand. Moreover, the bodies with both diatomite additions were more porous than the reference body. This result brings

about some advantages in transportation and mounting the art tiles

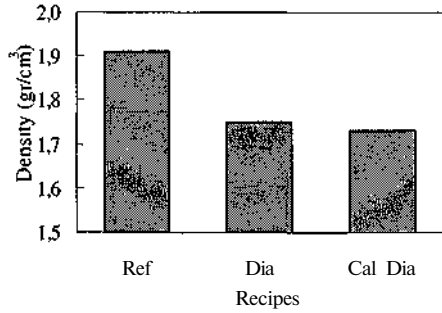


Figure 6 Density variations in the bodies

### 3 RESULTS

The results that can be derived from the tests earned out on the high silica art tile bodies after replacing the quartz sand with raw and calcined diatomites by 18% are summarized below

- Fired strength values of the bodies were increased by 2.5 and 3 times after raw and calcined diatomite addition, respectively
- Raw and calcined diatomite addition increases the total shrinkage of the art tile bodies
- Raw and calcined diatomite addition increases water absorption and porosity values. This is caused by the porous structure of the diatomite
- The density of the bodies with raw and calcined diatomite addition was decreased by 8.37% and 9.42%, respectively when compared to the reference body
- » Finally, it was proven that raw and calcined diatomite can be added to art tile bodies both to increase the fired strength and decrease the density of the bodies

### KAYNAKLAR

- Anmtaş, H Y, Albayrak, M, Saka, H A, Tokyay, M, 1998, Investigation of Diatomite Properties from Ankara-Kızılcahamam and Çankırı-Çerkeş Region, *Tr J of Engineering and Environmental Science*, 22, TÜBİTAK, Turkey, pp 337-343
- Atasoy N, Raby, J, 1989, *Türkiye'de Günümüze Gelen İznik Çimlen*, İstanbul Um Sosyal Bilimler Ens Yayını, 384 s
- Bentli, I, 2002, An Investigation into the Beneficiation of Kutahya-Alayunt Diatomite Ores, *4<sup>th</sup> Industrial*

- Minerals Symposium*, Ed Kose et al, (In Turkish), İzmir, pp 121-126
- Bozkurt, R, 2000, Diatomit, *üst of Industrial Minerals of Turkey*, İstanbul Mme Exporters Association (İMİB), Editors Onal et al, (In Turkish), İstanbul, pp 42-47
- Breese, R O Y, 1994, *Diatomite*, Industrial Minerals and Rocks, Carr (Ed), SMME, Colorado, USA pp 397-412
- Geçkin, A E, 1991, *lieu Teknoloji Malzemeleri*, İTÜ Kütüphanesi No 1454, İstanbul, 287 s
- Gyozo, G, 1986, Anatolian pottery from Izmir and Kutahya in Hungary in the 16th and 17th Centuries, 1 Uluslararası Tuik Çını ve Seramik Kongresi, Kutahya, 143-148
- Harben P W, 1995, *Diatomite*, The Industrial Minerals Handy Book, 57-61
- I Benth, N Ediz, I Tatar, 2004, Beneficiation of Kutahya-Alayunt Diatomite by Calcination, *W<sup>th</sup> International Mmeal Processing Symposium*, Ed Ipekoğlu, İzmir, pp 183-189
- I Tatar, N Ediz, I Benth, 2004, Diatomit Katkılı Çını Karo Bünye Üretimi, *5<sup>th</sup> Industrial Minerals Symposium*, Eds Akar&Seyrankaya, İzmir, pp 313-317
- Karadeniz, M, 1996, *Cevhei Zenginleştirme Tesis Ai tıkları-Çevi eye Etkileri-Onlemler*, MTA MAT Daire Başkanlığı, Ankara, 332 s
- Karaman, E, Kibici, E, 1999, *Temel Jeoloji Prensipleri Diatomit*, Devran Publication, Ankara, s 345 355
- Koktürk, U, 1997, *Endustriyel Hammaddeler*, Dokuz Eylül Üniversitesi Muh -Mim Fak Yayın No 205, izmir, 64-68
- Mete, Z, 1985, Kutahya-Alayunt Yoresi Diatomit Yataklarının izole Tuğla Yapımında Kullanılabilirliğinin Araştırılması, *Seramik Teknik Kongresi*, Ankara, 253-263
- Mete, Z, 1988, *Beneficiation of Kutahya Alayunt Diatomite Ores*, Akdeniz University Engineering Faculty Journal, Mining Section, Ed Yarmk, No 1, (In Turkish), İsparta, pp 184-201
- Onem, Y, 2000, *Sanayi Hammaddeleri*, Kozan Ofset, Ankara, 386 s
- Ozbey, G, Atamer, N, 1987, Kızılcahamam (Diatomit) Hakkında Bazı Bilgiler, *10 Türkiye Madencilik Bilimsel ve Teknik Kongresi*, TMMOB Maden Mühendisleri Odası, Ankara, 493 502
- Strnad, Z, 1986, *Glass-Ceramic materials*, Elsevier Science Publication Co
- TS EN 159, 1997, *Seramik Karolar Toz Halinde Preslenmiş*

## Solution of Clean Water Problem of Özberil Coal Washing Plant with Acrylamide Copolymer Flocculants

V Demz&H Delice

*Department of Mining Engmeei mg Sule\man Demuel University, İsparta Turkey*

**ABSTRACT:** Washing plant belonging to Ozberil Mining Co (Denizli Kale) has a capacity of 50 t/h and coal is washed with heavy media separation to increasing its quality Five settling tanks are used in the washing plant to separate slime from water by natural sedimentation Although using tanks for the wastewater, which does not contain appreciable amount of chemical pollutant Therefore, the amount of clean water which is needed for the plant can not be obtained due to very slow settling rate of solid ingredients in the tanks

The objective of this study is to get clear water for recirculating and separating fine solids in state of easy handling Therefore, laboratory flocculation experiments were carried out with the aim of designing the wastewater treatment facility for establishing optimum sedimentation conditions in this plant After the laboratory tests, engineering design was completed for the wastewater treatment plant Thus, in result of this study was found a suitable solution for the wastewater for Ozberil coal washing plant

### 1 INTRODUCTION

Sedimentation is the removal of suspended solid particles from a liquid stream by gravitational settling This is always the case in mineral processing where the carrier liquid is water (Kommek & Lash, 1979)

The efficiency of solid/liquid separation may be greatly improved by the application of synthetic polymeric flocculants, particularly in coal preparation where sedimentation, filtration and centrifugation processes are extensively used The term flocculation is often confused with coagulation, although the two refer to quite different processes Coagulation is basically electrostatic in that it is brought about by a reduction of the repulsive potential of the electrical double layer The term flocculation is derived from the Latin, "flocculus" literally a small tuft of wool, or a loosely fibrous structure Flocculation is brought about by the action of high molecular weight materials such as starch or polyelectrolytes, where the materials physically forms a bridge between two or more particles, uniting the solid particles into a random, three-dimensional structure which is loose and porous (Gnc & Lnc, 1978)

Nowadays, flocculants used for flocculation are non ionic, anionic and cationic polymers Non-ionic and anionic polymers cause to form big, fast sedimentation and fairly compact flocks However, it is preferable to use higher molecular weight anionic or non-ionic polymers over cationic flocculants for sedimentation process (Ateşok, 1987)

It is known through the literature that non ionic polymers are usually used in acidic slurries and high molecular weight anionic polymers are used in alkali slurries (Sabah & Yeşilkaya, 2000)

Although, the wastewater does not bear any appreciable amount of chemical pollutant nevertheless its appearance and very slow settling rate of solid ingredients make it unpleasant and unwelcome Thus, municipalities and inhabitants have been forcing coal washing plants to find an appropriate solution for the wastewater On the other hand, coal washing plants are advantageous find an appropriate solution, because of the cost of fully fresh water use either from wells or city network is getting unbearably high

Ozberil coal washing plant has a capacity of 50 t/h and coal, which is produced from underground, is washed to increase its quality Nowadays, this vast waste necessitates the Ozberil coal washing



Table 2 Particle size analysis of slime sample

Sieve Size (mm)	Weight(%)	Under Size(%)
+ 1 180	0 56	100 00
-1 180 + 0 850	0 96	99 44
-0 850 + 0 600	181	98 48
-0 600 + 0 300	5 32	96 67
-0 300 + 0 150	6 63	91 35
-0 150 + 0 075	10 17	84 72
-0 075 + 0 045	3 39	74 55
-0 045 + 0 038	2 99	71 16
-0 038	68 17	68 17
Total	100 00	

### 3 EXPERIMENTS

Sedimentation tests were done with slurry samples taken from the plant for experimental studies

Five different flocculant types were tested for five different amounts and 30 systematic sedimentation tests were applied Four Anionic flocculants produced by Ciba and one non-ionic flocculant produced by Cytec companies were used in tests Table 3 shows the flocculant type and properties in use experiments

Table 3 Characteristics of flocculants used

Commercial Name	Firm	Type	Dosage (%)
Magnafloc 155	Ciba	Anionic	0 02-0 1
Magnafloc 1011	Ciba	Anionic	0 02-0 1
Magnafloc LT25	Ciba	Anionic	0 02-0 1
Magnafloc LT27	Ciba	Anionic	0 02-0 1
SUPERFLOC N300	Cytec	Non-ionic	0 05-0 3

#### 3.1 Sedimentation test related to change of pulp solid concentration (without flocculant)

The pulp solids content affects the rate of settling since it determines the number of inter particle collisions Figure 2 shows the effect of changing the solid concentration on the settling rate of slimes It is noticed that settling rate increased as the solid concentration decreased The behaviour can partially be related to the change in the pulp viscosity The sedimentation velocity decreases with increasing the viscosity of a pulp by raising its density

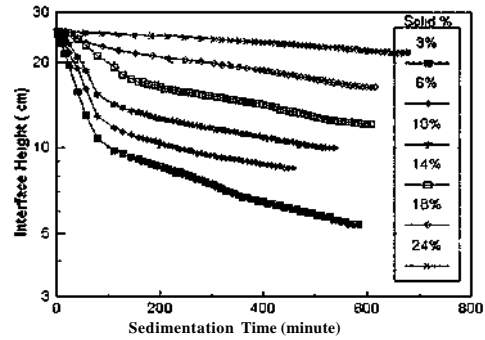


Figure 2 Sedimentation curve with different solid concentration

#### 3.2 Sedimentation test relate to flocculant dosage and type

To establish the most appropriate flocculant type and dosage for the efficiency of sedimentation, flocculation results obtained with non ionic and different molecular weight anionic polymers are shown in Figure 3-7

As seen in Figure 3-7, the optimum flocculant dosage for slimes that can be subjected to solid-liquid separation is 4 ppm for MagnaflocLT27 and Magnafloc101, 5 ppm for MagnaflocLT25, 10 ppm for Magnafloc 155 and 30 ppm for SuperflocN300 polymers In the tests performed in laboratory condition pH 8 and solid concentration of 6%, good results were obtained by using almost one-twenty of the anionic flocculants compared to non-ionic flocculant Because non-ionic flocculants usually hydrolyze in alkali slurry, even the use of high dosage SuperflocN300 did not provide an effective sedimentation

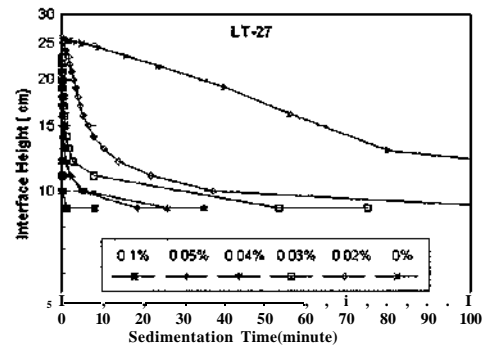


Figure 3 Sedimentation curve with different dosage in using MagnaflocLT27

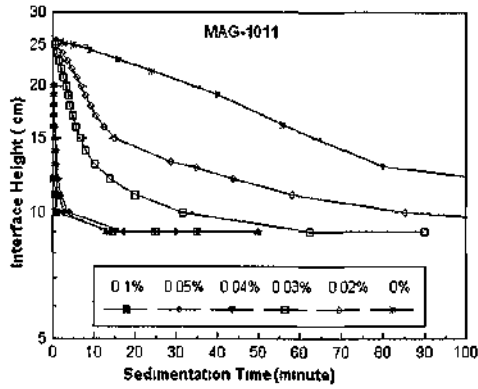


Figure 4 Sedimentation curve with different dosage in using Magnafloc101

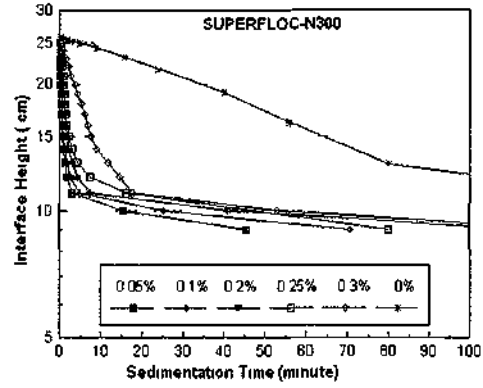


Figure 7 Sedimentation curve with different dosage in using SuperflocN300

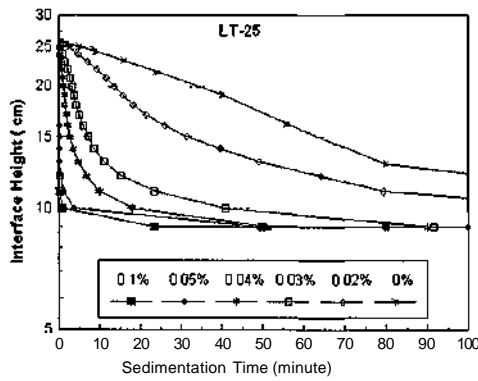


Figure 5 Sedimentation curve with different dosage in using MagnaflocLT25

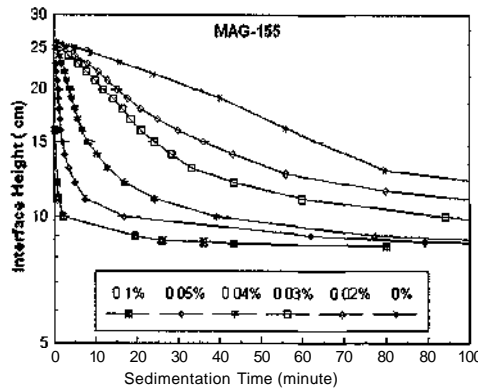


Figure 6 Sedimentation curve with different dosage in using Magnafloc155

The tests performed with four anionic and one non ionic flocculants showed relationships between sedimentation rate and flocculant dosage (Figure 8) As it can be seen in Figure 8, when 0.04% MagnaflocLT27 is used, 19.63 cm/mm sedimentation rate reached and again with the same dosage of Magnafloc101, MagnaflocLT25, Magnafloc155 and SuperflocN300, 12.74 cm/mm, 3.38 cm/mm, 14.3 cm/mm and 10.8 cm/mm, respectively

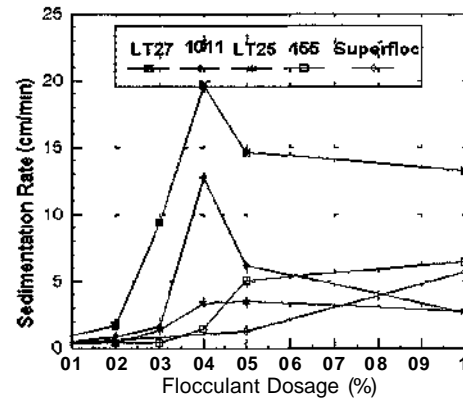


Figure 8 Effect of flocculant dosages on Sedimentation rate for different flocculant type

#### 4 CALCULATIONS OF THICKENER AREA

Figures 2-6 show the height of the interface of the settled pulp as a function of the sedimentation time, with different flocculant dosage and without

flocculant. It can be seen that the addition of the flocculant increases the sedimentation so that the final settling height of the slime slurry is readily reached.

The thickener design employed was first hypothesized by Kynch and later modified by Talmadge and Finch. Talmadge and Finch used this approach in determining the limiting flux and thus a prediction of the unit area for specific thickening applications. The value of the area (A) was developed by the following equation by Talmadge and Finch (Keane, 1986):

$$A = \frac{Q * t_m}{C_0 * H_0} \quad (1)$$

where, A is the thickener area, m<sup>2</sup>  
 g is feed solid rate (2.5 t/h)  
 t<sub>m</sub> is maximum time for underflow concentration (h)  
 H<sub>0</sub> is the initial height (0.26 m)  
 C<sub>0</sub> is the initial concentration (0.06 kg/l)

From the definition point of view, the thickener capacity is defined as the amount of the clear solution overflowing of slime slurry.

Thickener area was calculated for each flocculant type and without flocculant and results were showed in Table 3.

Table 3 summarizes the data of the above factors, affecting flocculation behaviour of slime, the thickener area needed for dewatering. The thickener area decreases with increase in flocculant dose for all flocculant types.

## 5 CONCLUSIONS

Increase in the sedimentation rate with increasing the molecular weight of the flocculant may be due to increase in the adsorption of the flocculant on the accessible particle surface.

All the flocculants tested were found be importantly to flocculant concentration. The effectiveness of the flocculants tested in coal tailing slime suspension was in order: LT27>101 l>LT25>155>Superfloc

Flocculation tests done with anionic flocculants, better flocks are obtained with high molecular weight MagnaflocLT27. Also flocculants are bound to surface of particles with electrostatic attraction forces along with polymer bridges. Consequently, with the use of MagnaflocLT27, an anionic flocculant, at concentration average 0.04%, which corresponds to 0.025 kg LT27 per ton pulp (0.31 kg

per ton solid), clear water to re-use in washing plant can be obtained.

A simple solid-liquid separation system may reclaim of the water input very efficiently.

Table 3. Effect of flocculant dose on the thickener area

Name	Dose (%)	Sediment rate cm/min	Thickener Area (m <sup>2</sup> )
None	0.0%	0.172	665
LT27	0.02%	1.738	97
	0.03%	9.42	75
	0.04%	19.63	18
	0.05%	14.63	8
	0.10%	13.22	3
1011	0.02%	0.855	226
	0.03%	1.662	104
	0.04%	12.741	11
	0.05%	6.218	3
	0.10%	2.620	0.5
	0.02%	0.399	372
	0.03%	1.382	112
	0.04%	3.381	48
LT25	0.05%	3.489	11
	0.10%	2.750	5
	0.02%	0.380	373
	0.03%	0.450	112
	0.04%	1.432	48
155	0.05%	5.083	11
	0.10%	6.481	5
	0.05%	1.309	141
	0.10%	5.687	120
	0.2%	6.146	101
	0.25%	8.478	75
S.Floc	0.30%	10.422	40

## REFERENCES

- Ateşok, G., 1987. Polimerlerin cevher hazırlamadaki yeri, kullanım özellikleri. *TMMOB Madencilik Dergisi*. Cilt 24, Sayı 3: 15-22.
- Keane, J.M., (ed. By Mular, A.L& Anderson, M.A), 1986. Laboratory testing for design of thickener circuits. *Design and Installation of Concentration and Dewatering Circuits*, SME, Colorado.
- Kominek, E.G. and Lash, L.D., (ed. by Schweitzer, P.A) 1979. Sedimentation, *Handbook of Separation Techniques for Chemical Engineers*. McGraw-Hill, NewYork.
- Gric, N.M. and Lric, B.D., 1978. Flucculation: Theory and Application, *Mining and Quarry Journal*. Vol. 5:1-8.
- Sabah, E. and Yeşilkaya, L., 2000. Evaluation of the settling behavior of Kırka borax concentrator tailings

*V Deniz & H Delice*

using different type of polymers *The Journal of Ore Dressing*, Issue 3-4 1-12  
Wills, B A, 1988 *Mineral Processing Technology*  
Pergamon Press, 3<sup>rd</sup> Ed., Oxford